MATHEMATICAL MODELS OF *DAPHNIA* EPIDEMICS

BY

VANESSA RIVERA QUIÑONES

DISSERTATION

Submitted in partial fulfillment of the requirements
for the degree of Doctor of Philosophy in Mathematics
in the Graduate College of the
University of Illinois at Urbana-Champaign, 2019

Urbana, Illinois

Doctoral Committee:

Professor Richard Laugesen, Chair
Associate Professor Zoi Rapti, Director of Research
Professor Lee DeVille,
Professor Carla Cáceres, School of Integrative Biology

Abstract

Disease ecology studies the interactions among hosts, pathogens, and the environment and how these shape the spread of disease. These interactions can be quite complex and lead to fascinating dynamics. Our system of study, *Daphnia* has a lot of interesting and complex features that can be analyzed with precision both biologically and mathematically. By using mathematical models we can study the underlying biological mechanisms that drive and/or inhibit the spread of disease. This dissertation explores, through a range of models, the many aspects that play a role in *Daphnia* epidemics. We begin with simple models and build models with higher complexity by adding more realistic biological assumptions.

From ordinary and partial differential equation models to stochastic models, through the chapters of this thesis, we zoom-in to the different aspects of *Daphnia* epidemics and and zoom-out to the bigger story that connects them. We give precise conditions under which short-term evolution of hosts can lead to the early termination of an epidemic. Moreover, overturning an assumption about hosts' ability to recover, we showcase the role of recovery from an infection in reducing disease prevalence and the number of secondary infections. Through this thesis we have gained more insight into the biology of our system, and more importantly we open the door to new and exciting questions. As new biological insights are discovered, we can use mathematical models to continue to unravel the many aspects of *Daphnia* epidemics.

For those whose shoulders I've stood on, those who will stand on mine, and those who could've been here and are not, this is for you.

Acknowledgments

This journey would have been over way before it really began without the love and support of my family. To my parents, Gloria and Rafael, my siblings Glorimar and Rafael José, thank you for your endless love and uttermost belief in me. You have shown me through your example how to persevere, to remain humble, and always be of service to others.

To my loving partner Gert, thank you for your endless support and confidence in me, for showing me that pursuing your dreams while prioritizing your well-being is possible. Also, for pointing out that these acknowledgements should include myself; so, thank you Vanessa for all your hard work. You did it!

I am grateful for the invaluable friendships of these group of amazing women: Alyssa, Emily H., Itziar, Marissa, Sarah, and Simone. I am in awe every day of you. You are my role models. Thank you for the laughs, the tears, and all the love.

To my advisor Zoi Rapti, you have made this thesis possible in the best ways. I've learned so much from you in the past few years. Thank you for always helping me find my path in my research, for everything. I think you are a fantastic mathematician, a wonderful mentor, and a truly kind person. I am grateful to have been your student.

I would also like to thank my committee members Richard Laugesen, Lee DeVille, and Carla Cáceres for your time and guidance. To the Cáceres Lab and my amazing collaborator Tara Stewart, thank you for sharing your love for *Daphnia* with me.

Lastly, I owe much gratitude to the National Academy of Sciences Ford Foundation Predoctoral Fellowship, and National Science Foundation, for the financial support from the grant DMS 1345032 MCTP: PI4: Program for Interdisciplinary and Industrial Internships at Illinois.

Table of Contents

Chapter 1

Introduction

1.1 Mathematics of Disease, Evolution, and Ecology

As new diseases continue to appear in populations, questions regarding the distribution and shape of infections have been of great interest to disease ecologists. Disease ecology focuses on the study of the interactions between the host, pathogen, and environment and how they affect the spread of an infection. By studying these interactions we can obtain valuable insights on how an epidemic could be prevented or minimized in a population.

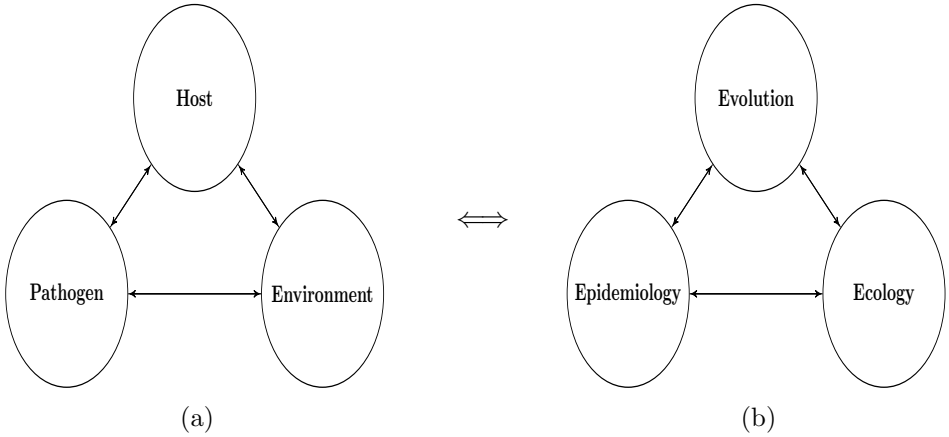

Figure 1.1: (a) Main interactions of study in Disease Ecology. (b) Main frameworks from which we will derive our mathematical models.

Some of the challenges that disease ecologists face is that each pairwise interaction in itself has an great amount of biological complexity and depends greatly on the specific biological system under study. Mathematical models have a long history improving our understanding of the mechanisms that lie underneath these interactions. Host-parasite interactions have been studied extensively in the past and continue to be a hot topic. Among the biological sciences, ecology has been one of the first and most developed areas that has used quantitative models [19]. One of the most commonly

used models in epidemiology are compartmental models, in which the population is divided into distinct compartments with assumptions about the rate of transfer from one compartment to another. The amount of compartments in which the population will be divided and structure of the model depends on the characteristics of a particular disease. Are host able to recover from the disease? Does the host gain immunity against reinfection? Is transmission direct or does it happen indirectly through environmental factors? Does the infection progress in stages? The answers to these questions will determine the characteristics of our models.

Daniel Bernoulli developed what was probably the first compartmental epidemic model in 1760 [5]. Some of the more well-known epidemiological models are the Susceptible-Infected (SI), Susceptible-Infected-Recovered (SIR), and Susceptible-Exposed-Infected-Recovered (SEIR). As seen in the early works of Anderson & May (1981), host–pathogen interactions can be understood from compartmental models that can be refined to account for more biologically realistic scenarios [6]. While the stages of a disease can be more complex, as in many modelling scenarios, we can use these models as a building block for more complicated models. There are many examples of infectious diseases such as measles, influenza, tuberculosis, malaria, sexually transmitted diseases that have been studied under this framework ([5], [57], [59]) providing evidence on how mathematical models can give insight to epidemiological processes.

Another key component to understanding disease ecology is evolution. How organisms adapt to changing environments has been a central question in biology and dates back to Darwin's *"On the Origin of Species "* [35]. Adaptation generally refers to changes that lead organisms to be suited to their local environment. The most common view of adaptation the process is as an optimization process: Given a set of conditions only the "best" adapted (i.e. fittest) to these conditions prevails. If only the best adapted prevail, how do we obtain diverse populations? What does mathematics tell us about these biological processes? In his work, Darwin argues that the most diversified descendants are favoured, which can lead to two distinct branches of sub-populations, ultimately explaining the emergence of two species from one [48]. This evolutionary process could explain the existence and drivers of diversity which can have implications in how diseases spread in a population.

There has been evidence that diverse populations can increase or decrease disease prevalence

(i.e. proportion of infected in a population) [30]. The effect where populations of hosts with high diversity inhibit disease spread is known as the dilution effect. Biologists have adopted two main perspectives on this effect, mainly, that loss of diversity is correlated with higher levels of disease prevalence; and conversely, that high parasite diversity needs high host diversity, thus increasing diversity will increase diseases [56]. Untangling the main factors of this effect can be complicated but mathematical models can help us predict these outcomes. Diversity, also referred to as variation, can happen at a genotypic level, where the composition of genes is altered, or at a phenotypic level, where the composition of observable traits changes.

It has been shown that hosts can vary in their susceptibility to infection, and thus the harm inflicted by a pathogen will vary among hosts ([14], [24], [25], [45], [41]). On one hand, this harm is characterized by the host's fitness, which accounts for the host's reproductive success. On the other hand, virulence, which can be defined as the cost to the host due to infection, translates into the reduction in host fitness [3]. Pathogens can affect host fitness and promote the evolution of defense strategies including resistance (i.e. avoiding or fighting infection), control (i.e. reducing parasite replication) and tolerance (i.e. living and reproducing with infection) [55].

The relationship between host susceptibility and virulence has been established by what is known as the trade-off hypothesis in which the parasite needs to harm the host in order to be transmitted. It argues that transmission and duration of an infection cannot be simultaneously maximized by a parasite. In fact, in the case of obligate killers such as *Metschnikowia*, the parasite may be expected to evolve very high virulence [46]. However, if virulence plays a role in other mortality sources (i.e. predation risk) other outcomes such as decreased virulence, evolutionary branching, and evolutionary cycles are possible [34]. We will explore some of these outcomes in more detail in Chapter 2.

Many studies have provided empirical support of the trade-off hypothesis between virulence and parasite transmission [3]. Three limitations of this hypothesis are that it relies on how virulence is defined, trade-offs might not be unique, and testing the trade-off hypothesis empirically is difficult [4]. Very little is known about the relationship between traits apart from what can be inferred from experimental data and biologists' understanding of the underlying mechanisms that come into play; thus, this hypothesis has its fair share of critiques [22].

The strength of the trade-off hypothesis lies in its simplicity. Adding a simple constraint to an epidemiological model allows one to make powerful predictions in evolutionary epidemiology [3]. Ecological and evolutionary dynamics can occur at similar or different timescales [23]. Thus, our assumptions on the timescale at which these interactions happen will play a role in deciding which mathematical framework to use. We will further study evolution in a short and long-term timescale by incorporating different trade-offs in Chapter 2 and Chapter 3.

1.2 Why study *Daphnia*?

Understanding the interplay between ecology, epidemiology, and evolution from a theoretical perspective has been a challenge. In the last few decades *Daphnia*, commonly known as the "water flea", has been a model system to provide insights about the connections between ecology, evolution, and infectious diseases [31]. Their importance is highlighted by the wide ecological roles they play which can be reviewed in the works of [70]. To study such interactions we focus on the zooplankter *Daphnia dentifera* which may experience yearly epidemics of the virulent fungus *Metschnikowia bicuspidata* in late summer and fall ([41], [42], [55]). We provide an illustration of the main interactions in the *Daphnia-Metschnikowia* system in Figure 1.2.

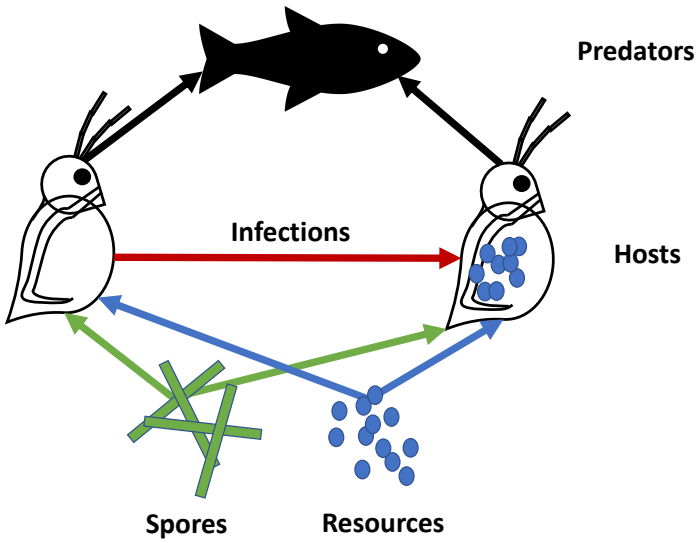

Figure 1.2: Main interactions among *Daphnia*, spores, resources, and predators.

Daphnia become infected when they encounter the fungal spores that are present in the water column through feeding. They are non-selective feeders and do not distinguish the fungal spores that make them sick from the algae they consume. The parasite is obligate killer since it depends on the host for reproduction and on the host's death for transmission. Once consumed, the spores must pierce the host's gut wall to reproduce within the host. When infected hosts die, spores are then released to the water column where they can infect new hosts.

In many midwestern lakes, *Daphnia dentifera* are preyed upon by visually oriented predators such as the blue gill sunfish. *Daphnia*, which are normally translucent, become more opaque as the infection progresses, and therefore more visible to predators [43]. Thus, infected host are preyed upon at a higher rate. Once infected *Daphnia* are consumed by the bluegill fish, it leads to a net loss of fungal spores [80].

Daphnia dentifera has been described as an ideal system to study host resistance since the parasite that afflicts it shows genetic diversity, which removes the possibility for coevolution. Thus, one can test for parasite-driven evolution directly [74]. In the case of our system of study *Daphnia–Metschnikowia*, this cost is compounded by the fact that infected individuals experience higher predation rates that uninfected host. Host susceptibility and virulence are not the only trade-off that has been observed in disease systems. Other examples of trade-offs suggested for the *Daphnia* system include: fecundity-tolerance, feeding rate versus spore yield and fecundity. We explore some of these trade-offs in more detail in Chapter 2 and Chapter 3.

1.3 Overview: Modelling *Daphnia* Epidemics

The use of compartmental models to understand the spread of disease in biological systems is not unique for the *Daphnia* system. Other vector-borne diseases transmitted by various species of mosquitoes such as the West Nile virus, dengue fever, malaria, Zika virus have been extensively studied under this framework [82]. In fact, similar to *Daphnia*, bumble bees experience infection through feeding, however the social hierarchy of bees requires a different definition of the compartments of the models ([16], [17], [29]). In this thesis, we build up from simple models and add complexity as we study different questions regarding how disease spreads in the *Daphnia-Metschnokawia* system. Here we provide a general overview of the models used throughout the

main text in hopes that the reader can get a bigger picture of what our models will attempt to answer and the assumptions that underlie them.

In Chapter 2, we use a Susceptible-Infected (SI) model (see Figure 1.3) to study the short-term evolution of host in our system. Similar models have been used in the literature ([41], [45]). In this formulation, we keep track of susceptible (S) and infected (I) individuals, and the transitions in/out and between compartments. We focus mostly on three main types of interactions: births, deaths, and infection. Using a Quantitative Genetics framework we show that the short-term evolution of hosts, can lead to the termination of an epidemic and reduced peak disease prevalence. Assuming a trade-off among virulence and two traits: host susceptibility and predation selectivity; we show virulence evolves to a lower value and increases disease prevalence.

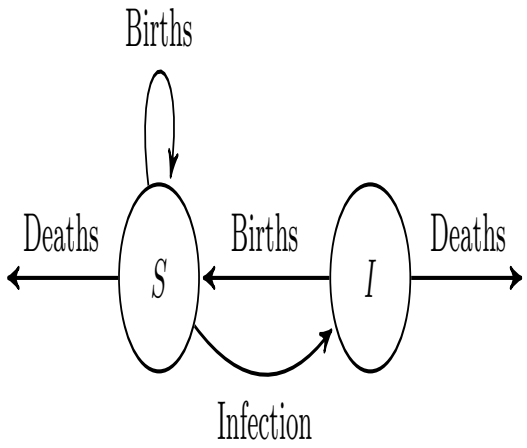

Figure 1.3: Illustration of Susceptible-Infected (SI) model.

The second model formulation we will use the Susceptible-Infected-Spore-Algae model, which we denote by $SIZA$ model as a short hand. Similar models to this formulation have been used to understand the role that spores, resources (i.e algae) and competitors play in the spread of disease [30]. By including the spore (Z) and algae (A) compartments, we can incorporate two new interactions: feeding and the release of spores back into the system through the death of infected individuals. This model extends our previous SI model (see Figure 1.4). We will use this formulation in Chapter 3, to explore *Daphnia's* role as consumers and how the long-term interactions of these four compartments impact the evolutionary outcomes for our system.

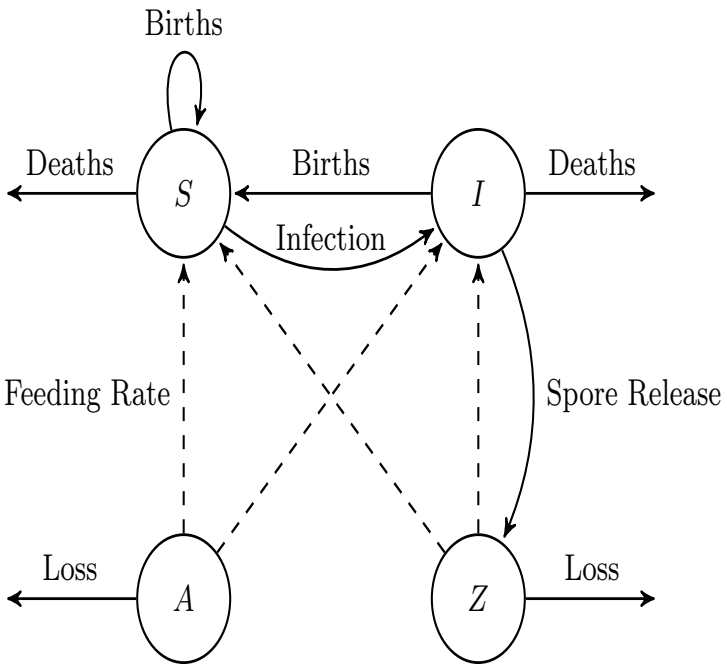

Figure 1.4: Illustration of Susceptible-Infected-Spores-Algae (SIZA) model.

In Chapter 4, we expand this formulation further by introducing an exposed compartment denoted by E (see Figure 1.5). Recent laboratory studies have data that newly suggests *Daphnia* are able to recover from an infection [79]. For simplicity, we exclude from the figure the births and death of susceptible, exposed, and infected individuals. In this joint work with Tara Stewart-Merrill, we use a differential equations model (i.e. $SEIZAS$ model), to study how these immune responses (clearance) and physiological barriers (resistance) impact the disease dynamics of our system. We show that these recovery mechanisms reduce disease prevalence and the number of secondary infections. In the absence of recovery, our system exhibits damped oscillations. Once recovery is introduced, these oscillations begin to dampen at a faster rate.

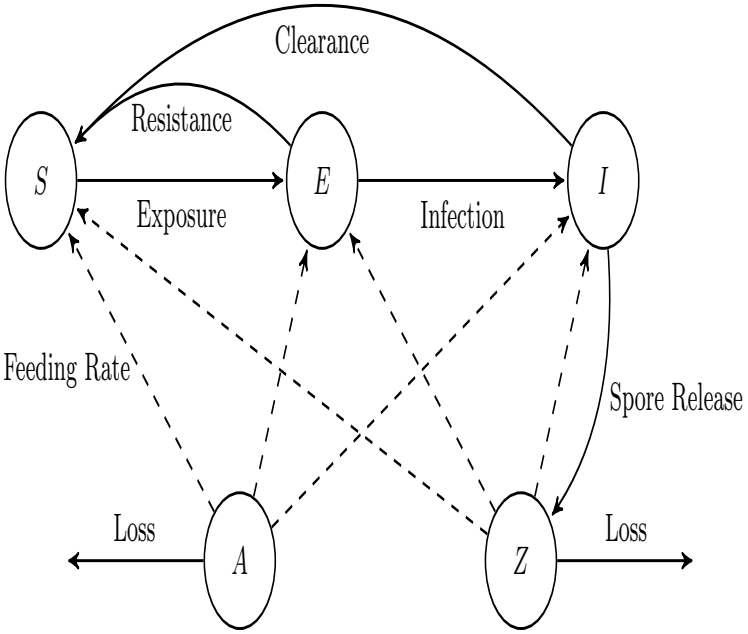

Figure 1.5: Illustration of Susceptible-Exposed-Infected-Spores-Algae (SEIZAS) model.

This inspired us to incorporate demographic stochasticity in our model, which has been shown to prevent the dampening of oscillations observed in deterministic models. By using a stochastic differential equation formulation, we capture two behaviors: sustained oscillations and extinction of the disease in Chapter 5. In Chapter 6, we incorporate clearance as a function of age since infection using a partial differential equation model. We show that clearance leads a reduction in secondary infections and disease prevalence. However, when compared with a model without clearance, its qualitative behavior does not change significantly. Finally, in Chapter 7 we provide an overarching summary of our findings and propose further directions of research.

Chapter 2

Short-term Evolution of Hosts

2.1 Introduction

When thinking about the processes that lead to biologically diverse populations, there has been evidence that changes at the individual level (e.g. genetic variation) and at the population level (e.g. introduction and persistence of new strategies or changes in the environment) exhibit very interesting feedback loops ([24], [62]). For example, changes in the size of populations and hence in the strength of the interaction among them can cause a change in the genotypes that are present [13]. We are interested in studying through different evolutionary frameworks the conditions in which these feedback loops result in changes in disease prevalence and duration of an epidemic. We will do so under two frameworks: Quantitative Genetics and Adaptive Dynamics. In this chapter, we will focus on using these methods to understand the short-term and long-term evolution of epidemiological relevant traits for our system: host susceptibility, virulence, predation, among others.

2.2 Quantitative Genetics Approach

Using Quantitative Genetic (QG) models we can study the evolution of a single trait due to genetic variation. These models are derived from the assumption that traits are determined by a large amount of genetic loci with small additive effects [1]. Thus, genetic variation is incorporated in these models by including the additive genetic variance of each trait of interest. This formulation allows us to model the mean change of a specific trait over time when mutations arise at a similar timescale as the ecology of a disease ([23], [66]). When evolutionary and ecological processes happen at similar timescales (e.g. within an epidemic season), it is often referred to as rapid evolution. We

can use the Quantitative Genetics approach to incorporate the genetic variation in the system and study short-term evolutionary dynamics. One advantage of this approach is that is allows us to couple the epidemiological and evolutionary processes with each other which can provide insights for experimental tests.

Susceptible-Infected (SI) Model

As a starting point, we consider a susceptible–infected (SI) model based on [41]. In this formulation, the susceptible class increases due to the births of both susceptible and infected individuals at a rate (b). However, infected individuals experience a lower fecundity due to the infection which we account with the parameter (ρ), for $0 < \rho < 1$. Births are controlled by incorporating a crowding parameter (c) which can be interpreted as the inverse to carrying capacity. Susceptible hosts die due to background mortality (d) and due to predation at a rate (p_S). Note that, the death rate of infected individuals is increased by v due to the infection (i.e virulence). Also, infected hosts are being preyed upon more intensely at a rate $\theta p_S > p_S$ due to selective predation arising from the fact that as spores reproduce within the host they become more opaque and thus more visible to predators. We can interpret θ as follows: if $\theta = 1$, implies no preference among host, and if, $\theta > 1$, predators prefer infected prey. The model then reads:

$$\frac{dS}{dt} = \overbrace{b(S+\rho I)(1-c(S+I))}^{\text{Births}} - \overbrace{(d+p_S)S}^{\text{Death}} - \overbrace{\beta SI}^{\text{Transmission}} \tag{2.1}$$

$$\frac{dI}{dt} = \overbrace{\beta SI}^{\text{Transmission}} - \overbrace{(d+v+\theta p_S)I}^{\text{Death}} \tag{2.2}$$

We are interested in obtaining the equation for the evolution of the mean transmission rate (β) which quantifies host susceptibility to the infection. We follow the proposed general recipe provided in [37] based on Quantitative Genetics, using the dynamical system (2.1)–(2.2) as an example. Assuming that transmission, β, is the only phenotype of the host of interest, we can formulate the following epidemiological model,

$$\frac{dS}{dt} = f[S, I; \vec{p}(\beta)], \tag{2.3}$$

$$\frac{dI}{dt} = r[S; \vec{p}(\beta)]I, \tag{2.4}$$

where S and I are the density of susceptible and infected host, $\vec{p}$ is a vector of all parameters in the model (some which could depend on β), f and r are the vectors of the expression for the dynamics the susceptible and infected class, respectively. The coupled evolutionary-ecological-epidemiological dynamics will be given by deriving an equation that describes the changes in host susceptibility over time. A formulation to obtain the mean change of the host susceptibility over one generation will be given by ([1], [2]),

$$\Delta\beta^* = \frac{(V_a/V_t)\int(\beta-\beta^*)W(\beta,\beta^*)P(\beta,\beta^*)d\beta}{\overline{W}}, \tag{2.5}$$

where V_a and V_t account for the additive and total phenotype variance, W is the individual fitness, P denotes the probability density of trait values β in a population with mean trait β^* and $\overline{W}$ represents the mean fitness of the population. The additive variance V_a captures the deviation from the mean phenotype due to inheritance between related allele's and their effect on the phenotype. The total phenotype variance V_t captures the additive effect of the total genetic and environmental variation. We can rewrite W by approximating the fitness function by its Taylor series about $\beta = \beta^*$.

$$W(\beta,\beta^*) = W(\beta^*,\beta^*) + (\beta-\beta^*)\frac{\partial W}{\partial\beta}\bigg|_{\beta=\beta^*} + \frac{1}{2}(\beta-\beta^*)^2\frac{\partial^2 W}{\partial\beta^2}\bigg|_{\beta=\beta^*} + \frac{1}{6}(\beta-\beta^*)^3\frac{\partial^3 W}{\partial\beta^3}\bigg|_{\beta=\beta^*} + ...$$

Under the assumption that β has a symmetric (usually normal) distribution function, all terms proportional to odd powers of $(\beta-\beta^*)$ of the integral expansion of become zero, and thus we are left with,

$$\begin{aligned}
\Delta\beta^* &= \frac{V_a}{V_t\overline{W}}\int\left[(\beta-\beta^*)W(\beta^*,\beta^*) + (\beta-\beta^*)^2\frac{\partial W}{\partial\beta}\bigg|_{\beta=\beta^*} + ...\right]P(\beta,\beta^*)d\beta, \\
&= \frac{V_a}{V_t\overline{W}}\int\left[(\beta-\beta^*)^2\frac{\partial W}{\partial\beta}\bigg|_{\beta=\beta^*} + ...\right]P(\beta,\beta^*)d\beta \\
&\approx \left(\frac{V_a}{V_t\overline{W}}\right)\left(V_t\frac{\partial W}{\partial\beta}\bigg|_{\beta=\beta^*}\right)
\end{aligned}$$

Clonal reproduction is an important aspect in the analysis of phenotypic plasticity, meaning the ability of one genotype to produce more than one phenotype when exposed to different envi-

ronments. With *Daphnia* , it is possible to identify phenotypes that can affect ecological dynamics through rapid evolution and the genotypes that underlie them [70]. Since *Daphnia* are clonal organisms, they are a model system of study and we can interpret the additive genetic variance (V_a) as the variance among clones which we denote by (V_c).

$$\Delta\beta^* = \left(\frac{V_a}{\overline{W}}\right)\left(\frac{\partial W}{\partial \beta}\Big|_{\beta=\beta^*}\right) = \left(\frac{V_c}{\overline{W}}\right)\left(\frac{\partial W}{\partial \beta}\Big|_{\beta=\beta^*}\right) \tag{2.6}$$

We can define the fitness W of individuals with a particular trait value as the instantaneous reproductive rate minus instantaneous death rate of individuals with that trait value [2]. Let $N = S+I$ denote the total population and suppose as in ([42], [45]) that the fitness W is maximized when the growth rate of susceptible individuals is maximized, namely,

$$W(\beta) = \frac{f(S,I;\beta)}{N} = \frac{b(S+\rho I)(1-c(S+I)) - (d+p_S)S - \beta SI}{N}$$

and that mean fitness will be given by $\overline{W(\beta)} = S/N$. Thus, the equation for the mean change in host susceptibility will be then given by,

$$\frac{d\beta}{dt} = -V_c I \tag{2.7}$$

Equation (2.7) tells us that transmission is a decreasing function over time and it decreases proportionally to the ratio of infected to susceptible hosts which is the same as the expression found derived by (Duffy and Sivars-Becker, 2007) ([45],[41]). However, to make this formulation biologically feasible β should always be positive or greater than zero ($\beta \geq 0$). Thus, as β decreases the clonal variation must decrease as well. In particular, we can assume that the variance is proportional to host susceptibility, $V(\beta) = V_c\beta$ [42]. The full formulation for the dynamical systems is then given by,

$$\frac{dS}{dt} = \overbrace{b(S+\rho I)(1-c(S+I))}^{\text{Births}} - \overbrace{(d+p_S)S}^{\text{Death}} - \overbrace{\beta SI}^{\text{Transmission}} \tag{2.8}$$

$$\frac{dI}{dt} = \overbrace{\beta SI}^{\text{Transmission}} - \overbrace{(d+v+\theta p_S)I}^{\text{Death}} \tag{2.9}$$

$$\frac{d\beta}{dt} = -V_c\beta I \tag{2.10}$$

Thus, the rate of host susceptibility depends on the density of infected host and mean host susceptibility. Host susceptibility evolves more rapidly as the number of infected increases.

2.3 Numerical Results

To analyze the effect of short-term evolution in host susceptibility, we performed numerical simulations. We see from Figure 2.1 that as the clonal variability increases prevalence decreases over time. In addition, the length of the epidemic decreases leading to a termination of the epidemic. These results indicate that variation in host susceptibility (i.e our transmission rate β) has important implication on the outcome of an epidemic and may lead to it's termination.

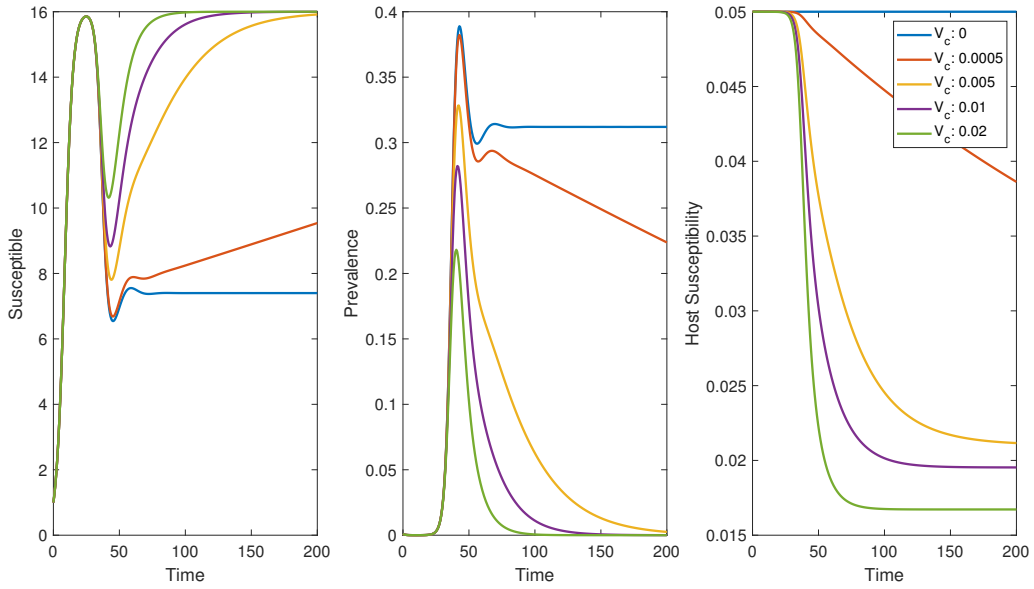

Figure 2.1: Populations densities for different levels of clonal variance (V_c).

These results illustrate that variability among hosts can result in a reduction in both epidemic duration and amount of infections due to short-term evolution of host susceptibility. This provides evidence how coupling ecological and evolutionary dynamics alter the observed behavior in our system. Mainly, as clonal variability among host increases we see a transition from an endemic to a disease-free state. In particular, as V_c increases, the mean host susceptibility decreases until it stabilizes at a fixed value corresponding to the absence of infected individuals. Also, the duration of the epidemic is reduced for higher values of clonal variation. While in all cases peak prevalence is

achieved in 40 days, the termination of the epidemic ranges from 100 to 150 days for higher values of clonal variation (i.e. $V_c \in \{0.01, 0.02\}$). Peak prevalence which was around 30% when there was no variation ($V_c = 0$), is reduced to approximately 23%.

Host susceptibility and virulence trade-off

Our model formulation assumes that other parameters in our model do not depend on host susceptibility (β) and this is the only parameter that experiences genetic variation. There is evidence that trade-offs can exist among traits and these can play a role in the spread of disease. Thus, instead of focusing on the mean change in host susceptibility as in equation (2.10), we will derive an expression for the mean change in virulence v. This will account for indirect effects of changes in virulence on host susceptibility. One of the most well studied one is the virulence-transmission trade-off in which the pathogen incurs in a cost when it increases transmission. Some of the common trade-offs assumed in the literature ([21], [73], [76], [81]) include: $\beta(v) = Cv^a, \beta(v) = \frac{Cv}{v+a} + B, \beta(v) = \frac{1}{A + Be^{-Cv}}$ and $\beta(v) = \frac{Cv}{v+a}\left(1 - Ke^{-\frac{(v-\tilde{v})^2}{\sigma^2}}\right)$. A common assumption is that transmission increases with virulence at an decelerating rate (i.e. $\beta'(v) > 0$ and $\beta''(v) < 0$). One could then consider how the evolution of virulence might affect our results. Suppose that the trade-off between virulence and host susceptibility is given by $\beta(v) = \frac{Cv}{(v+a)}$. We can find values for C and a by fitting this curve to two points, (0,0) and (0.05, 0.06).

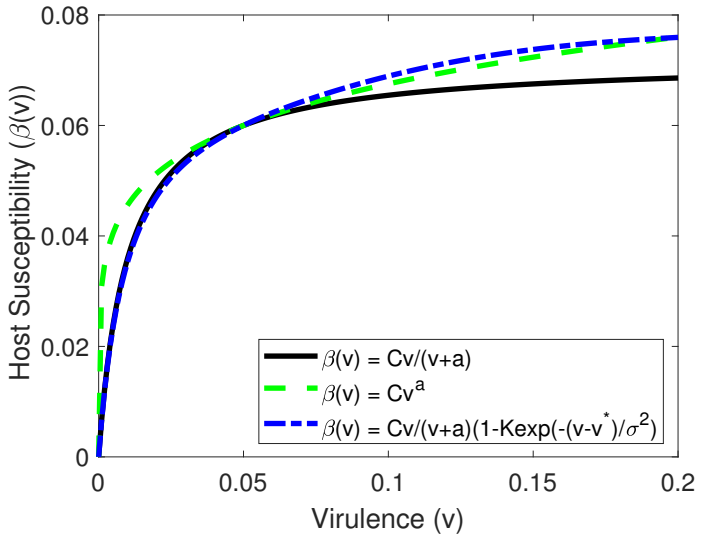

Figure 2.2: Examples of different trade-offs among host susceptibility and virulence.

Changes in parasite virulence affects can also affect other sources of host mortality and lead to more complicated interactions [34]. For example, if higher virulence leads to increased risk of predation then the parasite could evolve to decreased levels of virulence [33], evolutionary branching of the host [72], and even evolutionary cycles of virulence [61]. Since *Daphnia* experience selective predation we are interested in understanding how this affects the dynamics of our system. We can derive an equation for the mean change in virulence, by

$$\Delta v^* = \left(\frac{g}{\overline{W}}\right)\left(\frac{\partial W}{\partial v}\bigg|_{v=v^*}\right) \tag{2.11}$$

where g represents the genetic variance in virulence. Parasite fitness is maximized when the growth rate of infected individuals is maximized,

$$W(v) = \frac{\beta(v)SI - (d + v + \theta p_S)I}{N}, \text{ and that mean fitness will be given by } \overline{W(v)} = I/N$$

Hence, the equation for the mean change in virulence will by given by,

$$\frac{dv}{dt} = g\left(S\frac{d\beta}{dv} - p_S\frac{d\theta}{dv} - 1\right) \tag{2.12}$$

Thus, the full formulation for the dynamical systems is then given by,

$$\begin{aligned}
\frac{dS}{dt} &= \overbrace{b(S+\rho I)(1-c(S+I))}^{\text{Births}} - \overbrace{(d+p_S)S}^{\text{Death}} - \overbrace{\beta SI}^{\text{Transmission}} \\
\frac{dI}{dt} &= \overbrace{\beta SI}^{\text{Transmission}} - \overbrace{(d+v+\theta p_S)I}^{\text{Death}} \\
\frac{dv}{dt} &= g\left(S\frac{d\beta}{dv} - p_S\frac{d\theta}{dv} - 1\right)
\end{aligned} \tag{2.13}$$

First, we study the case where θ is constant. From the model (2.13), we can compute the equilibrium value for virulence by,

$$\frac{dv}{dt} = g\left(S\frac{d\beta}{dv} - 1\right) = 0 \Rightarrow \frac{d\beta}{dv} = \frac{1}{S^*}$$

In this case, we see that g does not play a role in determining the equilibrium value for virulence

since it does not depend on virulence itself. However, this doesn't lead to significantly different qualitative results. By solving for v, in the equation above, we obtain that, $v^* = \sqrt{ad + a\theta p_S} = 0.05664$ for $\beta(v) = Cv/(v + a)$, and $v^* = \dfrac{ad + a\theta p_S}{1 - a} = 0.0631$ for $\beta(v) = Cv^a$. To study the effect of letting θ be a function of virulence, we consider two trade-offs found in the literature: a linear [33] and a saturating function of virulence [61]. Linear and saturating functional responses for predators types have been analyzed for the *Daphnia* in [54] where predation is dependent on predator density, a prey handle time, and attack risk. Here we only account for predation through p_S and the predator selectivity parameter θ which we allow to depend on virulence v as seen in Figure 2.3.

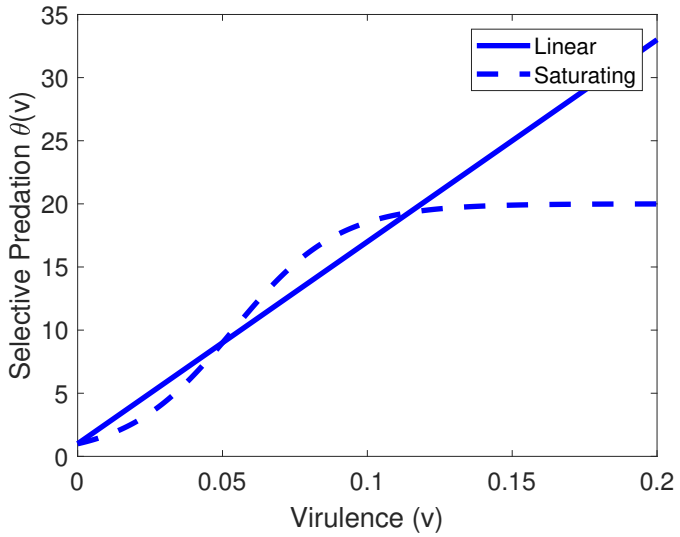

Figure 2.3: Selective predation parameter (θ) as a function of virulence (v).

In the first case, suppose $\theta(v) = \theta_0 + \theta_1 v$, where θ_0 is the baseline predation increase experienced by infected host, and θ_1 the rate at which it changes due to virulence. We fit this line across two data points, mainly $(0, 1)$ and $(0.05, 9)$. To obtain, $\theta(v) = 1 + 160v$. Secondly, suppose $\theta(v) = \dfrac{m}{e^{-lv} + n}$. As v goes to infinity $\theta(v)$ approaches the value m/n, and l allows us to control the shape of θ [61]. Ranges for θ ($1 \leq \theta \leq 20$) were chosen according to ([54], [77]), thus we take $m = 20n$ so that $\theta(v)$ saturates to the value 20. In both cases, considering the effect host susceptibility and predation selectivity as a function of virulence leads to virulence decreasing and disease prevalence increasing over time, as shown in Figure 2.4.

Using equation (2.12) we see that for the linear case virulence stabilizes at $v^* = \sqrt{\frac{a(d+\theta_0 p_S)}{1+\theta_1 p_S}} = 0.01176$. While we cannot solve for v^* explicitly for the saturating case we find that $v^* = 0.01337$ numerically. For $g = 0$, which corresponds to the case where there is no genetic variability, prevalence stabilizes at approximately 37%. When considering $\theta(v)$ as a saturating function of virulence, disease prevalence is increased from 70 % to 77% which is due to the fact virulence evolves to a slightly higher value over time. Thus, accounting for the mean change of virulence over time leads to roughly a 40% increase in disease prevalence.

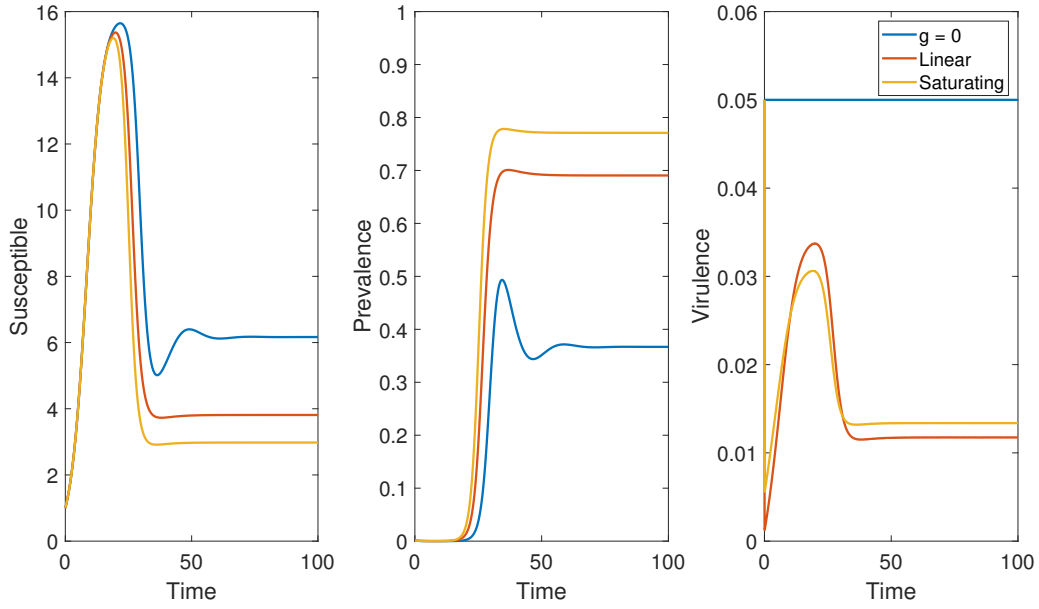

Figure 2.4: Populations densities for different levels of genetic variance g with $\beta(v) = \frac{Ca}{(v+a)}$. (a) Linear functional response, $\theta(v) = 1 + 160v$. (b) Saturating functional response, $\theta(v) = m/(\exp(-lv) + n)$, where $m = 20n, n = 0.0526, l = 54.89$.

2.4 Discussion–Future Directions

Using Quantitative Genetics, we have seen the effects of short-term evolution of host susceptibility and predation selectivity in *Daphnia* populations. In our model given by equations (2.8)–(2.10) genetic variability in host susceptibility leads to the early termination of an epidemic and lower values of peak disease prevalence. This is due to the fact that mean host susceptibility decreases over times as clonal variation increases which is also seen in the works of [45].

By assuming an explicit trade-off among both host susceptibility and virulence there was not a significant difference in the dynamics of our system. However, when both host susceptibility and our predation selectivity parameter were taken as a function of virulence, we observed that virulence evolves to a lower value and increases disease prevalence. Using a saturating trade-off for our selective predation parameter leads to higher prevalence. This suggests the shape chosen for the trade-off among traits leads to quantitative but not qualitative differences. Contrary to the previous model, which only considered the evolution of host susceptibility, the amount of genetic variance did not affect the results significantly.

A future direction would be to also consider trade-offs that account for within-host replication process and virulence. In his work (Day, 2002), provides evidence that virulence may evolve through host exploitation [36]. Mainly, when pathogens rely on the host to increase their spore production and the infected host's death to be transmitted this can lead to increased virulence. When within-host replication is taken into account new trade-offs can emerge for our system. Let ϵ denote the level of within-host replication, we can write a functional form for our parameters by: $v(\epsilon) = \epsilon$, $\beta(\epsilon) = 2(1 - \exp(-\xi\beta\epsilon))\exp(-\epsilon), \sigma(\epsilon) = (1 - \exp(-\xi\sigma\epsilon))$. In the next section, we incorporate the effects of long term evolution and how this may affect the interaction among competing hosts with different traits. In particular, we explore the effect long-term variability and potential effect of host susceptibility on other parameters in our model using an Adaptive Dynamics framework.

Chapter 3

Long-term Evolution of Hosts

3.1 Introduction

Another important approach to understanding the evolution of traits is Adaptive Dynamics (AD) ([50], [68]). In contrast to models based on Quantitative Genetics, one central assumption of this approach is that evolution happens at a slower timescale than ecological processes. This approach allows us to consider the long-term behaviour of a system in which a new individual enters a population that is at its equilibrium. In particular, it considers the situation when mutations are of small effect and happen rarely. This framework treats the host which has experienced mutations as an invader. By applying an invasion analysis, we can then predict the outcome of the interactions between a resident and mutant host. Will the resident or mutant population persist exclusively or is there a possibility that they will coexist? Based on evolutionary game-theory, evolutionary invasion analysis has become a widely used tool in evolutionary biology [58]. This theory has been used to understand a variety of biological problems such as the maintenance of genetic variation, co-evolutionary dynamics, diversification of species, among others ([39], [49], [60], [83]).

We will use the Adaptive Dynamics framework to derive an expression of the growth rate of a rare mutant which is introduced to a population composed of resident traits, which we call the invasion fitness function. In this context, the invasion fitness is defined as the growth rate of the rare mutant y in a population of x as $s(y, E_x)$. To distinguish this as the invasion fitness, where y is rare we can also denote it as $s_x(y)$ for shorthand. Our invasion fitness tells us how a rare individual with trait y grows in an environment determined by a population of traits x. In particular, we are interested in deriving mathematical conditions that determine the competitive outcomes between these two populations. To do this, we will analyze the properties of the invasion fitness function. Since $s_x(x) = 0$ by definition, the Taylor Expansion of $s_x(y)$ about $y = x$ is given by,

$$\begin{aligned} s_x(y) &\approx D_1(x)(y-x) + \frac{1}{2}D_2(x)(y-x)^2 + ..., \\ \text{where } D_1(x) &= \left.\frac{\partial s_x(y)}{\partial y}\right|_{y=x} \text{ and } D_2(x) = \left.\frac{\partial^2 s_x(y)}{\partial y^2}\right|_{y=x} \end{aligned} \tag{3.1}$$

A mutant trait y can successfully invade if $s_x(y) > 0$. Only mutants with $y > x$ or $y < x$ can invade so that $D_1(x)$ is non-zero and the direction that the population evolves is certain. Since we can define this invasion fitness for all pairs x and y, we can construct the fitness landscape, which is a 3-D plot of x, y, and $s_x(y)$. On this landscape we can follow the evolution of the population. In particular, we know that the population will move through the trait space according to the fitness landscape until we have a point where $D_1(x)$ is equal to zero.

Definition 3.1.1. We call x^* an **evolutionary singular strategy**, if $D_1(x) = \left[\frac{\partial s_x(y)}{\partial y}\right]_{y=x^*} = 0$.

The adaptive dynamics of the trait x will be determined by its fitness gradient $D_1(x)$.

$$\frac{dx}{dt} = mD_1(x) = \frac{1}{2}N\mu\sigma^2 D_1(x) \tag{3.2}$$

where the parameter m is related to the mutation processes (i.e. mutation rate μ and variance σ), the population size N which for now we assume to be constant, though it could also depend on the trait x ([28], [39]). Combining equations (3.1) and (3.2) we see that if $D_1(x) > 0$, then only mutants with $y > x$ can invade and there will be an increase in x. If $D_1(x) < 0$, then only mutants with $y < x$ can invade and there will be an decrease in x. However, we can't predict the evolution of this point using the fitness gradient $D_1(x)$. Therefore, we need other conditions to help us classify the behavior of these points.

Any singularity can be categorized in one of eight types of singularities based on its second derivative [20]. Let x^* denote an evolutionary singular strategy and consider the Taylor expansion of the invasion fitness function about $y = x^*$. By definition $D_1(x^*) = 0$ and $s_{x^*}(x^*) = 0$; thus, our invasibility condition depends on the second derivative of $s_x(y)$.

$$s_x(y = x^*) \approx s_{x^*}(x^*) + D_1(x)(x^* - x) + \frac{1}{2}D_2(x)(x^* - x)^2 + ... = \frac{1}{2}D_2(x)(x^* - x)^2 + ...$$

When $D_2(x) > 0$ the invasion fitness function $s_x(y)$ has a local minimum with respect to y at the critical point (x^*, x^*); therefore x^* can be invaded by near by traits. On the other hand, when $D_2(x) < 0$, $s_x(y)$ has a local maximum with respect to y and x^* cannot be invaded by nearby traits. We summarize these conditions below,

$$s_x(y) > 0 \iff D_2(x) = \left[\frac{\partial^2 s_x(y)}{\partial y^2}\right]_{y=x=x^*} > 0 \iff x^* \text{ can be invaded} \tag{3.3}$$

$$s_x(y) < 0 \iff D_2(x) = \left[\frac{\partial^2 s_x(y)}{\partial y^2}\right]_{y=x=x^*} < 0 \iff x^* \text{ cannot be invaded} \tag{3.4}$$

However, it may be invaded by a distant mutant. Thus, another important question we must ask is, can x^* be achieved through the evolution of the trait? In some cases, the answer is no. Because, the population moves along the fitness gradient, we must have that $s_x(y) > 0$ for values of y closer to x^* than x (i.e. $|x^* - x| > |x^* - y|$) and conversely, $s_x(y) < 0$ for values of x closer to x^* than y (i.e. $|x^* - y| > |x^* - x|$). This occurs only if the derivative of the fitness gradient with respect to x is negative, namely,

$$\left.\frac{\partial D_1(x)}{\partial x}\right|_{y=x=x^*} = \left.\frac{\partial^2 s_x(y)}{\partial y^2}\right|_{y=x=x^*} + \left.\frac{\partial^2 s_x(y)}{\partial x \partial y}\right|_{y=x=x^*} < 0 \tag{3.5}$$

When a singularity is both evolutionary stable and convergence stable, meaning it satisfies equations (3.4) and (3.5), it represents a stable endpoint of evolution. This type of singularity is called a continuously stable strategy (CSS). We can have an evolutionary attractor or repellor, in which the trait evolves to or away from this singular point, respectively.

Definition 3.1.2. An evolutionary singular strategy (ess) is **convergence stable** if the population evolves towards x^* so that mutants are only invaded by the strategies close to x^*.

However, if a singularity is convergence stable but not evolutionary stable, meaning equation (3.5) holds but (3.4) fails, it leads to the evolution towards the singularity and the disruption of it into two different traits. This type of singularity is called evolutionary branching point.

Definition 3.1.3. An evolutionary singular strategy is a **branching point** if the population evolves towards x^* and around the critical point it is possible for both $s_y(x^*) > 0$ (x^* invasible by nearby mutants) and $s_{x^*}(x) > 0$ (x^* can invade nearby populations).

This last type of singularity could lead to an environment in which multiple traits coexist. We are interested in studying if evolutionary branching is possible in our system.

3.2 *Daphnia* in their role as hosts

It has been shown in the past that host may experience evolutionary branching through the evolution of different defense mechanisms. For example, hosts with different resistance and tolerance mechanisms are able to coexist ([15], [26]). In addition, there is evidence that the presence of a predator may lead to evolutionary branching of the host [72]. Thus, we study the role of these mechanisms on the long-term outcomes when only infected individuals experience mutations, when both susceptible and infected classes are affected by mutations, and finally, how are these previous results altered once we include resource acquisition.

To compare the effects of short-term and long-term evolution in our system, we expand on the SI model given by equations (2.1)–(2.2), previous susceptible-infected model given by introducing mutant susceptible and infected classes S_m and I_m when the resident population S, I have reached an equilibrium as in ([25], [26]).

Only Infected *Daphnia* Mutate

To find the invasion fitness of a mutant strain, we extend the previous model to include a resident, (S, I), and mutant host I_m of the infected class by considering,

$$\begin{aligned}
\frac{dS}{dt} &= b(S+\rho I))(1-c(S+I+I_m)) - (d+p_S)S - (\beta(v)I + \beta(v_m)I_m)S, \\
\frac{dI}{dt} &= \beta(v)SI - (d+v+\theta p_S)I, \\
\frac{dI_m}{dt} &= \beta(v_m)SI_m - (d+v_m+\theta p_S)I_m,
\end{aligned} \tag{3.6}$$

where $N = S+I+I_m$ denotes the total population. Following the work of [81], in which only infected individuals will experience mutations, we assume host susceptibility will depend on virulence. For our system, we obtain six equilibrium points. The trivial equilibrium in which all populations become extinct, $(0, 0, 0)$, the disease free equilibrium, where $I^* = I_m^* = 0$, we see that the susceptible class reaches $S_{df} = \dfrac{1}{c}(b-(d+p_S))$. If there are no longer any resident nor mutant infected host (i.e.

$I^* = 0$ or $I_m^* \neq 0$), we obtain, $(S^*, 0, I_m^*)$ and respectively $(S^*, I^*, 0)$ in which one host out-competes the other and we one remains in the system. Finally, our equilibrium point of interest is when all populations remain present (S^*, I^*, I_m^*).

One way to determine the invasion fitness function for our system is by performing a linear stability analysis. First, we compute the Jacobian matrix for our system. The elements of the jacobian matrix, $a_{i,j}$, (i.e. the term in the i^{th} row and j_{th} column of J) are the per capita effect of species j on the rate of increase of species i, with all other species at their equilibrium.

$$J = \begin{bmatrix} \frac{\partial S'}{\partial S} & \frac{\partial S'}{\partial I} & \frac{\partial S'}{\partial I_m} \\ \frac{\partial I'}{\partial S} & \frac{\partial I'}{\partial I} & \frac{\partial I'}{\partial I_m} \\ \frac{\partial I'_m}{\partial S} & \frac{\partial I'_m}{\partial I} & \frac{\partial I'_m}{\partial I_m} \end{bmatrix} = \begin{bmatrix} J_{\text{res}} & P \\ O & J_{\text{mut}} \end{bmatrix}$$

At the equilibrium where the resident populations is at it's equilibrium and no mutant is present, $(S^*, I^*, 0)$, the invasion fitness for the rare mutant will be determined by the sub-matrix J_{mut},

$$\begin{aligned} s_v(v_m) &= \beta(v_m)S^* - (d + v_m + \theta p_S) && (3.7) \\ &= \beta(v_m)\left[\frac{d + v + \theta p_S}{\beta(v)}\right] - (d + v_m + \theta p_S) && (3.8) \end{aligned}$$

Assuming the same trade-off among host susceptibility and virulence as in the previous section, $\beta(v) = Cv/(v + a)$, we can find the evolutionary stable strategy (ess) which makes equation (3.8) equal to zero.

$$\left.\frac{\partial s_v(v_m)}{\partial v_m}\right|_{v_m = v = v^*} = \beta'(v^*)\left[\frac{d + v^* + \theta p_S}{\beta(v^*)}\right] - 1 = 0 \qquad (3.9)$$

Hence, $v^* = (ad + \theta p_S)/(a - 1)$. which for our parameter values is equal to $v^* = 0.0566$ which is not that different to our default value for virulence. This suggests that for an invader to survive in the system under our chosen trade-off it must evolve to have a similar virulence as the resident strain.

Susceptible and Infected *Daphnia* Mutate

Similarly, we can extend the previous model to incorporate the assumption that both susceptible and infected host experience mutations as follows,

$$\begin{aligned}
\frac{dS}{dt} &= b(S+\rho I)(1-cN) - (d+p_S)S - \beta S(I+I_m), && (3.10)\\
\frac{dI}{dt} &= \beta S(I+I_m) - (d+v+\theta p_S)I, && (3.11)\\
\frac{dS_m}{dt} &= b_m(S_m+\rho_m I_m)(1-c_m N) - (d+p_S)S_m - \beta_m S_m(I+I_m), && (3.12)\\
\frac{dI_m}{dt} &= \beta_m S_m(I+I_m) - (d+v_m+\theta_m p_S)I_m, && (3.13)
\end{aligned}$$

where $N = S + I + S_m + I_m$ denotes the total population. This is following [25] in which infection of either strain is related to the combined density of the infected. Here b denotes the maximal birth rate from both susceptible (S) and infected class (I), however we assume infected individuals suffer from a lower fecundity rate which we account by (ρ), and that births will be density dependent through consumption of resources (c). The susceptible class is reduced due to the background mortality rate (d) and predation rate (p_S). Individuals will become infected with host susceptibility (β), which we allow to depend on the disease induced mortality (v).

The system (3.10)–(3.13) has six equilibrium points. The trivial equilibrium point $(0,0,0,0)$ where both host classes become extinct is obtained by inspection. When there are no infected individuals present (i.e. $I = I_m = 0$) then the disease-free equilibrium points are given by $(S_{df},0,0,0)$ and $(0,0,S_{df}^{(m)},0)$ where $S_{df} = \dfrac{b-(d+p_S)}{cb}$ and $S_{df}^{(m)} = \dfrac{b_m-(d+p_S)}{c_m b_m}$. Other equilibrium points correspond to a single infected strain, namely, $(S^*,I^*,0,0)$ and $(0,0,S_m^*,I_m^*)$. Finally, we obtain the endemic equilibrium (S^*,I^*,S_m^*,I_m^*). In this formulation, we do not specify a particular functional trade-off between transmission and other model parameters.

Invasion Fitness Function: SI model

The invasion fitness function of a mutant can be derived in a variety of ways. One may chose a biological argument that focuses on computing the average number of off-springs of the mutant or study the stability of the equilibrium in which the resident population is at it's steady state. In this section, we give the derivation of the invasion fitness function for our models using linear

stability analysis and verify this result by using a more biologically motivated analysis in Appendix A.3. The Jacobian matrix for this model is given by,

$$J = \begin{bmatrix} J_{\text{res}} & P \\ O & J_{\text{mut}} \end{bmatrix}$$

So, the invasion fitness for the rare mutant will be determined by the sub-matrix J_{mut} at the equilibrium point in which the resident population is at its steady state and the mutant is introduced (i.e. $(S^*, I^*, 0, 0)$),

$$J_{\text{mut}} = \begin{bmatrix} b_m(1 - c_m(S^* + I^*)) - (d + p_S) - \beta(v_m)I^* & b_m\rho_m(1 - c_m(S^* + I^*)) \\ \beta_m I^* & -(d + v_m + \theta_m p_S) \end{bmatrix}$$

has trace and determinant given by,

$$\text{trace}(J_{\text{mut}}) = b_m(1 - c_m(S^* + I^*)) - (d + p_S) - \beta_m I - (d + v_m + \theta p_{S_m}), \text{ and}$$
$$\det(J_{\text{mut}}) = (b_m(1-c_m(S^*+I^*))-(d+p_{S_m})-\beta_m I^*)(-(d+v_m+\theta_m p_{S_m}))-b\rho_m\beta_m(1-c_m(S^*+I^*))I^*$$

If $\det(J_{\text{mut}}) > 0$ we notice that $\text{trace}(J_{\text{mut}}) < 0$ so a sufficient condition for stability is given by $\det(J_{\text{mut}}) > 0$. After some algebraic manipulations that the fitness function is given by,

$$s(\vec{p}, \vec{p}_m) = b_m(1-c_m N_r^*)-(d+p_S)+\frac{\beta_m I^*}{(d + v_m + \theta_m p_S)}(b_m\rho_m(1-c_m N_r^*)-(d+v_m+\theta_m p_S)) \quad (3.14)$$

This expression allows us to identify key parameters that could determine the competitive outcome of the resistant versus mutant host traits. We can obtain by symmetry the invasion fitness function for the resident host,

$$s(\vec{p}_m, \vec{p}) = b(1 - cN_m) - (d + p_S) + \frac{\beta I_m^*}{(d + v + \theta p_S)}(b\rho(1 - cN_m) - (d + v + \theta p_S)) \quad (3.15)$$

Here N_r^* and N_m^* denote the total resident and invader population, respectively. Both the resident and mutant host are able to coexist if $s_{\vec{p}}(\vec{p_m}) > 0$ and $s_{\vec{p_m}}(\vec{p}) > 0$. Note that the outcome of evolutionary models under this framework rely on the assumption of the existence of a trade-off and it's shape. These boundaries will be connected by the trade-off function.

Numerical Results

One can visually analyze the outcomes of an invasion by using techniques such as trade-off invasion plot (TIP). On a TIP, we obtain boundaries that indicate for which trait combinations the resident trait can be invaded by a rare mutant trait, and reciprocally, when can a mutant strain be invaded by a resident trait. To visualize these invasibility conditions, we use the fitness functions and determine when the fitness of the resident trait is zero (i.e $s_x(y) = 0$) and the fitness of the mutant strain is zero (i.e. $s_y(x) = 0$), respectively since a successful invasion will be achieved if the value of $s_x(y) > 0$ and $s_y(x) < 0$ or, $s_x(y) < 0$ and $s_y(x) > 0$.

Using equations (3.14) and (3.15), we can obtain parameter regions where that capture the different outcomes of competing between the resident and mutant host [27]. In Figure 3.1, we compare how changes in host susceptibility (β) and other parameters related to infection that can lead to coexistence of our populations. Mainly, we are see that host susceptibility in relation with fecundity reduction (ρ), virulence (v), predator selectivity (θ) could potentially lead to coexistence. The biggest coexistence region is given by a relationship between virulence and host susceptibility. Host are able to coexist for higher values of virulence and lower values of host susceptibility.

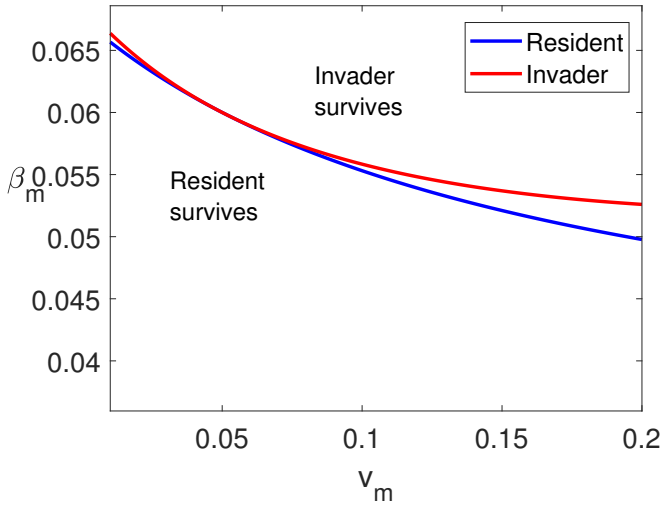

(a) Host Susceptibility vs. Virulence.

Figure 3.1: Trade-off invasibility plot (TIP) for host susceptibility β_m versus (a) virulence v_m and (b) fecundity reduction ρ_m (c) predator selectivity θ_m. Default values are $(v_m, \beta_m) = (0.05, 0.06)$, $(\rho_m, \beta_m) = (0.75, 0.06)$, $(\theta_m, \beta_m) = (9, 0.06)$. The blue and red curves denote the fitness boundary for the resident and mutant host, respectively. Coexistence regions correspond to the areas between the two curves.

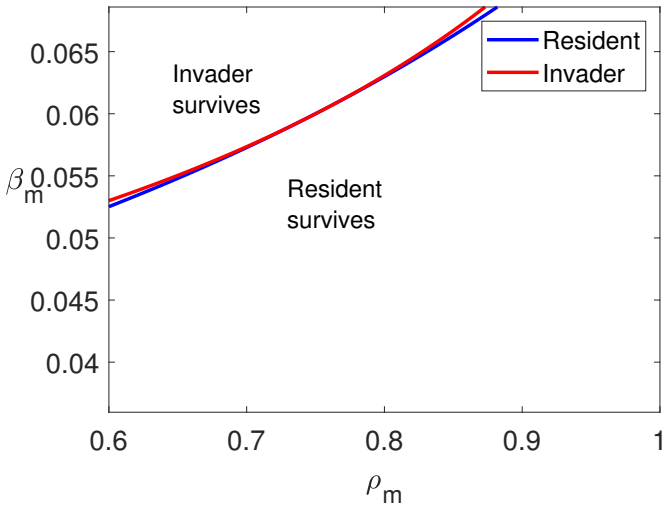

(b) Host Susceptibility vs. Fecundity Reduction.

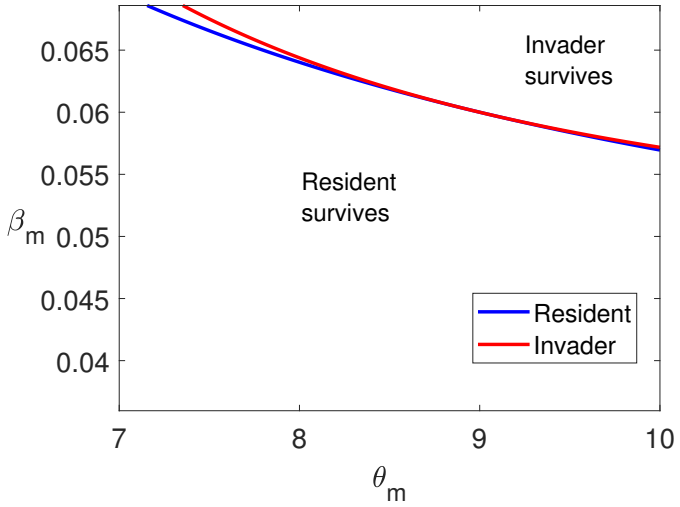

(c) Host Susceptibility vs. Predator Selectivity.

Figure 3.1: (cont.) Trade-off invasibility plot (TIP) for host susceptibility β_m versus (a) virulence v_m and (b) fecundity reduction ρ_m (c) predator selectivity θ_m. Default values are $(v_m, \beta_m) = (0.05, 0.06)$, $(\rho_m, \beta_m) = (0.75, 0.06)$, $(\theta_m, \beta_m) = (9, 0.06)$. The blue and red curves denote the fitness boundary for the resident and mutant host, respectively. Coexistence regions correspond to the areas between the two curves.

Geometrical Tools

When a functional trade-off among traits can be established another visual way to see the outcome of an series of invasions is using a Pairwise-Invisibility plot (PIP) [28]. These plots show, for each resident trait value x all the values of y for which the fitness function $s_y(x)$ described

above is positive and its intersection with the 45°line $x = y$ will give us the singular points in which the selection gradient vanishes. This allows us to classify points in which different evolutionary behaviours can be observed. We see an geometrical example of these classifications in Figure 3.2.

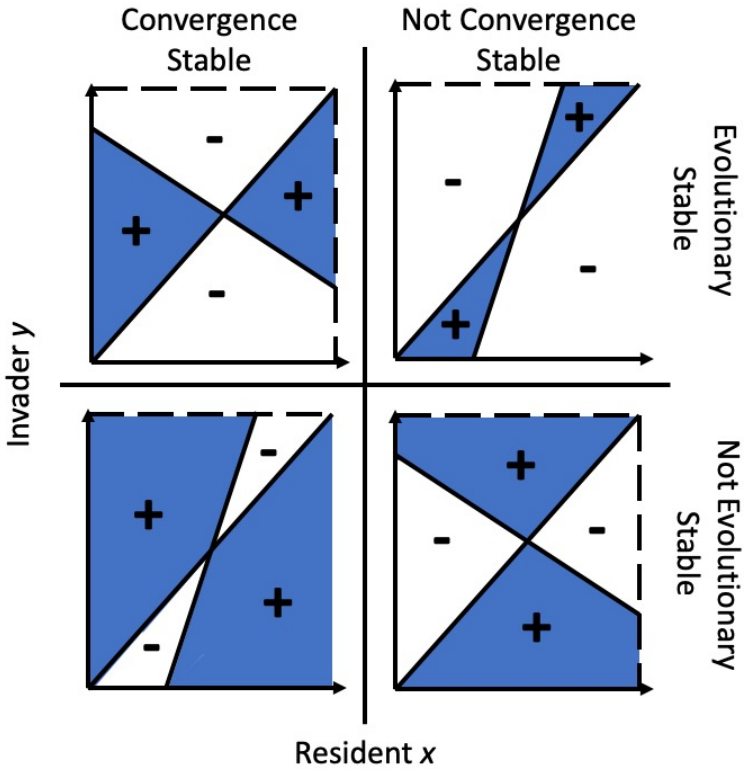

Figure 3.2: Example of Pairwise-Invisibility Plots based on [28].

As discussed in ([20], [50], [28]), we can use a PIP plot to classify the behavior of singular points, as follows:

(a) If a vertical line through the evolutionary singular points lies entirely in the positive region, the singular point is uninvasible.

(b) If a horizontal line through the point lies entirely in the positive regions, the singular point can invade when rare.

(c) If the line perpendicular to $y = x$ lies in positive regions, the singular point leads to coexistence. Overlapping positive regions obtained by reflecting the image along the line $y = x$ determines which traits coexist.

(d) If the positive region lies above the line $y = x$ for values left of the singular point and below the region for values right of the point, then the point is convergence stable.

Therefore, Figure 3.3a indicates that host susceptibility evolves until an optimal fitness and there is no selective disruption for this trade-off in the case where only infected individuals mutate. Figure 3.3b illustrate that v^* is uninvasible but not convergence stable under our assumptions.

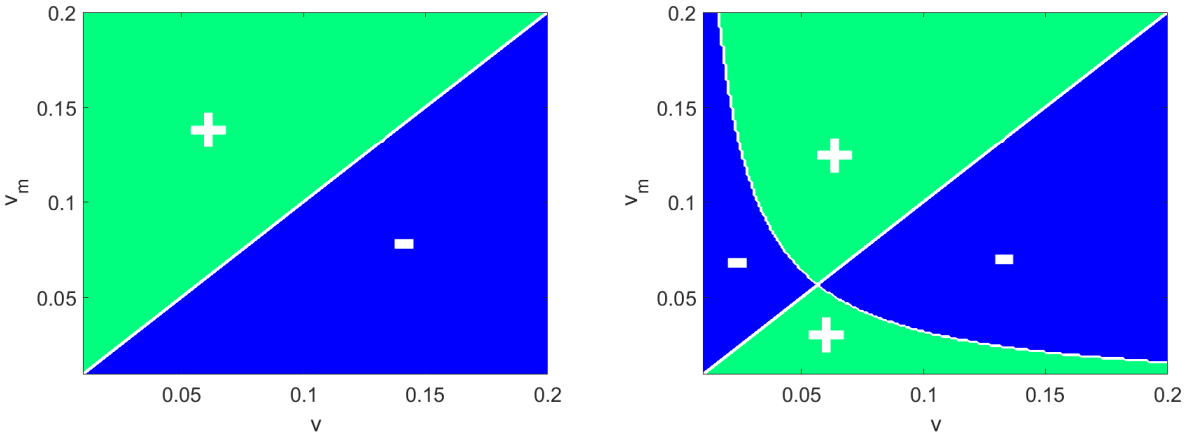

(a) Only infected *Daphnia* mutate.

(b) Susceptible and Infected *Daphnia* Mutate

Figure 3.3: Pairwise Invasibility Plot under various assumptions and $\beta(v) = \dfrac{Ca}{v + a}$.

3.3 *Daphnia* in their role as consumers

We extend the previous model by also considering the resources that *Daphnia* consume since host becomes infected by ingesting an the fungus *Metschnikowia bicuspidata*. There has been evidence that *Daphnia-dentifera* exhibit a trade-off between fecundity and resistance to *Metschnikowia biscupidata* that is driven by a variation in feeding rate [44]. In particular, slow feeders consume less fungal spores which acts as a resistance mechanism but leads to less energy to produce offspring. In addition, *Daphnia* species that are less susceptible to a parasite create a dilution effect that inhibits outbreaks in *Daphnia dentifera* ([30], [53], [70]). Thus, consumption of resources plays and important role in disease transmission.

Models which incorporate environmental transmission through free-living spores have been studied in the past ([21], [69]). Their work suggests that evolutionary branching is possible when considering different defense strategies or due to selective predation. However, their models do not

consider the effects other sources of resources may change the observed outcomes. To this end, we include two new populations classes mainly algae (A) and fungal spores (Z).

$$\frac{dS}{dt} = \overbrace{e_S f_S(A)(S+\rho I)}^{\text{Births}} - \overbrace{(d+p_S)S}^{\text{Deaths}} - \overbrace{\mu\frac{f_S(A)}{A}SZ}^{\text{Transmission}} \tag{3.16}$$

$$\frac{dI}{dt} = \overbrace{\mu\frac{f_S(A)}{A}SZ}^{\text{Transmission}} - \overbrace{(d+v+\theta p_S)I}^{\text{Increased mortality}} \tag{3.17}$$

$$\frac{dZ}{dt} = \overbrace{\sigma e_S f_S(A)(d+v)I}^{\text{Spore Release}} \overbrace{-\lambda Z}^{\text{Mortality}} - \overbrace{\frac{f_S(A)}{A}(S+I)Z}^{\text{Removal}} \tag{3.18}$$

$$\frac{dA}{dt} = \overbrace{r\left(1-\frac{A}{K}\right)A}^{\text{Logistic growth}} - \overbrace{f_S(A)(S+I)}^{\text{Algae Consumption}} \tag{3.19}$$

What we considered host susceptibility in our previous SI formulation, will be separated into different mechanisms that contribute to transmission. Susceptible individuals move into the infected class after being successfully infected by the parasite as governed by the transmission rate. The transmission rate, in turn, depends on host density S, the hosts feeding rate $f_S(A)$, the relative density of spores to algal resources Z/A, and the per spore infectivity μ. We assume that *Daphnia* are non-selective feeders, hence the spores experience the same risk of being eaten as the algae. Spore production (spore yield upon death of infected hosts) increases with host growth rate. We use a functional response to model the intake rate of a consumer as a function of food density (A). In the case of invertebrates such as *Daphnia* one can consider a Holling Type II given by,

$$f_S(A) = \frac{f_{S_0}A}{h_S + A},$$

where f_{S_0} denotes the maximal feeding rate and h_S denotes the half-saturation constant. In Figure 3.4, we see the behaviour of this function. In particular, for larger quantities of algae $f_S(A)$ approaches it's maximum value f_{S_0} and at the half-saturation constant is where half of the maximum intake is reached. This functional response gives us an idea on how much (f_{S_0}) and how fast (h_S) algae is consumed.

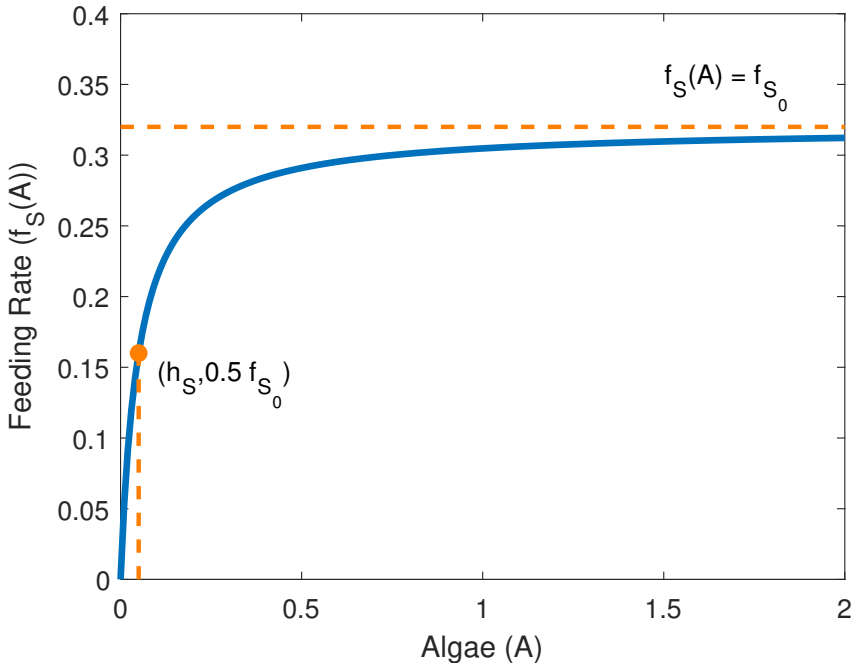

Figure 3.4: Illustration of the Holling Type II functional response for the feeding rate $f_S(A)$ for $f_{S_0} = 0.32$ and $h_S = 0.05$.

In this model, the birth rate depends on the feeding rate $f_S(A)$ and is proportional to the conversion efficiency e_S of the consumed algal resources into *Daphnia* biomass. Susceptible *Daphnia* die at a constant background rate d and are preyed upon at a constant rate p_S. But this mortality rate can vary among the host classes. Hence, spores (Z) are released in the water column at a rate proportional to the per capita yield of spores $\sigma(A) = \sigma e_S f_S(A)$ and the death rate of infected hosts $(d + v)I$. Spores are removed from the water column when consumed by *Daphnia* at a rate proportional to their feeding rate or by other causes (e.g., sinking, UV radiation) at a rate λ. Algae (A) grows logistically in the absence of any *Daphnia* at an intrinsic rate r and with carrying capacity K.

Similar to our susceptible-infected (SI) model, we can analyze the outcome of rare mutant host being introduced to the system, by expanding our previous model and considering the dynamics of the resident (S and I) and a mutant host (S_m and I_m) classes as follows,

$$
\begin{aligned}
\frac{dS}{dt} &= e_S f_S(A)(S+\rho I) - (d+p_S)S - \mu\frac{f_S(A)}{A}SZ \\
\frac{dS_m}{dt} &= e_S f_{S_m}(A)(S_m+\rho_m I_m) - (d+p_S)S_m - \mu_1\frac{f_{S_m}(A)}{A}S_m Z \\
\frac{dI}{dt} &= \mu\frac{f_S(A)}{A}SZ - (d+v+\theta p_S)I \\
\frac{dI_m}{dt} &= \mu_m\frac{f_{S_m}(A)}{A}S_m Z - (d+v_m+\theta_m p_S)I_m \\
\frac{dZ}{dt} &= e_S f_S(A)\sigma(d+v)I + e_S f_{S_m}(A)\sigma_m(d+v_m)I_m - \lambda Z \\
&- \frac{f_S(A)}{A}(S+I)Z - \frac{f_{S_m}(A)}{A}(S_m+I_m)Z \\
\frac{dA}{dt} &= r\left(1-\frac{A}{K}\right)A - f_S(A)(S+I) - f_{S_m}(A)(S_m+I_m)
\end{aligned}
\tag{3.20}
$$

There are seven possible equilibrium solutions to this system. $E_0 = (0,0,0,0,0,0)$, corresponds to the total extinction of our six populations, and $E_A = (0,0,0,0,0,K)$, corresponds to the survival of only the algae. The disease-free equilibrium, $E_S = (S^*,0,0,0,0,A^*)$ and $E_{S_m} = (0,S_m^*,0,0,0,A_m^*)$ corresponds to a single uninfected strain. In the absence of infection, the competition exclusion principle applies to our system. Suppose there are no spores present in the system, (i.e. $Z^* = 0$) this leads to no infected host being present (i.e. $I^* = I_m^* = 0$). It follows from equations (3.20) that,

$$e_S f_S(A) = (d+p_S) \text{ and } e_S f_{S_m}(A) = (d+p_S)$$

which implies that $f_S(A) = f_{S_m}(A)$. This leads to the coexistence of the single uninfected hosts E_S and E_{S_m}. If $S \neq 0$ this implies that $e_S f_S(A) = (d+p_S)$ which allows us to obtain,

$$A_C^* = \frac{h_S(d+p_S)}{e_S f_{S0} - (d+p_S)} \text{ and } S_C^* + S_{m,C}^* = \frac{r(1-A_C^*/K)A_C^*}{f_S(A_C^*)}$$

If the strains have different feeding rates, i.e. $f_S(A) \neq f_{S_m}(A)$ then either,

$$S^* = 0 \text{ and } S_m^* = \frac{r(1-A_m/K)A_m}{f_S(A_m)} \text{ or } S_m^* = 0 \text{ and } S^* = \frac{r(1-A/K)A}{f_S(A)}$$

implying that the host with the best feeding rate "wins". This simply illustrates what biologists

refer to as the competitive exclusion principle, which illustrates how species competing for the same limiting resource cannot coexist. As soon as one species has an advantage over the other, it will dominate in the long-term. Another equilibrium point corresponds to the survival of either the resident or mutant host (i.e.E_{SIZA} or $E_{S_mI_mZA}$). Finally, our last equilibrium point corresponds to the coexistence of the two strains, which we denote by $E = E_{SIZAS_mI_m} = (S^*, I^*, Z^*, A^*, S_m^*, I_m^*)$.

Invasion Fitness Function: SIZA Model

By taking the variables in the order S, I, Z, A, S_m, I_m. At the equilibrium $(S^*, I^*, Z^*, A^*, 0, 0)$, the Jacobian takes the following form,

$$J = \begin{pmatrix} J_{\text{res}} & P \\ O & J_{\text{mut}} \end{pmatrix}$$

Here J_{res} is a 4×4 matrix representing the stability of the resident population $SIZA$ in the absence of the mutant strain S_m, I_m (and therefore has negative eigenvalues since the resident only equilibrium is stable in the absence of the mutant). O represents a 4×2 matrix in which all elements are zero and therefore the 2×4 matrix P does not influence stability. Stability is therefore determined by the 2×2 matrix J_{mut} which is defined as follows.

$$J_{\text{mut}} = \begin{pmatrix} e_S f_{S_m}(A^*) - (d + p_S) - \mu_m \left(\frac{f_{S_m}(A^*)}{A^*}\right) Z^* & e_S f_{S_m}(A^*)\rho_m \\ \mu_m \left(\frac{f_{S_m}(A^*)}{A^*}\right) Z^* & -(d + v_m + \theta_m p_S) \end{pmatrix}$$

By computing the trace and determinant of the Jacobian matrix, we can derive the invasion fitness function,

$$\begin{aligned} \text{trace J} &= e_S f_{S_m}(A^*) - (d + p_S) - \mu_m \left(\frac{f_{S_m}(A^*)}{A^*}\right) Z^* - (d + v_m + p_S\theta_m), \\ \det \text{J} &= \left(e_S f_{S_m}(A^*) - (d + p_S) - \mu_m \left(\frac{f_{S_m}(A^*)}{A^*}\right) Z^*\right) \times \{-(d + v_m + \theta_m p_S)\} \\ &\quad - \left(\mu_m \left(\frac{f_{S_m}(A^*)}{A^*}\right) Z^*\right) \times \{e_S f_{S_m}(A^*)\rho_m\} \end{aligned}$$

Note that if det $J > 0$, then

$$e_S f_{S_m}(A^*) - (d + p_S) - \mu_m \left(\frac{f_{S_m}(A^*)}{A^*} \right) Z^* < 0$$

which implies that the trace of J is negative. Thus, the linear invasion stability is equivalent to the positivity of det J. If the determinant is positive it means that the equilibrium $(S^*, I^*, Z^*, A^*, 0, 0)$ is stable. If the determinant is negative, then the equilibrium is unstable and the mutant (S_m, I_m) can invade. After some algebraic manipulation, we obtain the following invasion criterion,

$$\begin{aligned} s_{\text{SIZA}}(\vec{p}, \vec{p}_m) &= e_S f_{S_m}(A^*) - (d + p_S) - \mu_m \left(\frac{f_{S_m}(A^*)}{A^*} \right) Z^* + \frac{e_S f_{S_m}(A^*) \rho_m}{d + v_m + \theta p_S} \times \mu_m \left(\frac{f_{S_m}(A^*)}{A^*} \right) Z^* \\ &= e_S f_{S_m}(A^*) - (d + p_S) - \mu_m \left(\frac{f_{S_m}(A^*)}{A^*} \right) Z^* \left(1 - \frac{e_S f_{S_m}(A^*) \rho_m}{d + v_m + \theta p_S} \right) > 0 \end{aligned} \tag{3.21}$$

which is identical to equation (A.3) as expected. Similarly, to the previous section we can obtain the invasion fitness function for the resident by symmetry,

$$s_{\text{SIZA}}(\vec{p}_m, \vec{p}) = e_S f_S(A_m^*) - (d + p_S) - \mu \left(\frac{f_S(A_m^*)}{A_m^*} \right) Z_m^* \left(1 - \frac{e_S f_S(A_m *) \rho}{d + v + \theta p_S} \right) > 0 \tag{3.22}$$

In the next section, we consider the outcomes of an invasion for different parameter regions. While we don't specify a particular trade-off we can get an idea of the invasion outcomes by plotting the parameter regions where we observe the resident or invader exclusively and the coexistence.

Numerical Results

We assume a fixed resident strain which corresponds to the default values of our model without the invader and a range of possible values for the invader. The resident strain is then paired up with each invader parameter and the invasion fitness function (3.21)–(3.22) are evaluated in each case. We obtain invisibility plots for but do not assume a specific trade-off among the traits. Figure 3.5 shows that as the invader's virulence increases the areas for coexistence increase for both the maximal feeding rate and half-saturation constant. However, these exhibit inverse relationships to virulence when the invasion fitness functions for the resident and invader are zero. In particular, the maximum feeding rate increases while the half-saturation constant decreases as a function

of virulence. This makes sense since the maximal feeding rate and half-saturation constant are inversely related in the definition of $f_S(A)$. In Figure 3.6, we consider a trade-off among the host's feeding rate (f_{S_0}, h_S) and per spore infectivity μ. We observe regions of coexistence are possible for lower values of per spore infectivity. However, similar to the previous figure, the maximal feeding rate and half-saturation constant exhibit an inverse relationship.

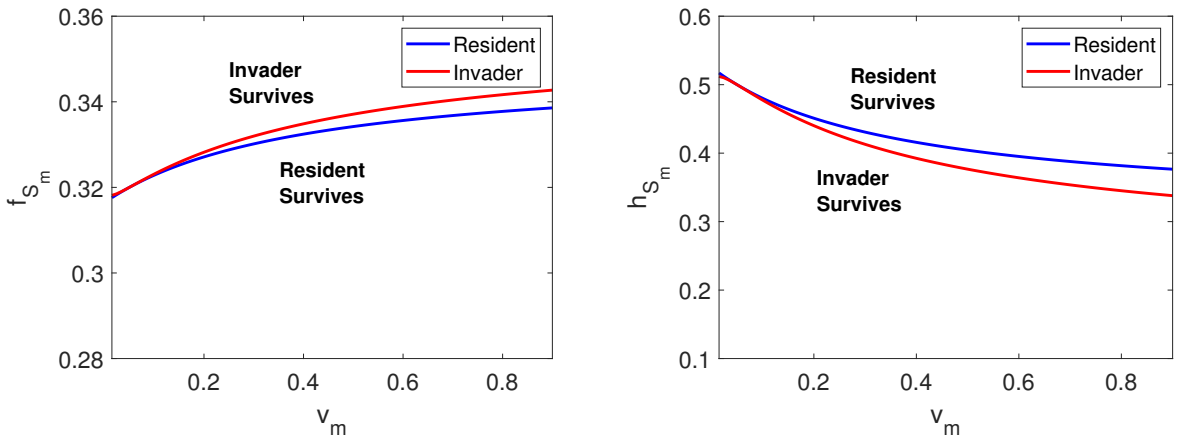

(a) (b)

Figure 3.5: Trade-off invasibility plot (TIP) parameters related to transmission and virulence. We compare the outcomes for different levels of virulence (v_m) versus (a) the maximal feeding rate (f_{S_m}), and (b) half-saturation constant (h_{S_m}). Default values are $(v_m, f_{S_m}) = (0.05, 0.32)$, $(v_m, h_{S_m}) = (0.05, 0.05)$, and $K = 2$.

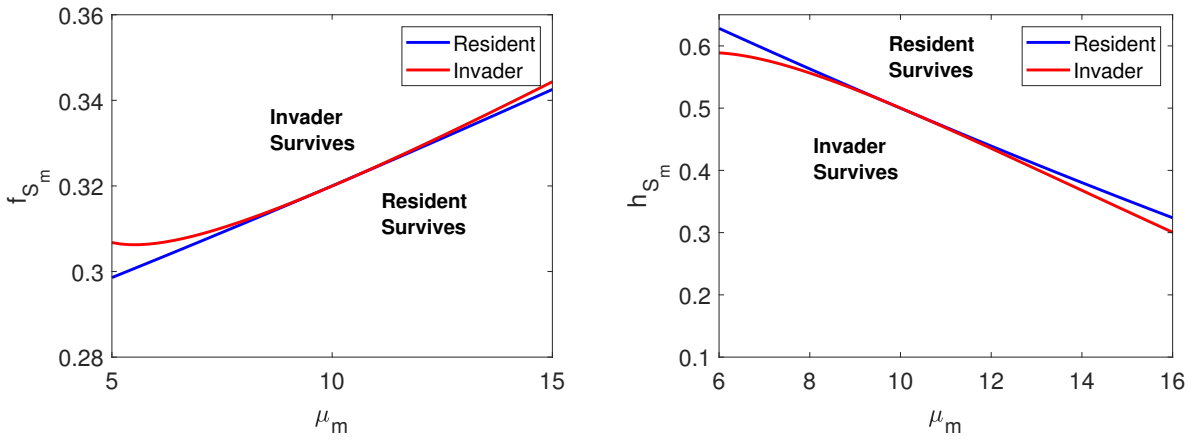

(a) (b)

Figure 3.6: Trade-off invasibility plot (TIP) parameters related to per spore infectivity. We compare the outcomes for different levels of infectivity (μ_m) versus (a) the maximal feeding rate (f_{S_m}), and (b) half-saturation constant (h_{S_m}). Default values are $(\mu_m, f_{S_m}) = (10, 0.32)$, $(\mu_m, h_{S_m}) = (10, 0.05)$, and $K = 2$.

3.4 Discussion–Future Directions

Under the Adaptive Dynamics framework we explored the effect of long-term mutations in our system. Using the expression for our invasion fitness function, obtained trade-off invisibility plots (TIPs) for a wide combination of parameter ranges. Previously, it has been suggested that *Daphnia* exhibit trade-offs among parasite transmission and birth rate in some lakes [9]. For our $SIZA$ model formulation, the birth rate of susceptible individuals depends on the conversion efficiency e_S, feeding rate $f_S(A)$. We did not find evidence of a trade-off among transmission and the conversion efficiency e_S. We found coexistence regions for trade-offs among virulence (v), per spore infectivity (μ), and feeding rate (f_{S_0}, h_S). Since births and transmissions are mediated through feeding, it is difficult to untangle the trade-off among parasite traits and these two events.

Chapter 4

Resistance and Clearance in *Daphnia* Epidemics

4.1 Introduction

Daphnia epidemics vary from pond to pond and year to year. We are interested in understanding transient dynamics that drive these changes. Until recent studies [79], recovery from an infection was thought impossible for *Daphnia* populations. This assumption has led researchers to largely ignore the within-host stages that encompass the process of infection. It has been shown that infections, which are caused by the ingestion of fungal spores from the parasite *Metschnikowia*, can be prevented due to physical structures of resistance in the host (i.e. a robust gut) and that only a subset of early infections lead to late infections indicating that an immune response to infection can lead to it's clearance [79]. To account for host resistance, we introduce an exposed class, which describes hosts that are under attack from fungal spores but are not infected yet. It has been shown for other disease models, such as those for the West Nile virus, that adding an exposed compartment leads to a reduction in the basic reproduction number ([12], [63], [84]). We will use an ordinary differential equation model, to incorporate these two new mechanisms of recovery: resistance and clearance; and, determine their effect on the basic reproduction number R_0 and disease prevalence.

SEIZA Model

To analyze the stages in which *Daphnia* progress through an infection, we divide the population into three compartments: susceptible S, exposed E, and infected I. We denote the fungal spores by Z and algea by A. We incorporate two new mechanisms for recovery: clearance c and resistance γ . Our system can be written as follows:

$$\frac{dS}{dt} = \overbrace{e_S f_S(A)\,(S+E+\rho I)}^{\text{Births}} - \overbrace{(d+p_S)S}^{\text{Deaths}} - \overbrace{\mu\frac{f_S(A)}{A}SZ}^{\text{Exposure}} + \overbrace{cI}^{\text{Clearance}} + \overbrace{\gamma E}^{\text{Resistance}} \tag{4.1}$$

$$\frac{dE}{dt} = \overbrace{\mu\frac{f_S(A)}{A}SZ}^{\text{Exposure}} - \overbrace{(d+p_S+\gamma+\alpha)E}^{\text{Loss of Exposed}}, \tag{4.2}$$

$$\frac{dI}{dt} = \overbrace{\alpha E}^{\text{Infection}} - \overbrace{(d+v+\theta p_S+c)I}^{\text{Loss of Infected}}, \tag{4.3}$$

$$\frac{dZ}{dt} = \overbrace{\sigma e_S\frac{f_S(A)}{A}(d+v)I}^{\text{Spore Release}} - \overbrace{\lambda Z}^{\text{Mortality}} - \overbrace{f_S(A)\,(S+E+I)\,\frac{Z}{A}}^{\text{Spore Consumption}} \tag{4.4}$$

$$\frac{dA}{dt} = \overbrace{r\left(1-\frac{A}{K}\right)A}^{\text{Logistic Growth}} - \overbrace{f_S(A)\,(S+E+I)}^{\text{Algae Consumption}}. \tag{4.5}$$

The susceptible class (4.1) increases due to births from susceptible, exposed, and infected hosts. However, the infected class experiences a reduced birth rate due to the infection which we denote by $0 \leq \rho < 1$. Births will depend on the feeding rate $f_S(A)$ and are proportional to the conversion efficiency e_S of the consumed algae into *Daphnia*. Susceptible individuals move into the exposed class at a rate dependent on the per spore infectivity μ, the feeding rate $f_S(A)$, the proportion of spores to algae resources $\frac{Z}{A}$, and density of susceptible. We use a functional response to model the intake rate of a consumer as a function of food density (A). In the case of invertebrates such as *Daphnia* one can consider a Holling Type II given by,

$$f_S(A) = \frac{f_{S_0}A}{h_S + A},$$

where f_{S_0} denotes the maximal feeding rate and h_S denotes the half-saturation constant. In particular, for larger quantities of algae $f_S(A)$ approaches it's maximum value f_{S_0} and at the half-saturation constant is where half of the maximum intake is reached.

The exposed class (4.2) is characterized by *Daphnia* that have consumed fungal spores but have a structural defense that prevents infection [79]. Individuals in the exposed compartment, can either transition to the susceptible class at a constant rate γ or move to the infected class at a rate α. Infected individuals may move to the susceptible class through clearance of the infection

at a constant rate c.

Susceptible and exposed individuals die at a background mortality rate d and are preyed upon at a rate p_S. Infected individuals experience a higher death rate due to infection v and increased predation at a rate θp_S where $\theta > 1$. As *Daphnia* become infected, they become more visible to predators and hence are preyed upon at a higher rate. Spores (4.4) which reproduce within infected hosts are released into the water column at a rate proportional to the spore yield $\sigma(A) = \sigma e_S \frac{f_S(A)}{A}$, where $\sigma(A)$ represents the spores per death infected *Daphnia*, and the death rate of infected hosts $(d+v)I$. This spore yield formulation is different from those assumed in the previous chapters and can be seen in Figure 4.1.

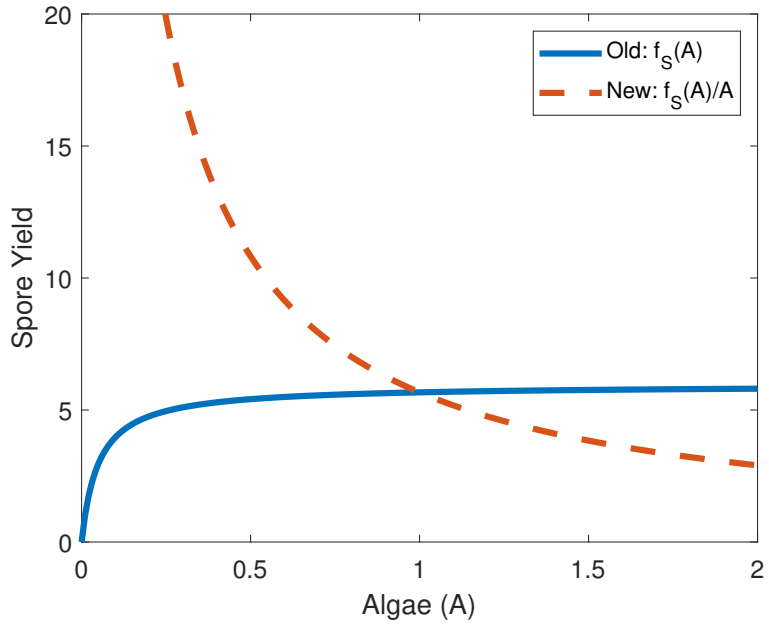

Figure 4.1: Spore yield formulations: $\sigma(A) = \sigma e_S f_S(A)$ (old) and $\sigma(A) = \sigma e_S \frac{f_S(A)}{A}$ (new).

Spores are removed from the water column by being consumed by *Daphnia* at a rate proportional to the feeding rate $f_S(A)$ and due to other causes at a rate λ. Finally, algae (4.5) grows logistically at a intrinsic rate r with carrying capacity K and decreases due to consumption by all host classes. In the model, our classes denote the density of hosts (i.e. $S(t), E(t)$, and $I(t)$), fungal spores $Z(t)$, and algae $A(t)$. To be biologically feasible each should always be positive or greater than zero. To guarantee our model preserves this biological intuition we show the following,

Lemma 4.1.1. *The subset* $\Omega = \{(S(t), E(t), I(t), Z(t), A(t)) | S(t) \geq 0\, E(t) \geq 0, I(t) \geq 0, Z(t) \geq$

$0, A(t) \geq 0\} \subset \mathcal{R}^5$ *is forward invariant for our system.*

Proof. If $S = 0$ we see from equation that (4.1), $\frac{dS}{dt} \geq 0$ for $(S, E, I, Z, A) \in \Omega$. Similarly, from equations (4.2)–(4.4), we obtain that $E = 0$, $I = 0$, and $Z = 0$ which implies that $\frac{dE}{dt} \geq 0$, $\frac{dI}{dt} \geq 0$, and $\frac{dZ}{dt} \geq 0$ for $(S, E, I, Z, A) \in \Omega$. Finally, if $A = 0$ we see from equation (4.5) that $\frac{dA}{dt} \geq 0$. □

Equilibrium points

To understand the possible long term behaviour of our system we compute it's equilibrium points. We see by inspection that the trivial equilibrium $E_0 = (0, 0, 0, 0, 0)$ and the algae only equilibrium $E_K = (0, 0, 0, 0, K)$ are admitted in our system. When there is no disease present (i.e. $E = I = Z = 0$) we obtain the disease-free equilibrium, $E_{df} = (S_{df}, 0, 0, 0, A_{df})$ where $A_{df} = \frac{(d+p_S)h_S}{e_S f_{S0} - (d+p_S)}$ and $S_{df} = \frac{e_S r\left(1 - \frac{A_{df}}{K}\right)A_{df}}{d+p_S}$. Finally, we obtain the endemic equilibrium where all our populations are present $E_e = (S^*, E^*, I^*, Z^*, A^*)$. For mathematical convenience let us define,

$$R(A) = \frac{\mu\alpha\sigma e_S \frac{f_S(A)}{A}(d+v)r(1-\frac{A}{K})}{(\lambda + r(1-\frac{A}{K}))(d+v+\theta p_S + c)(d+p_S+\gamma+\alpha)}$$

Then, we can write the endemic equilibrium densities as follows,

$$S^* = \frac{(\lambda + r(1-\frac{A^*}{K}))(d+v+\theta p_S+c)(d+p_S+\alpha+\gamma)}{\alpha\mu\sigma e_S(\frac{f_S(A^*)}{A^*})^2(d+v)} = \frac{r(1-\frac{A^*}{K})A^*}{R(A^*)f_S(A^*)} \tag{4.6}$$

$$Z^* = \frac{d+p_S+\gamma+\alpha}{\mu\frac{f_S(A^*)}{A^*}} \frac{e_S(f_S(A^*) - f_S(A_{df}))}{\left[(d+p_S+\alpha) - e_S f_S(A) - \frac{\alpha(e_S f_S(A^*)\rho + c)}{(d+v+\theta p_S+c)}\right]} \tag{4.7}$$

$$E^* = \frac{r(1-\frac{A^*}{K})A^*}{R(A^*)f_S(A^*)} \frac{e_S(f_S(A^*) - f_S(A_{df}))}{\left[(d+p_S+\alpha) - e_S f_S(A) - \frac{\alpha(e_S f_S(A^*)\rho + c)}{(d+v+\theta p_S+c)}\right]} \tag{4.8}$$

$$I^* = \frac{\alpha r(1-\frac{A^*}{K})A^*}{(d+v+\theta p_S+c)R(A^*)f_S(A^*)} \frac{e_S(f_S(A^*) - f_S(A_{df}))}{\left[(d+p_S+\alpha) - e_S f_S(A) - \frac{\alpha(e_S f_S(A^*)\rho + c)}{(d+v+\theta p_S+c)}\right]} \tag{4.9}$$

by using equation (4.5) we obtain a cubic polynomial in A^* which we can solve for A^* (see Appendix B). We are interested in how the equilibrium densities of our system depend on the carrying capacity K, resistance γ, and clearance c. In Figure 4.2, we see that for a carrying capacity $K < 1.0484 = A_{df}$, only algae remains in the system. This corresponds to the scenario in which resources are too low to sustain the host population. For intermediate values of K, the observe

the disease-free equilibrium in which only the susceptible host and algae are present. Finally, for higher resource availability we observe the endemic equilibrium in which all the populations are present in our system. Thus, as K increases, the parasite is able to better sustain itself since there are more susceptible hosts to infect.

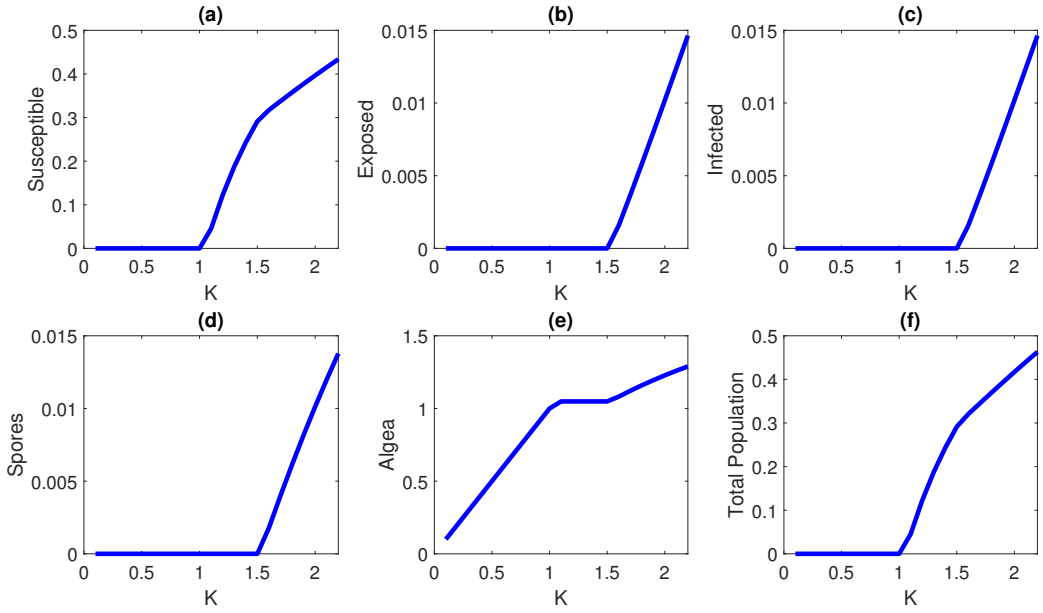

Figure 4.2: Equilibrium densities as a function of carrying capacity (K).

To compare how the equilibrium densities depend on resistance and clearance, we vary each parameter γ and c independently of each other over similar ranges while all other parameters remain fixed. Figure 4.3 shows that, as resistance increases, the density of susceptible hosts increases while the exposed, infected, and spore densities decrease. A similar behavior can be observed for increasing values of clearance; however, for high clearance rates ($c \geq 0.4$) we transition from the endemic to the disease-free equilibrium. This suggests that among our two mechanisms of recovery, clearance has a higher impact in controlling the infection than resistance.

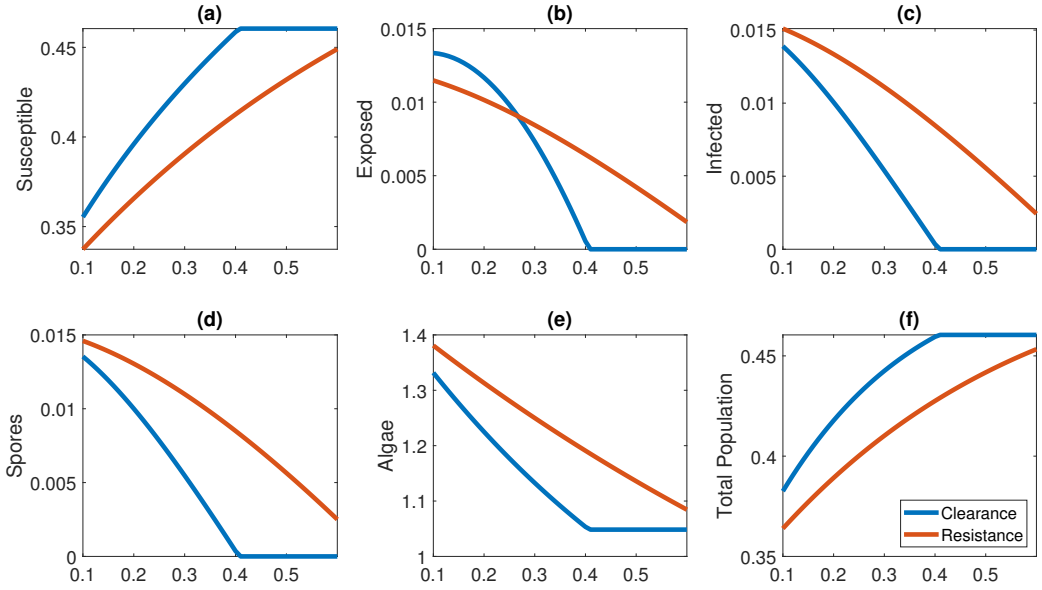

Figure 4.3: Equilibrium densities as a function of clearance (blue line) and $\gamma = 0$, and resistance (red line) and $c = 0$ where $0 \leq c, \gamma \leq 0.6$. All other parameters are fixed at their default values.

4.2 Basic Reproduction Number

The basic reproduction number R_0 is defined as the number of secondary infections produced when a single infected individual is introduced into a completely susceptible population. The expression for R_0 gives us a threshold condition for the parasite's persistence in the system. Using the next-generation approach, R_0 is computed as the spectral radius of the matrix FV^{-1}, denoted by $\rho(FV^{-1})$, where F is the transmission matrix describing the generation of secondary infections in the E, I, Z compartments, and V is the transition matrix describing how individuals move in/out of the E, I, Z compartments of our model ([38], [82]). It follows that,

$$F = \begin{bmatrix} 0 & 0 & \mu \frac{f_S(A_{df})}{A_{df}} S_{df} \\ 0 & 0 & 0 \\ 0 & 0 & 0 \end{bmatrix} \text{ and } V = \begin{bmatrix} d + p_S + \gamma + \alpha & 0 & 0 \\ -\alpha & d + v + \theta p_S + c & 0 \\ 0 & -\sigma e_S \frac{f_S(A_{df})}{A_{df}} (d + v) & \lambda + \frac{f_S(A_{df})}{A_{df}} S_{df} \end{bmatrix}$$

Thus, the basic reproduction number is given by,

$$R_0 = \rho(FV^{-1}) = \mu \frac{f_S(A_{df})}{A_{df}} S_{df} \frac{\alpha\sigma e_S f_S(A_{df})(d+v)}{A_{df}(\lambda + \frac{f_S(A_{df})}{A_{df}} S_{df})(d + p_S + \gamma + \alpha)(d + v + \theta p_S + c)} \tag{4.10}$$

To interpret (4.10) we see that R_0 is proportional to the exposure rate per infective spore propagule $\mu \frac{f_S(A_{df})}{A_{df}} S_{df}$, the rate of release of spores propagules per dead infected individual and infection rate $\alpha\sigma e_S \frac{f_S(A_{df})}{A_{df}}(d+v)$, the time individuals spend in the exposed and infected compartments respectively, $(d + p_S + \gamma + \alpha)^{-1}$ and $(d + v + \theta p_S + c)^{-1}$, and life span of spore propagules, $\left(\lambda + \frac{f_S(A_{df})}{A_{df}} S_{df}\right)$. In the following theorem, we show that R_0 provides a threshold such that when $R_0 < 1$, the disease dies out, and when $R_0 > 1$, the parasite persists in the system.

Theorem 4.2.1. *The disease-free equilibrium $E_{df} = (S_{df}, 0, 0, 0, A_{df})$ is locally asymptotically stable if $R_0 < 1$ and unstable if $R_0 > 1$.*

Proof. To analyze the stability of the disease-free equilibrium we compute the Jacobian matrix of our system (see Appendix B) and evaluate it at the disease-free equilibrium E_{df}. At the disease-free equilibrium, $E_{df} = (S_{df}, 0, 0, 0, A_{df})$ the eigenvalues of the Jacobian matrix satisfy,

$$(\Lambda^2 - \left[r\left(1 - 2A_{df}/K\right) - f'_S(A_{df})S_{df}\right]\Lambda + e_S S_{df} f'(A_{df}) f_S(A_{df}))g(\Lambda) = 0 \tag{4.11}$$

Let $c_1 = r\left(1 - 2A_{df}/K\right) - f'_S(A_{df})S_{df}$ and $c_0 = e_S S_{df} f'(A_{df}) f_S(A_{df}) > 0$, so that,

$$\Lambda^2 - c_1\Lambda + c_0 = 0 \iff \Lambda = \frac{c_1 \pm \sqrt{c_1^2 - 4c_0}}{2} \tag{4.12}$$

the two eigenvalues will be negative or have negative real part if $c_1 < 0$. After some algebraic manipulation it can be shown that, $c_1 < 0$ if and only if $K - h_S - 2A_{df} < 0$. The remaining eigenvalues satisfy the following cubic polynomial,

$$g(\Lambda) = \Lambda^3 + a_2\Lambda^2 + a_1\Lambda + a_0 = 0 \tag{4.13}$$

Using the Routh Hurtwitz stability criterion (see Appendix B), $g(\Lambda)$ has all roots in the open left half plane if and only if a_2, a_1, a_0 are positive and $a_2 a_1 > a_0$, where the coefficients of $g(\Lambda)$ are

given by,

$$\begin{aligned}
a_2 &= 2d + v + (\theta + 1)p_S + c + \gamma + \alpha + \lambda + \frac{f_S(A_{df})}{A_{df}} S_{df} > 0 \\
a_1 &= (d + v + \theta p_S + c)(d + p_S + \gamma + \alpha) + (2d + v + (\theta + 1)p_S + c + \gamma + \alpha) \left(\lambda + \frac{f_S(A_{df})}{A_{df}} S_{df} \right) > 0 \\
a_0 &= (d + v + \theta p_S + c)(d + p_S + \gamma + \alpha) \left(\lambda + \frac{f_S(A_{df})}{A_{df}} S_{df} \right) (1 - R_0)
\end{aligned}$$

We see that $a_0 > 0$ if and only if $R_0 < 1$. Finally, after some algebraic manipulations we obtain,

$$a_2 a_1 - a_0 = a_2(2d + v + (\theta + 1)p_S + c + \gamma + \alpha) \left(\lambda + \frac{f_S(A_{df})}{A_{df}} S_{df} \right) +$$
$$(d + v + \theta p_S + c)(d + p_S + \gamma + \alpha) \left(2d + v + (\theta + 1)p_S + c + \gamma + \alpha + R_0 \left(\lambda + \frac{f_S(A_{df})}{A_{df}} S_{df} \right) \right) > 0$$

Thus, the disease-free equilibrium is locally asymptotically stable if $R_0 < 1$ and unstable otherwise, as desired. □

In the next theorem, we ascertain the stability of the remaining equilibrium points of our system by using the standard linear stability analysis.

Theorem 4.2.2. *(i) The trivial equilibrium E_0 is a saddle for all parameter values. (ii) The algae only equilibrium E_K is linearly asymptotically stable for $K < A_{df}$ and a saddle otherwise. (iii) The equilibrium E_{df} is linearly asymptotically stable if $K - h_S - 2A_{df} < 0$ and $R_0 < 1$ (the parasite cannot invade).*

Proof. (i) It follows from the standard linear stability analysis, that at the trivial equilibrium $E_0 = (0, 0, 0, 0, 0)$, we have the Jacobian is a diagonal matrix with eigenvalues given by $\Lambda_1 = -(d + p_S) < 0, \Lambda_2 = -(d + p_S + \alpha + \gamma) < 0, \Lambda_3 = -(d + v + \theta p_S + c)/\alpha < 0, \Lambda_4 = -\lambda < 0$, and $\Lambda_5 = r > 0$, thus the trivial equilibrium is unstable. (ii) Similarly for E_K, the eigenvalues are given by, $\Lambda_1 = -\lambda < 0, \Lambda_2 = -r < 0, \Lambda_3 = -(d + v + \theta p_S + c) < 0, \Lambda_4 = -(d + p_S + \alpha + \gamma) < 0$, and $\Lambda_5 = e_S f_S(K) - (d + p_S)$. After some algebraic manipulation, we see that $\Lambda_5 < 0$ if and only if $K < A_{df}$. □

From these results we see that in general, E_0 is unstable for this type of consumer resource model. The equilibrium E_K, is only stable when there are not enough resources available to sustain

the host population, $K < A_{df}$. When $K = A_{df}$, the equilibrium E_K undergoes a transcritical bifurcation. It can be shown that A^* satisfies the following,

$$R(A^*) = 1+M(A^*)+\frac{\alpha M(A^*)}{(d+v+\theta p_S+c)}, \text{ where } M(A^*) = \frac{e_S(f_S(A^*)-f_S(A_{df}))}{\left[d+p_S+\alpha-e_S f_S(A^*)-\frac{\alpha(e_S f_S(A^*)\rho+c)}{(d+v+\theta p_S+c)}\right]}$$

When $A^* = A_{df}$ then $M(A^*) = 0$, $R(A^*) = R(A_{df}) = R_0 = 1$, and $S^* = S_{df}$. It follows from equation (4.8), that at $A^* = A_{df}$, $Z^* = 0$, which leads to $E^* = I^* = 0$. Thus, we transition from the endemic to the disease-free state. From equation (4.8), we see that for $Z^* > 0$ to be possible,

$$d+p_S+\alpha-e_S f_S(A^*) = \alpha+e_S(f_S(A_{df})-f_S(A^*)) > \frac{\alpha(e_S f_S(A^*)\rho+c)}{d+v+\theta p_S+c} \tag{4.14}$$

Condition (4.14) states that spores remain in the system as long as the net loss of exposed individuals is greater than the proportion of gains and loss of infected individuals. Notice that this condition does not depend on the resistance parameter γ. Which could explain why resistance reduces the spore populations at a much slower rate than clearance, as seen in Figure 4.3.

Model without Exposed Class

To compare the effect of adding an exposed class to our system we compute the expression for R_0 for the model without the exposed class.

$$R_0^{\text{SIZA}} = \mu\frac{f_S(A_{df})}{A_{df}}S_{df}\frac{\sigma e_S f_S(A_{df})(d+v)}{A_{df}(\lambda+\frac{f_S(A_{df})}{A_{df}}S_{df})(d+v+\theta p_S+c)} \tag{4.15}$$

By inspection, considering an exposed class reduces R_0^{SIZA} by a factor of $\mathcal{E} = \dfrac{\alpha}{(d+p_S+\alpha+\gamma)}$ regardless of the resistance level. However, for a fixed infection rate α, this factor reduces R_0 as γ increases which suggest that resistance reduces the amount of secondary infections in our system. Furthermore, both R_0 and R_0^{SIZA} are decreasing functions of clearance. Thus, the combined effect of the two recovery mechanisms and inclusion of an exposed class lead to a combined reduction in secondary infections.

Elasticity Analysis

Using our explicit expression for R_0, we perform an elasticity analysis to determine how influential our model predictions are to particular parameters. This type of analysis is important since it allows us to identify parameters that should be measured more precisely. A highly sensitive parameter should be carefully estimated since a small change in that parameter could lead to qualitatively different results. We can define the normalized forward sensitivity index for R_0 for the parameter p by,

$$I_p^{R_0} = \frac{\partial R_0}{\partial p}\frac{p}{R_0}.$$

This expression approximates the fractional change in R_0 due to fractional change in parameter p while all other parameters remain fixed ([8], [32], [63], [75]). For example, we can interpret elasticity in terms of percentages as follows, if $I_p^{R_0} = 1$, then a 1% increase in p leads to a 1% change in R_0. By considering the proportion instead of absolute changes in a parameter p, we can compare the effect of parameters that vary in scale or units.

Parameter	Sensitivity Index $\left(I_p^{R_0}\right)$	Parameter	Sensitivity Index $\left(I_p^{R_0}\right)$
α	0.3151	K	0.7465
c	-0.24	λ	-0.6776
d	-0.7435	μ	1.0
e_S	5.4085	p_S	-4.1282
f_{S_0}	5.4085	r	0.6776
γ	-0.1370	σ	1.0
h_S	-1.7465	θ	-0.6
v	0.525		

Table 4.1: Sensitivity of R_0 to parameter values.

In Table 4.1, we see that the expressions for $I_\mu^{R_0}$ and $I_\sigma^{R_0}$ do not depend on other parameter values. In addition, the variables with the highest index are e_S and f_{S_0} which reflects the fact that infection is highly dependent on feeding and conversion of algae into *Daphnia*. As expected, both resistance and clearance decrease the value of R_0, however clearance has a higher influence in decreasing R_0.

We can further analyze the combined dependence of R_0 on the infection rate α, resistance rate

γ, and clearance rate c by computing the value of R_0 over a range of values of our parameters. In Figures 4.4a and 4.4b we see that as resistance and clearance increase, larger values of infection rate are needed to sustain the epidemic. For $\alpha \in [0, 0.7]$ there exist a threshold for which the disease is controlled. In particular, a pathogen would not be able to persist for $\gamma \geq 0.55$ and $c \geq 0.35$. In Figure 4.4c, we combine the effect of both resistance and clearance for a fixed infection rate, $\alpha = 0.5$. As resistance increases, we see that lower values of clearance are needed to contain the disease.

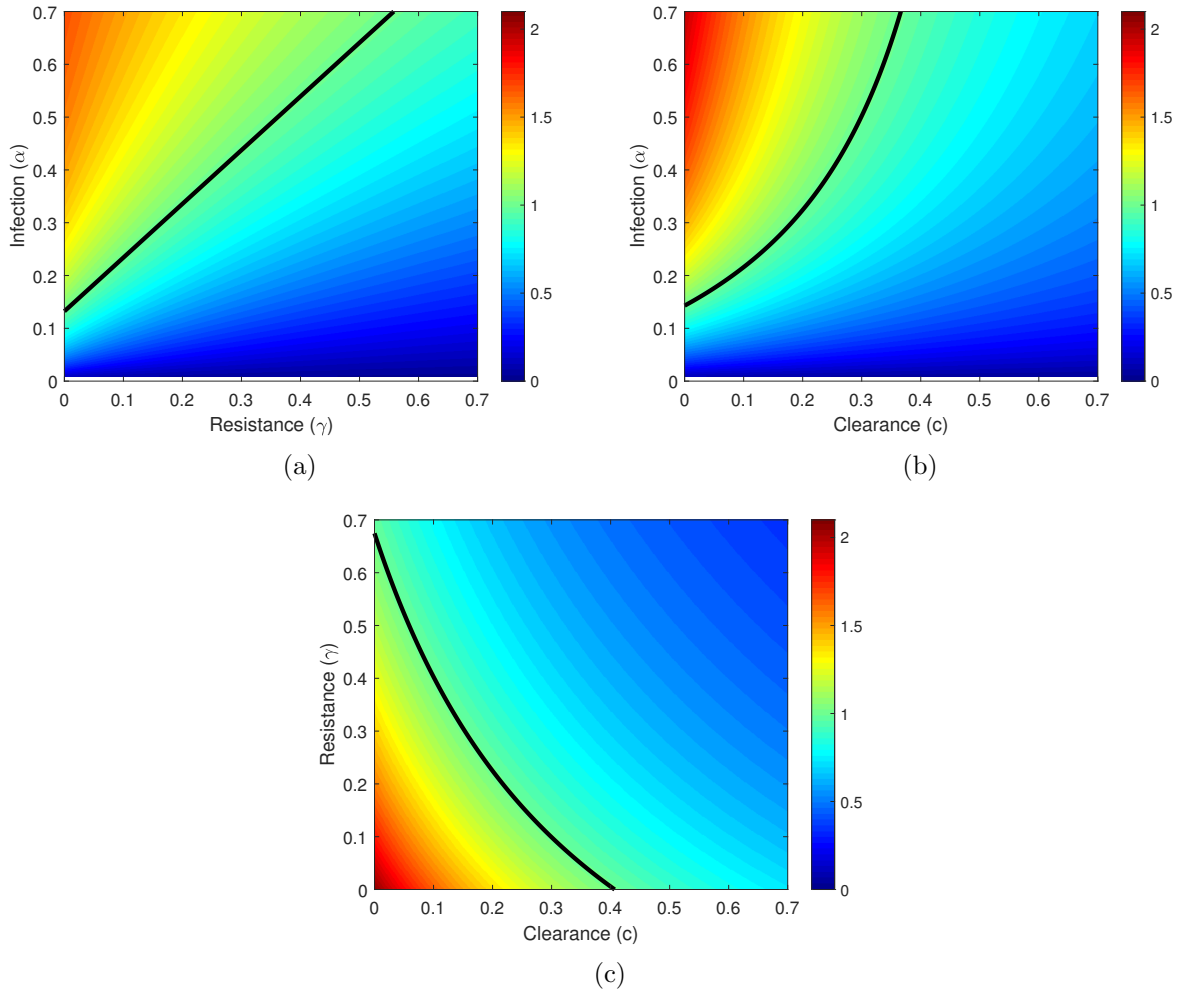

Figure 4.4: (a) R_0 as a function of resistance and infection rate, $c = 0.12$. (b) R_0 as a function of clearance and infection rate, $\gamma = 0.1$. (c) R_0 as a function of clearance and resistance for $\alpha = 0.5$. The black line serves as a visual aid for $R_0 = 1$.

From our elasticity analysis of R_0, we expect predation to have a big impact in the intensity of an epidemic. In Figure 4.5, we see how lower values of predation lead to needing higher values of

clearance and resistance to observe the disease free equilibrium (i.e. $R_0 < 1$). This indicates that predation plays an important role in suppressing the epidemic. In particular, if $p_S < 0.09$, the endemic state persists our range of clearance values and for our range of resistance values if $p_S < 0.095$.

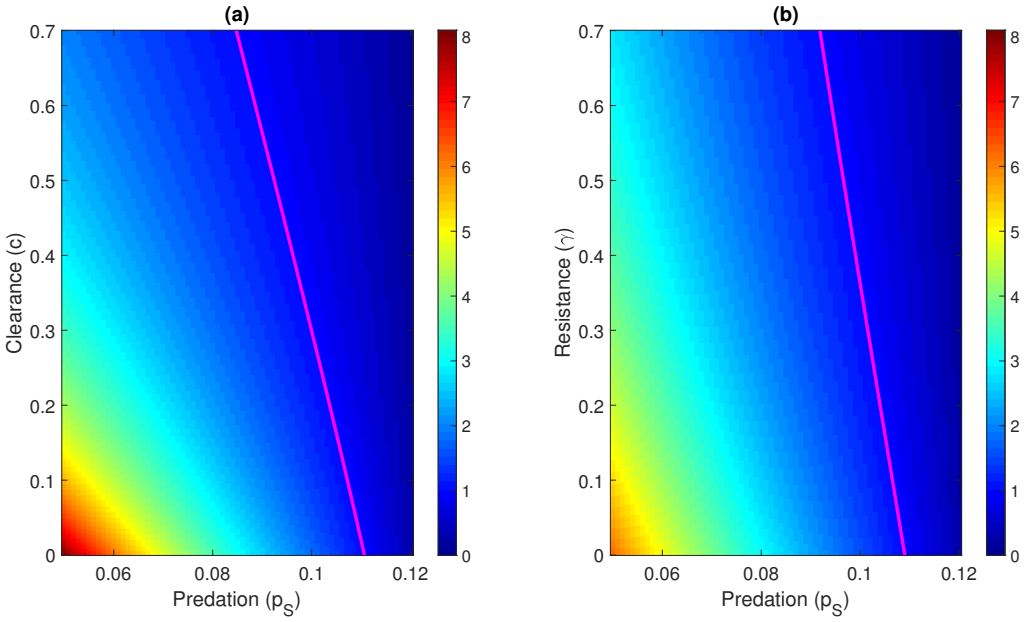

Figure 4.5: R_0 as a function of clearance (left) and resistance (right) for $p_S = 0.09$. The magenta line serves as a visual aid for $R_0 = 1$.

4.3 Numerical Experiments

We analyzed the transient and long-term behaviour of our system under different assumptions by plotting how population densities change over time. Figure 4.6 shows when there is no recovery (i.e. $\gamma = 0$ and $c = 0$) the system exhibits higher levels of oscillations that dampen over time. As we incorporate resistance or clearance, the height of the oscillations decreases. However, once clearance is introduced the populations stabilize at a much faster rate and converge to either the endemic or disease-free equilibrium. We repeat our numerical simulations to consider a lower predation rate $p_S = 0.09$. As seen in Figure 4.7, once the predation rate is reduced prevalence increases and the oscillations become more pronounced and dampen at a slower rate.

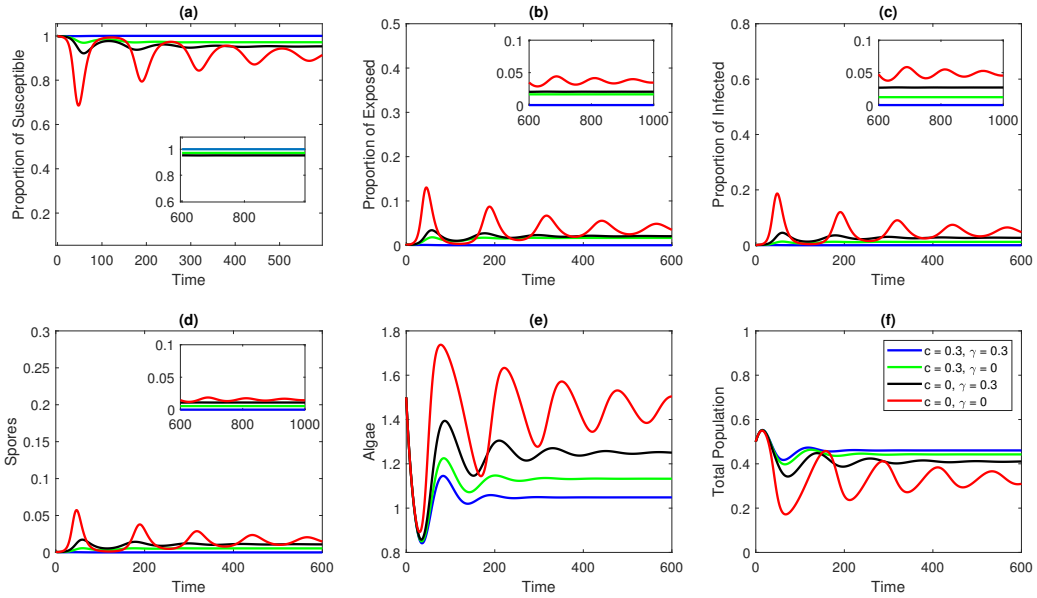

Figure 4.6: Simulations of our ODE system for different recovery scenarios. Clearance and resistance (blue), only clearance (green), only resistance (black), no recovery (red). Initial Conditions: (0.5,0,0,0.001,1.5) and $p_S = 0.1$.

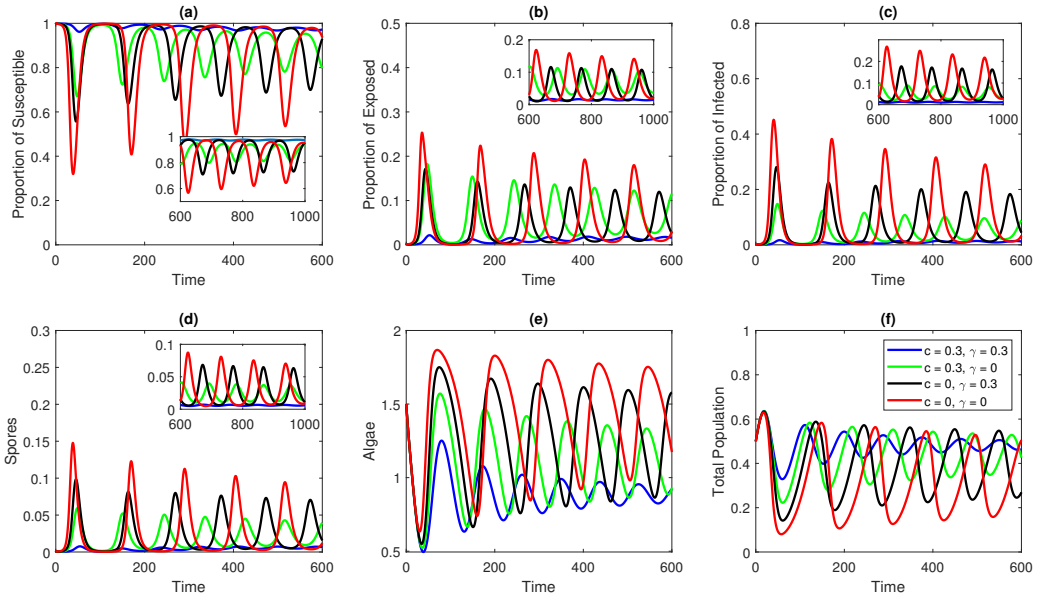

Figure 4.7: Simulations of our ODE system for different recovery scenarios. Clearance and resistance (blue), only clearance (green), only resistance (black), no recovery (red). Initial Conditions: (0.5,0,0,0.001,1.5), $p_S = 0.09$.

Initial conditions will play a big role in the dynamics observed for our system. Figures 4.8

and 4.9 show that for high susceptible initial populations and low spore dose (which is what you would expect at the start of an epidemic), there is large peak at the beginning of epidemic which reaches very low densities in approximately 100 days for $p_S = 0.1$ and 70 days for $p_S = 0.09$, and is proceeded by small oscillations after a period of time. For $p_S = 0.1$, this period is around 250 days while for $p_S = 0.09$ this period is approximately 180 days.

This is a big contrast to the previous scenarios in which the we observe oscillations that are frequent and dampen over time. For our default predation rate, $p_S = 0.1$, we see that only in the case where there is higher level of resistance and clearance is the disease controlled. But similar to Figure 4.7, when predation is lower, $p_S = 0.09$, oscillations remain present for a longer period of time. In fact, in 4.9, even when resistance and clearance are high, the exposed and spore populations which had remained close to zero begin to increase at around 800 days.

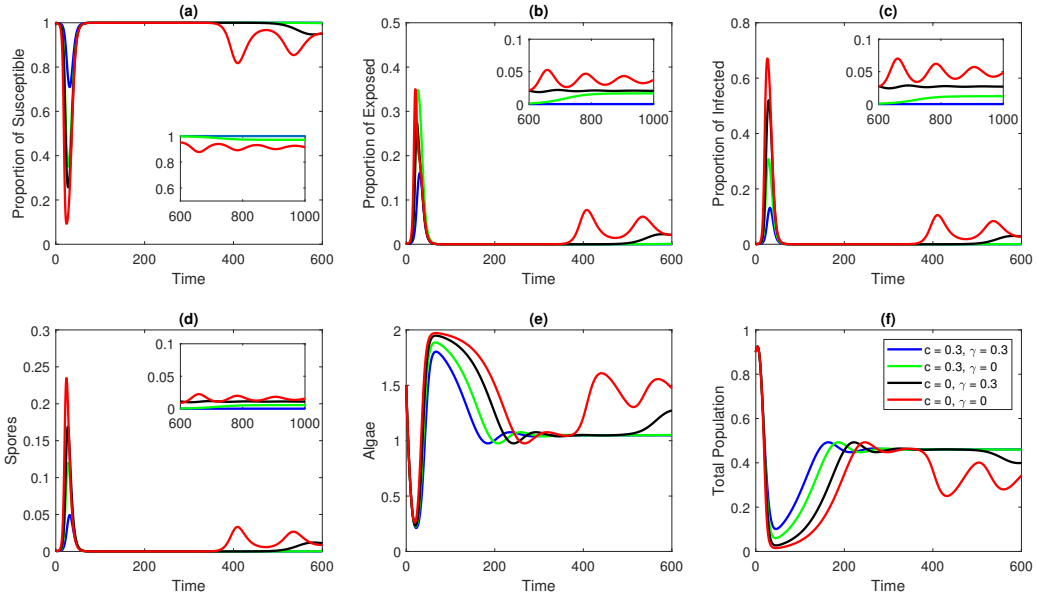

Figure 4.8: Simulations of our ODE system for different recovery scenarios. Clearance and resistance (blue), only clearance (green), only resistance (black), no recovery (red). Initial Conditions: (0.9,0,0,0.001,1.5) and $p_S = 0.1$.

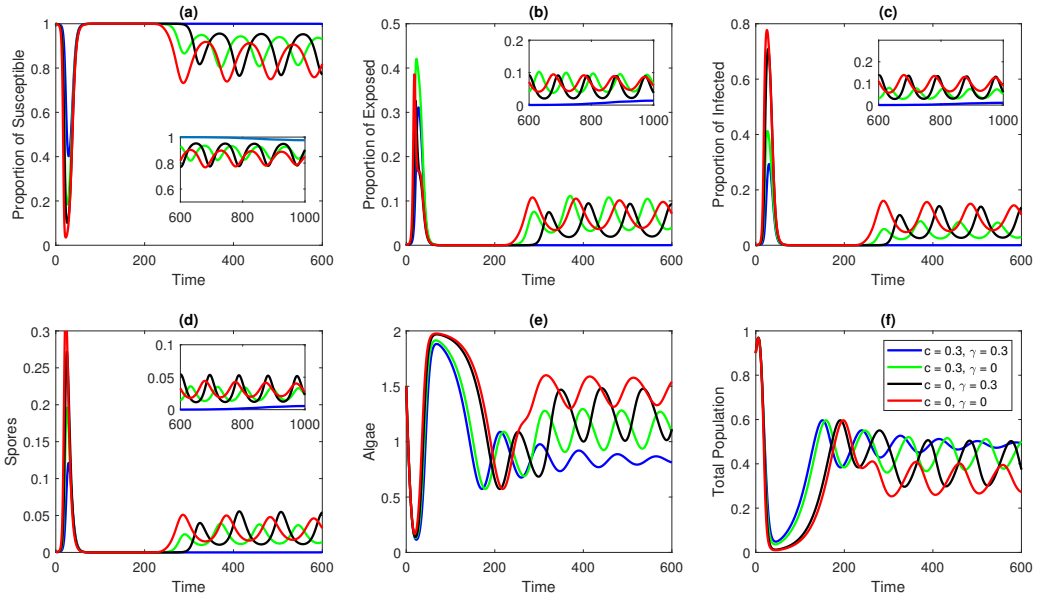

Figure 4.9: Simulations of our ODE system for different recovery scenarios. Clearance and resistance (blue), only clearance (green), only resistance (black), no recovery (red). Initial Conditions: (0.9,0,0,0.001,1.5) and $p_S = 0.09$.

4.4 Discussion–Future Directions

In models of disease such as the West Nile Virus and Malaria, the inclusion of an exposed class leads to the reduction of R_0 [5] and disease prevalence [67], which we observe also for our system. When considering two recovery mechanisms, resistance and clearance, this reductions is made more significant. In the absence of recovery, we have shown our system undergoes damped oscillations for a long period of time. As we include resistance and clearance, this dampening occurs at a much faster rate. Additionally peak disease prevalence, which can be analyzed as the peaks of our observed oscillations is reduced. When comparing the effects of resistance versus clearance, we have shown that clearance has a much larger effect in reduction both secondary infections (i.e. R_0) and disease prevalence. There has been evidence that considering a model with non-exponentially distributed exposed and infectious periods, might lead to an increase in R_0 and periodic behavior [65]. It has been shown that adding non-exponential infection distributions destabilizes the endemic equilibrium in an SIR model. Including more realistic infectious periods could allow us to account for recurrent outbreaks of *Daphnia* epidemics.

Our results also showcase the importance of initial conditions for our system. When there is a high level of susceptible individuals ($S(0) = 0.9$) and low spore densities ($Z(0) = 0.001$), our model predicts a high prevalence peak which is followed by low values ($\approx 10^{-6}$) and begins to rebound. In [65], the author argues that the ability of infected individuals to rebound from low levels is a unrealistic feature of deterministic epidemic models. To explore this further we will reformulate our model as a stochastic model in Chapter 5 and analyze it's behavior.

Another future direction for this work would be to translate the disease progression stages discussed in [79] into stages in our infectious class. So far we have assumed the rates of resistance and clearance remain constant over time; thus the chance of recovery within a given time interval is constant, regardless of the time since infection. We will study clearance as a fuction of age since infection in Chapter 6.

Chapter 5

Demographic Stochasticity

5.1 Introduction

Many disease models used to describe populations dynamics rely on deterministic differential equations to track changes in populations over time. The use of deterministic models in ecology and epidemiology has a long history and a strong body of research. These models are still widely used to understand population dynamics [78]. They are characterized by the basic reproduction R_0 (i.e. the amount of secondary infections produced by a single infected individual in a completely susceptible population), which if greater than one, predicts that the populations will eventually converge to an endemic equilibrium usually through damped oscillations ([7], [52]). However, it has been recognized that these models can have limitations in capturing the behavior of a system when there exists a very low number of infected individuals or when modeling recurrent outbreaks which would exhibit sustained oscillations [65]. The threshold conditions for R_0 found in Chapter 4 may not hold for stochastic models. Mainly, the disease may go extinct even if $R_0 > 1$, depending on the stochastic fluctuations [67].

For example, diseases such as measles, whopping cough, avian flu exhibit sustained oscillations that capture recurrent disease dynamics. Many types of extensions of the Susceptible-Infected-Recovered (SIR) models have resulted in sustained oscillations. Some of these extensions show that sustain oscillations can happen implicitly or through the periodical forcing of model parameters such as transmission [12]. In his work (Barlett, 1957), recognized that by adding stochastic terms associated with the discrete nature of births, deaths, immigration and emigration processes (i.e. demographic stochasticity) one could bridge the gap between what the theory predicted and the observed statistics for measles epidemics ([11], [18]).

While stochastic effects are preset in all populations, they are particular relevant when popula-

tions sizes are small. It has been shown that deterministic models with added stochasticity could give recurrent dynamics by constantly perturbing the system away from its steady state. Whereas deterministic models treat the number of individuals in each state as a continuous variable stochastic models treat the number of individuals as discrete, and the process is more appropriately modeled as a Markov Chain. The phenomena where a system with stochastic fluctuation sustains an oscillatory behavior while the deterministic model converges to an stable equilibrium is know as coherence resonance ([7], [52]).

5.2 Stochastic Model

Stochastic models are characterized by considering the probability of an individual in a population transitioning to different compartments of our system. As in [7], to compare the deterministic and stochastic simulations we introduce a scale factor Ω to account for the fact we would measure individuals rather than the population densities. One can interpret Ω as the size of our population or in this case our system. In other stochastic disease models this has usually been related to only the hosts population size. In our case, we can interpret Ω as the overall size of the system including: hosts, spores, and algae.

To determine which parameters need re-scaling, we analyzed how each parameter's units scaled when we consider that the population is now given by the number of individuals in each class. Only the spore release (σ), half saturation constant (h_S), and the carrying capacity (K) did not scale linearly with our units; therefore, they must be re-scaled.

$$\frac{dS}{dt} = e_S f_S(A)\left(S+E+\rho I\right) - (d+p_S)S - \mu\frac{f_S(A)}{A}SZ + cI + \gamma E \tag{5.1}$$

$$\frac{dE}{dt} = \mu\frac{f_S(A)}{A}SZ - (d+p_S+\gamma+\alpha)E, \tag{5.2}$$

$$\frac{dI}{dt} = \alpha E - (d+v+\theta p_S+c)I, \tag{5.3}$$

$$\frac{dZ}{dt} = \sigma e_S \Omega\frac{f_S(A)}{A}(d+v)I - \lambda Z - f_S(A)\left(S+E+I\right)\frac{Z}{A} \tag{5.4}$$

$$\frac{dA}{dt} = r\left(1-\frac{A}{\Omega K}\right)A - f_S(A)\left(S+E+I\right). \tag{5.5}$$

where $f_S(A)$ is now given by,

$$f_S(A) = \frac{f_{S_0} A}{h_S \Omega + A}$$

Starting from our ODE model, we can obtain a stochastic model by interpreting the deterministic rates (e.g. births, deaths, exposure, etc.) as stochastic rates. We summarize the types of events, the transition probabilities, and the effect of each event on the population. In this stochastic framework, we take into account our populations S, E, I, Z and denote s, e, i, z as the number of individuals in each class. Denote the general state of the system as $n = (s, e, i, z)$. The transition probability per unit time from state n to the state n' will be denoted as $T(n'|n)$ in which n' is obtained by shifting each state variable in n by $+1$ or -1.

Event	Effect	Transition Probabilities
Births/Gain	$s \to s+1$	$e_S f_S(a)\,(s + e + \rho i)\,\Delta t$
	$z \to z+1$	$\sigma \Omega e_S \frac{f_S(a)}{a}(d+v) i \Delta t$
	$a \to a+1$	$ra\Delta t$
Deaths/Loss	$s \to s-1$	$(d + p_S) s \Delta t$
	$e \to e-1$	$(d + p_S) e \Delta t$
	$i \to i-1$	$(d + v + \theta p_S) i \Delta t$
	$z \to z-1$	$\lambda z + f_S(a)\,(s + e + i)\,\frac{z}{a}\Delta t$
	$a \to a-1$	$r\frac{a^2}{\Omega K} + f_S(a)\,(s + e + i)\,\Delta t$
Exposure	$(s, e) \to (s-1, e+1)$	$\mu \frac{f_S(a)}{a} s z \Delta t$
Infection	$(e, i) \to (e-1, i+1)$	$\alpha e \Delta t$
Clearance	$(s, i) \to (s+1, i-1)$	$ci\Delta t$
Resistance	$(s, i) \to (s+1, e-1)$	$\gamma e \Delta t$

Table 5.1: Transition probabilities for different events.

By using the transition probabilities in Table 5.1, we can construct the master equation ([7], [47]) which describes the evolution over time of our system.

$$\frac{dP(n;t)}{dt} = \sum_{n' \neq n} T(n|n') P(n';t) - \sum_{n' \neq n} T(n'|n) P(n;t) \tag{5.6}$$

where $n = (s, e, i, z, a)$ represents the state of the system, $P(n|n')$, is the probability of the system in the state n at time t, and the change of this quantity with time is given by the sum of transitions into the state n from all the other states n', and minus the sum of transitions out of the state n into all the other states n'. We summarize the types of events, the transition probabilities, and the effect of each event in Table 5.1.

Due to the complexity of this equation, studying it analytically is a challenge. We can further study the master equation (5.6) numerically by implementing stochastic simulations in MATLAB using Gillespie's algorithm [51]. Both this algorithm and the master equation are derived from the same Markovian assumptions thus there is an exact correspondence among the two [19]. In the Gillespie algorithm, the state of the system is updated by determining the time to the next event, and which event will occur next. This algorithm assumes that at any given time step only one event can occur and that times are exponentially distributed. A brief outline of the algorithm is given below ([11], [78]).

Step 1: Initialize populations, parameters, and denote by e_i the transition probability corresponding to each possible event in Table 5.1.

Step 2: Select two random numbers from an uniform distribution between $(0, 1)$, (i.e. $u_1, u_2 \in U(0, 1)$).

Step 3: Compute the time when the next event occurs: $t_{j+1} = t_j + \Delta t$ where $\Delta t = \dfrac{-\log(u_1)}{\sum_i e_i}$

Step 4: To select which event occurs we divide the interval $[0, 1] = (0, p_1] \cup (p_1, p_2] \cup ... \cup (p_{N-1}, 1]$ into sub-intervals corresponding to the probability of each event happens p_i. If $u_2 \in (p_i, p_{i+1}]$ event e_i happens.

Step 5: Update populations according to Table 5.1 and repeat.

5.3 Numerical Results

Using the Gillepsie algorithm we obtained sample stochastic realizations of our model. In Chapter 4, we noticed that predation plays a big role in the observed behaviour of the determinstic version of our model. Thus, we perform our simulations for $p_S = 0.1$ and $p_S = 0.09$. In Figure

5.1, we compute the frequency of the disease-free and endemic equilibria for different values of Ω. Recall, we can think of Ω as the size of our system, thus our populations are proportional to Ω. In the case where populations are small $\Omega = 1000$, we only observe the disease-free equilibrium for all values of p_S considered. This suggest in contrast to the results presented in Chapter 4, that when populations are too low we should expect the extinction of the parasite. As the size of the system increases we start to observe the endemic equilibrium at a higher frequency.

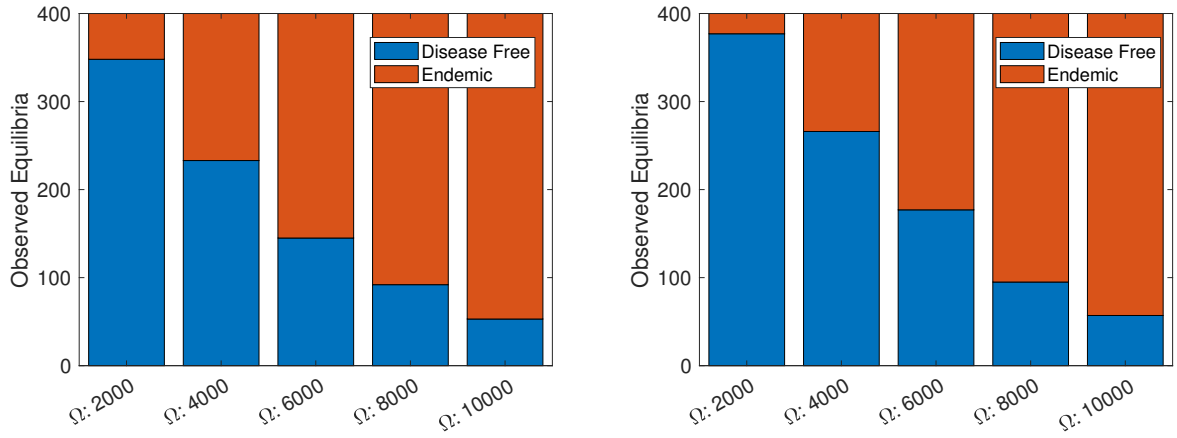

(a) $p_S = 0.09$ (b) $p_S = 0.1$

Figure 5.1: Frequency of disease-free (blue) and endemic (red) equilibria for different scale factor values $\Omega = \{2000, 4000, 6000, 8000, 10000\}$.

In fact, as shown in Figures (5.2)–(5.5), when the system is large enough (i.e. large values for Ω), our realizations exhibit sustained oscillations while our deterministic model shows dampening. Thus, under this formulation sustained oscillations are possible for large enough populations. The stochastic realizations exhibit sustained oscillation regardless of the rate of predation p_S. For $p_S = 0.1$, these oscillations show higher variation when compared to its deterministic counterpart. When $p_S = 0.09$, the stochastic realization follows the deterministic behaviour more closely.

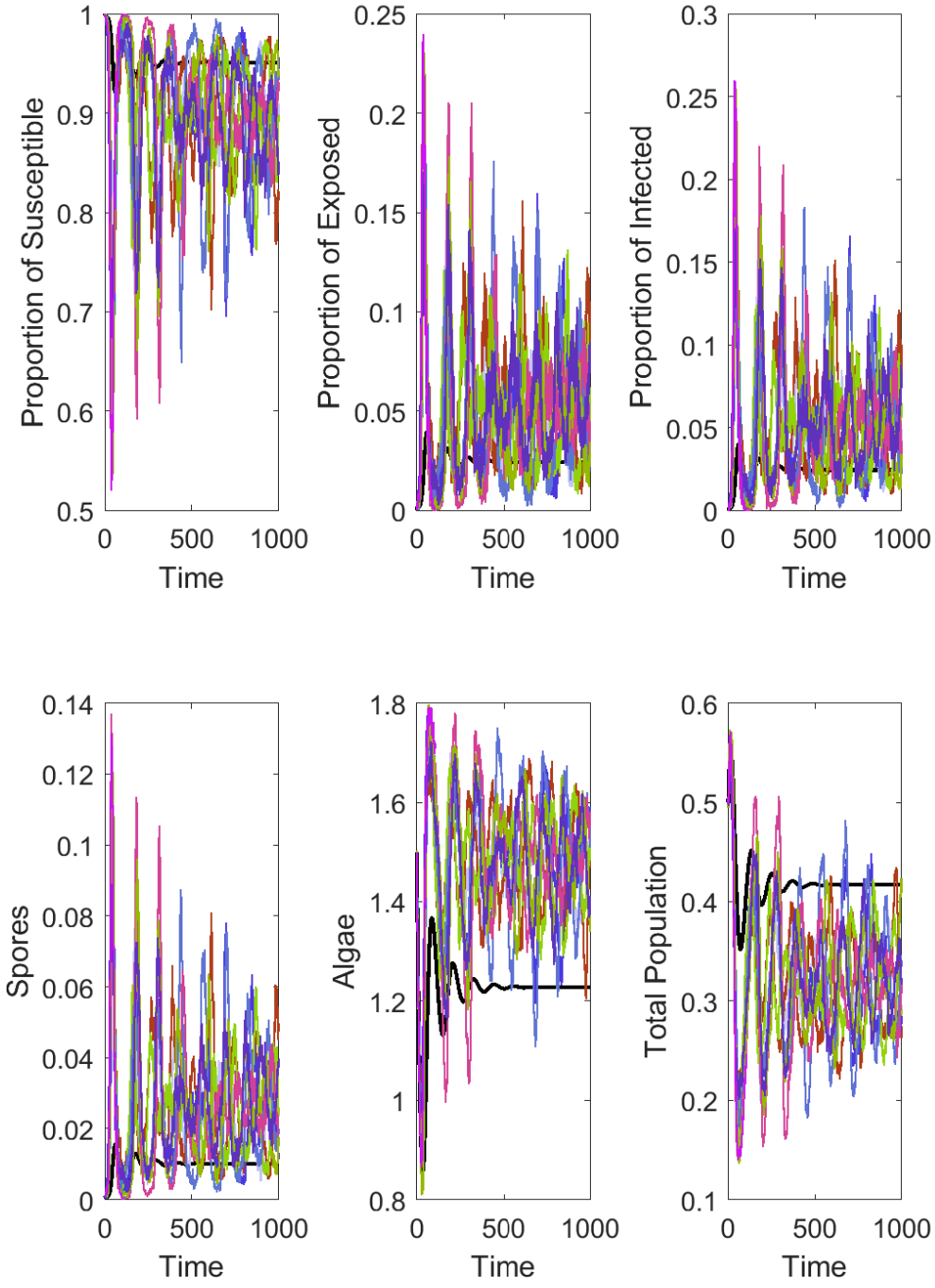

Figure 5.2: Deterministic (black line) vs. Stochastic (other curves) simulation with scale factor $\Omega = 5000$, $p_S = 0.1$, $c = 0.12$, and $\gamma = 0.1$.

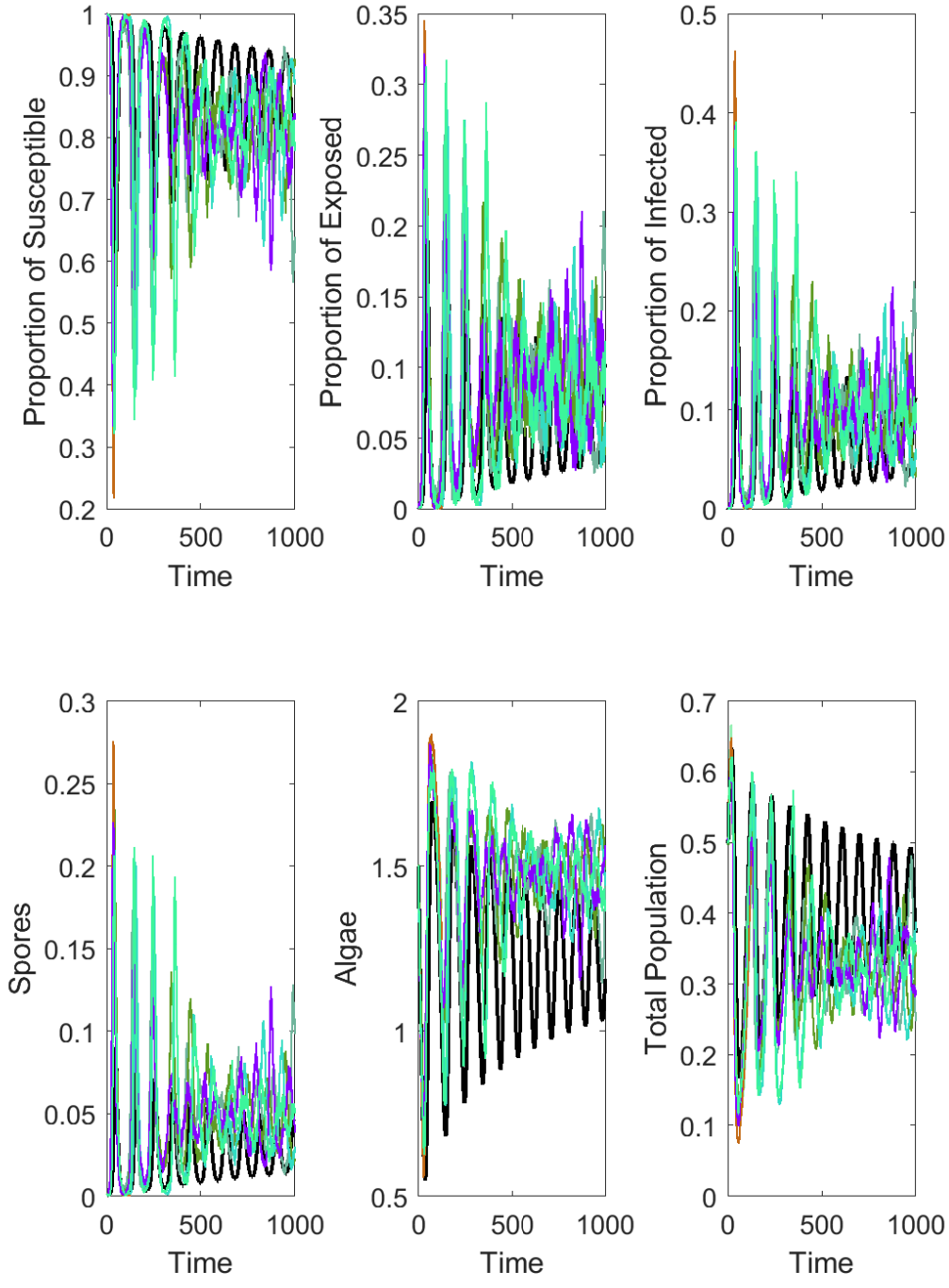

Figure 5.3: Deterministic (black line) vs. Stochastic (other curves) simulation with scale factor $\Omega = 5000$, $p_S = 0.09$, $c = 0.12$, and $\gamma = 0.1$.

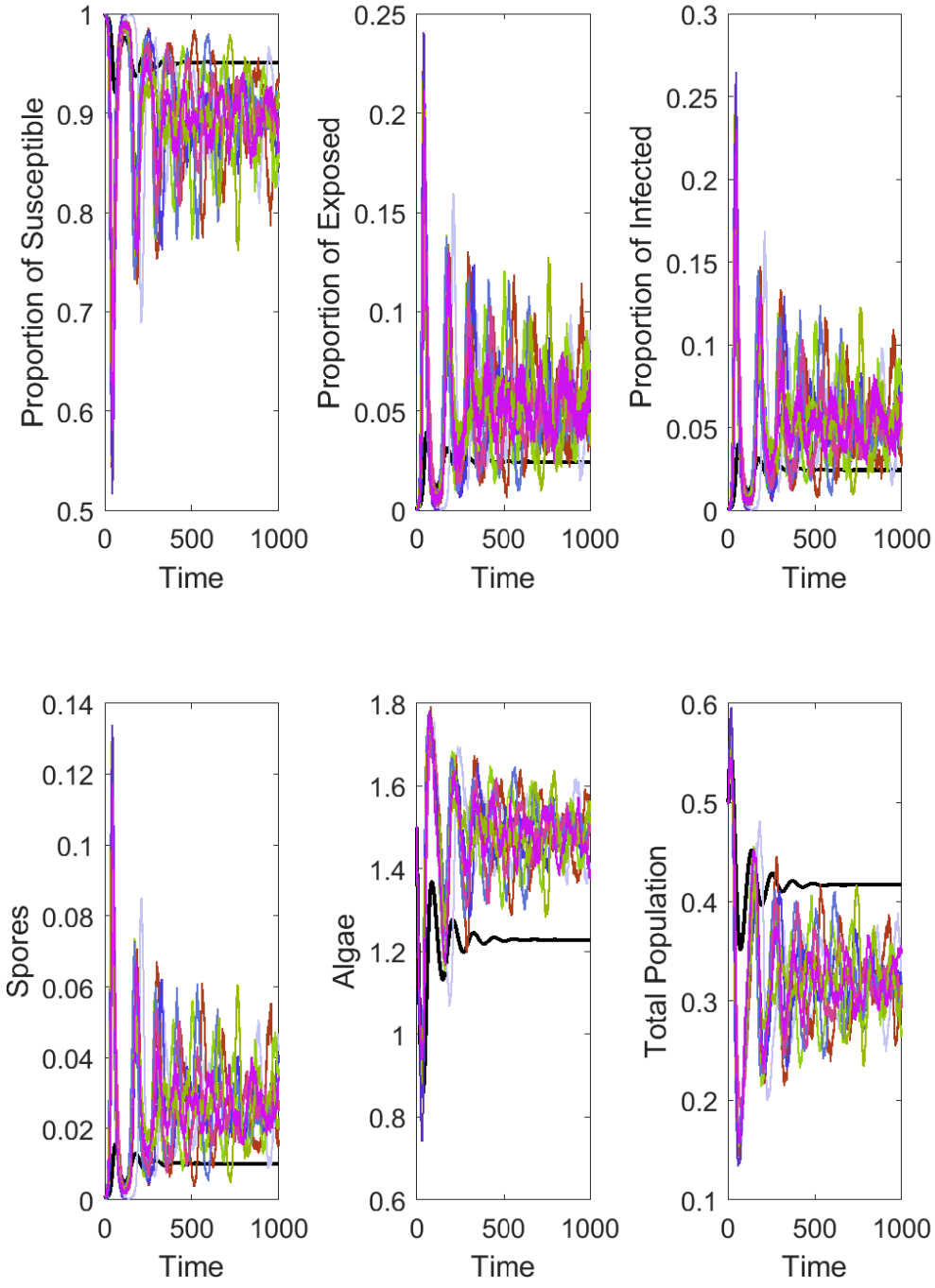

Figure 5.4: Deterministic (black line) vs. Stochastic (other curves) simulation with scale factor $\Omega = 10000$, $p_S = 0.1$, $c = 0.12$, and $\gamma = 0.1$.

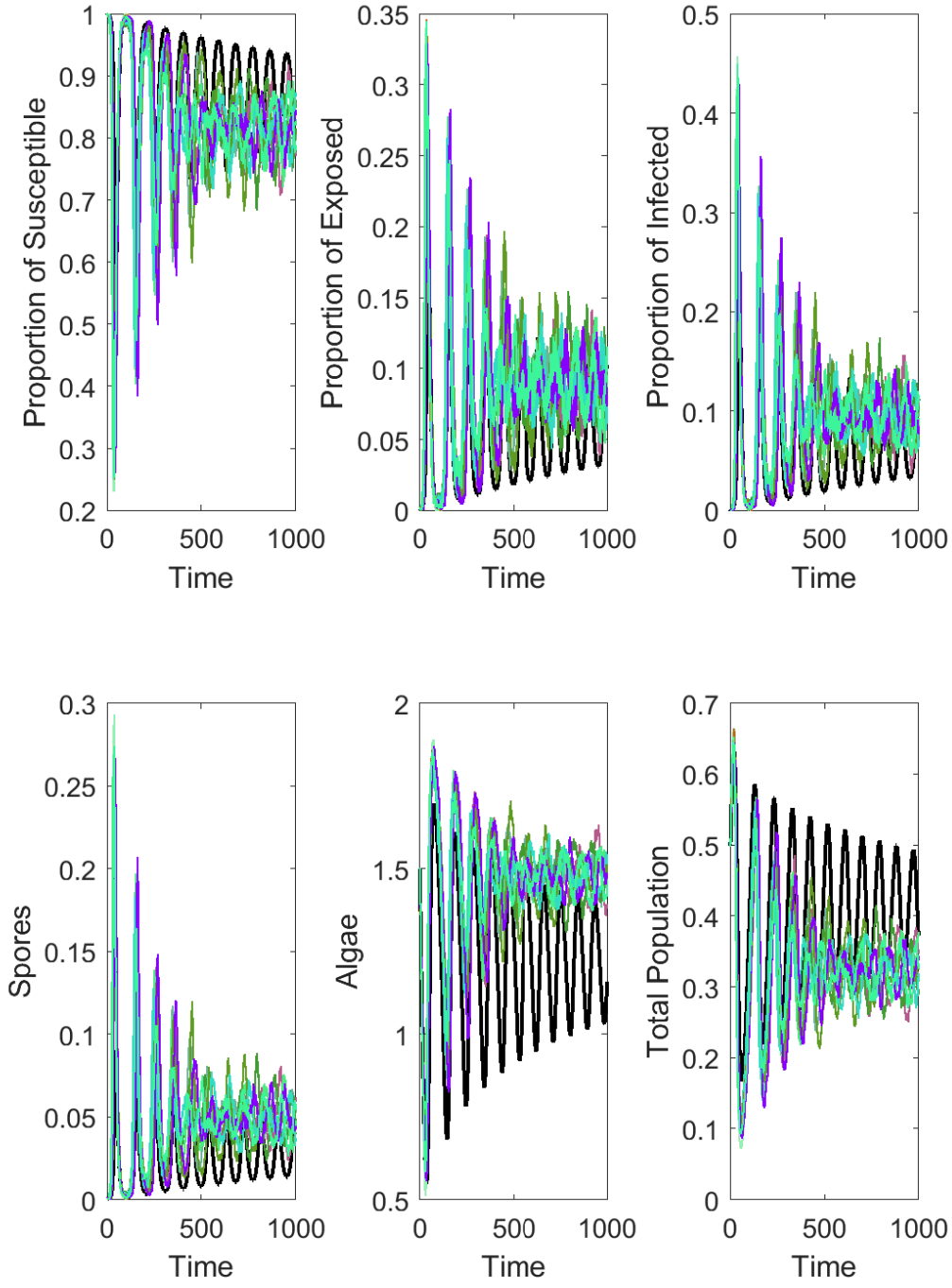

Figure 5.5: Deterministic (black line) vs. Stochastic (other curves) simulation with scale factor $\Omega = 10000$, $p_S = 0.09$, $c = 0.12$, and $\gamma = 0.1$.

The Gillespie algorithm generates exact realizations of the stochastic process when parameters are time-independent, however, it is computationally intensive for large systems since it tracks each transition in the population. To further understand the effect of the magnitude of the scale factor in the dynamics of our stochastic system, we analyzed the computational time of our simulations for different values of Ω. As seen in Figure 5.6, regardless of the values for rate of predation p_S, as Ω increases, the computational time increases. While this is not a constraint for the amount of samples considered in this section, it could become a computational constraint for larger amounts of samples.

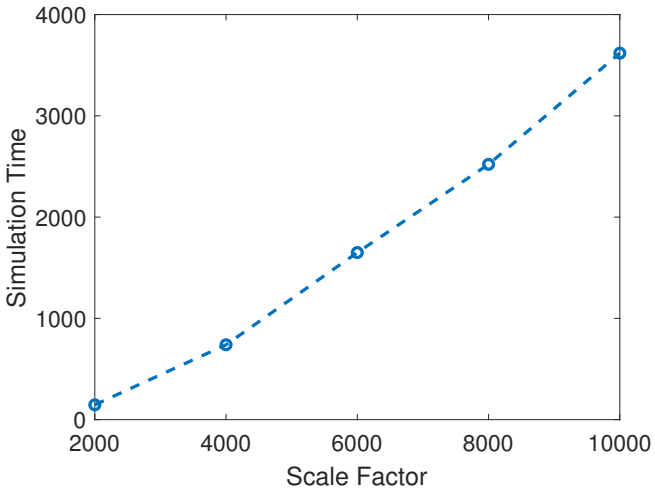

(a) $p_S = 0.09$

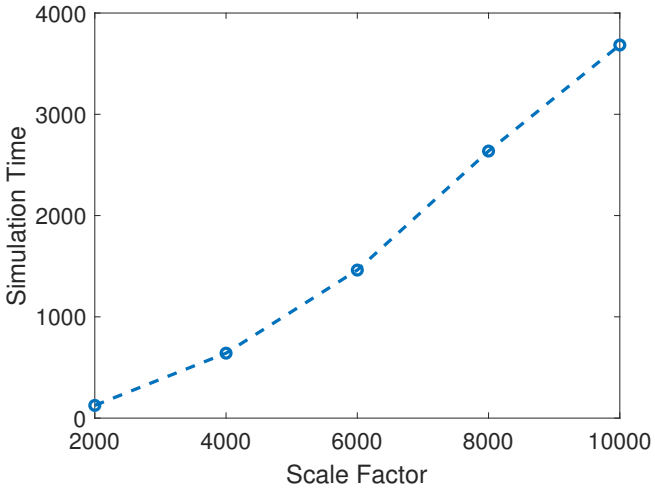

(b) $p_S = 0.1$

Figure 5.6: Computational time of simulations for different scale factor values $\Omega = \{2000, 4000, 6000, 8000, 10000\}$.

5.4 Discussion–Future Directions

Using a stochastic formulation of the model presented in Chapter 4 we have shown two behaviors not captured by our deterministic model: sustained oscillations and parasite extinction for low spore populations. This opens the door for questions regarding the biological assumptions made in our modeling framework. By introducing a scale factor, we studied how the size of our system leads to different behaviors for our system. In particular, as the size of the system increases we observed the endemic equilibrium at a higher frequency; however, it increases computational time. This is due to the fact that as the system of the size increases the time to extinction is longer. Sustained oscillations have been also observed, when transmission is modeled as a function of time. In many models of recurrent epidemics, account for seasonal forcing by assuming that the contact rate is a periodic function of time ([12], [18], [64], [78]). A future direction for this work would be to include these seasonal effects.

Chapter 6

Age-Since-Infection Model

6.1 Introduction

Age of infection has been shown to influence host fecundity and mortality through parasite virulence. Specifically, in many systems, mortality increases, while fecundity decreases as the disease progresses. In their work, (Rapti and Cáceres, 2016) showed how the timing of intrinsic mortality, which tends to increase with age, and extrinsic mortality, which tied to predators, affects the size of epidemics [77]. The ability of the infected host to recover through clearance of the infection may also depend on the age of infection. The longer an individual remains infected, the more unlikely it will be to recover from the disease. These changes, in turn, affect the between-host transmission. To investigate how these mechanisms affect disease transmission, we extend the model presented in [77] to include a recovery mechanism and investigate how epidemiological relevant quantities such as disease prevalence and the basic reproductive number R_0 depend on them.

The objective of the model is to investigate how clearance, as a function of age of infection, influences the disease dynamic for the *Daphnia-Metschnikowia* system. Using a partial differential equation (PDE) formulation, we explicitly model disease induced mortality and recovery as functions of the age of infection. There are two independent variables in our system: the time t and the age of infection $0 \leq a \leq a_0$, where a_0 is the maximum age of infection. Here S, I, Z, and A denote the susceptible and infected hosts, the pathogen spores, and the algal resources, respectively. The coupled differential equations model reads:

$$\frac{dS}{dt} = \overbrace{e_S f_S(A)\left(S + \int_0^{a_0} \rho(a) I(t,a) da\right)}^{\text{Births}} - \overbrace{(d + p_S)S}^{\text{Deaths}} - \overbrace{\mu \frac{f_S(A)}{A} SZ}^{\text{Transmission}} + \overbrace{\int_0^{a_0} c(a) I(t,a) da}^{\text{Clearance}} \quad (6.1)$$

$$\frac{\partial I}{\partial t} + \frac{\partial I}{\partial a} = -(\overbrace{d + v(a) + \theta(a) p_S}^{\text{Death}} + \overbrace{c(a)}^{\text{Clearance}})I, \quad I(t,0) = \overbrace{\mu \frac{f_S(A)}{A} SZ}^{\text{Initial Conditions}} \quad (6.2)$$

$$\frac{dZ}{dt} = \overbrace{\sigma e_S f_S(A) \int_0^{a_0} (d + v(a)) I(t,a) W(a) da}^{\text{Spore Release}} - \overbrace{\lambda Z - f_S(A)\left(S + \int_0^{a_0} I(t,a) da\right)\frac{Z}{A}}^{\text{Spore Loss}} \quad (6.3)$$

$$\frac{dA}{dt} = \overbrace{r\left(1 - \frac{A}{K}\right)A}^{\text{Logistic Growth}} - \overbrace{f_S(A)\left(S + \int_0^{a_0} I(t,a) da\right)}^{\text{Algae Loss}}. \quad (6.4)$$

We incorporate a new transitions from the infected class to the susceptible class due to clearance of the disease. We consider the effect of the time and an individual remains infected by allowing the parameters relevant to the infection class to depend on age of infection (a).

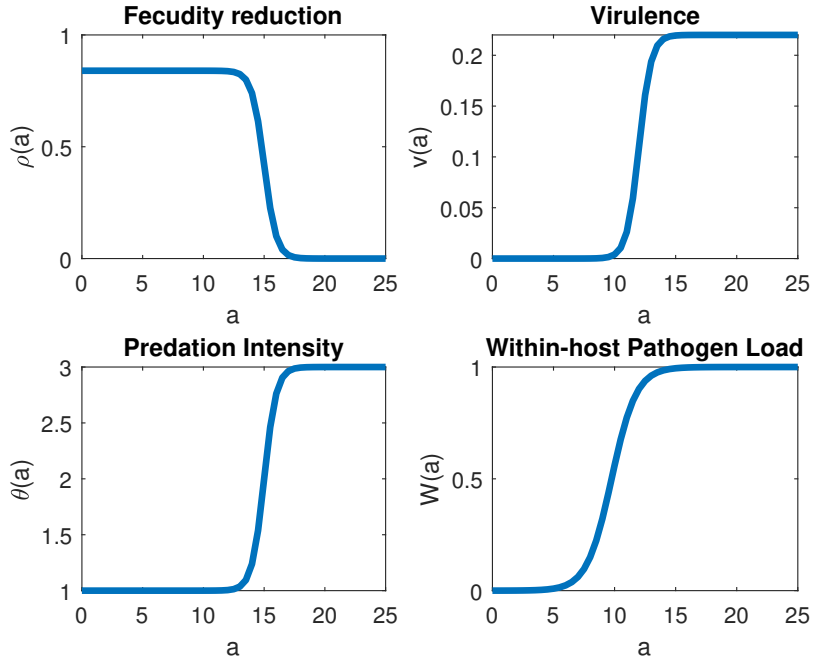

Figure 6.1: Parameters as a function of age. **a)** fecundity parameter, $\rho(a) = 0.5\rho_0(1-\tanh(a-h_\rho))$ with $\rho_0 = 0.84$. **b)** disease-induce mortality $v(a) = 0.5v_0(1+\tanh(a-h_v))$, with $v_0 = 0.22$. **c)** selective predation parameter $\theta(a) = 1+0.5(\theta_0-1)(1+\tanh(a-h_\theta))$ with $\theta_0 = 5$ and half-saturation constant $h_\theta = 15$. **d)** within-host pathogen load $W(a) = 1/(1+\exp(-0.99+9.6582))$

.

We use a partial differential equation (PDE) to describe the dynamics of the infected host, where the number of infected host in a time t in a particular age range $[a_1, a_2]$ is given by $\int_{a_1}^{a_2} I(t,a)da$. Infected individuals suffer from a reduction in fecundity ($\rho(a)$), disease induced mortality (i.e. virulence, $v(a)$), a higher rate of predation which we account by the selective predation parameter ($\theta(a)$), and are able to remove the infection due to clearance ($c(a)$).

Spores reproduce within the infected host and are released to the system after infected individuals die due to background mortality (d) and virulence. To account for this process, we incorporate $W(a)$ as a weight that represent the within-pathogen load as a function of age of infection. Previous studies have shown that $W(a) = \frac{1}{1+\exp(-0.99a+0.96582)}$, establishing that weight is an increasing function of age since infection (see Figure 6.1) [10].

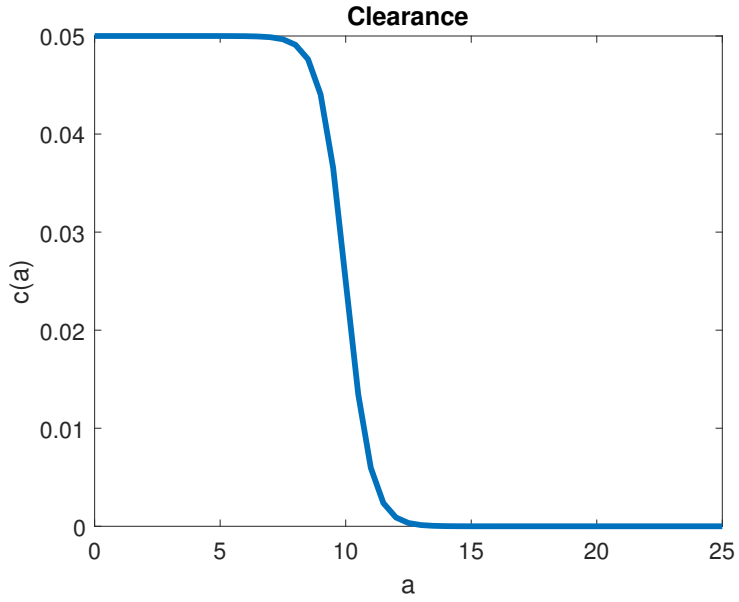

Figure 6.2: Recovery due to clearance as a function of age, $c(a) = 0.5c_0(1 - \tanh(a - h_c))$

Steady States

The system admits four steady states. The first two are the trivial steady state $E_0 = (0, 0, 0, 0)$ and the algae-only steady state $E_A = (0, 0, 0, K)$, which exist for all parameter values. Next, is the disease-free steady state $E_{df} = (S_{df}, 0, 0, A_{df})$ is given by $A_{df} = \frac{(d+p_S)h_S}{e_S f_{S0} - (d+p_S)}$ and $S_{df} = \frac{e_S r\left(1-\frac{A_{df}}{K}\right)A_{df}}{d+p_S}$. It is biologically feasible if $e_S f_{S0} - (d + p_S)$ which essentially states that the growth

rate of the susceptible hosts is higher than their death rate and $A_{df} < K$ which states that the resource requirement for the host is less than the carrying capacity. Finally, there is the endemic steady state $E_e = (S_e, Q_e, Z_e, A_e)$, where $Q_e = \int_0^{a_0} I_e(a)da$ is the total infected host population. The steady state population densities are given in Appendix B and are found as functions of the algae equilibrium density A_e which satisfies a cubic polynomial. The dependence of E_e on various parameters related to clearance (i.e. c_0, h_c), host intrinsic (i.e. v_0, h_v), and extrinsic mortality (i.e. θ_0, h_θ) will provide us with new insights on the role of each mechanism in disease dynamics.

6.2 Basic Reproduction Number

One of the most important and common metrics of epidemics is the basic reproductive ratio R_0. It is equal to the number of secondary infections produced by a single infectious host in a population of entirely susceptible hosts [57]. It is therefore an important quantifier of epidemic frequency and severity. We can obtain R_0 by linearization of the system around the disease-free equilibrium point. This yields a linear eigenvalue problem for the time-independent perturbations corresponding to an eigenvalue Λ. The characteristic equation of this eigenvalue problem is

$$R(\Lambda) \equiv \mu \frac{f_S(A_{df})}{A_{df}} S_{df} \frac{\sigma e_S f_S(A_{df}) \int_0^\infty W(a)(d+v(a)) e^{-\int_0^a (\Lambda + d + v(\tau) + \theta(\tau) p_S + c(\tau))d\tau} da}{\Lambda + \lambda + \frac{f_S(A_{df})}{A_{df}} S_{df}} = 1. \quad (6.5)$$

When $\Lambda = 0$ expression (6.5) implies $R(0) = R_0$, where R_0 is the basic reproduction ratio of the system given by the equation

$$R_0 = \mu \frac{f_S(A_{df})}{A_{df}} S_{df} \frac{\sigma e_S f_S(A_{df}) \int_0^{a_0} W(a)(d+v(a)) e^{-\int_0^a (d + v(\tau) + \theta(\tau) p_S + c(\tau))d\tau} da}{\lambda + \frac{f_S(A_{df})}{A_{df}} S_{df}}. \quad (6.6)$$

Equation (6.6) states that R_0 depends on the average spore release over the lifespan of the infected host $\sigma e_S f_S(A_{df}) \int_0^{a_0} W(a)(d+v(a)) e^{-\int_0^a (d + v(\tau) + p_S \theta(\tau) + r(\tau))d\tau} da$, the transmission rate per infective propagule $\mu \frac{f_S(A_{df})}{A_{df}} S_{df}$, and the lifespan of the free-living infective prapagules $\left(\lambda + \frac{f_S(A_{df})}{A_{df}} S_{df}\right)^{-1}$.

Theorem 6.2.1. *If $R_0 < 1$ then the disease-free equilibrium is locally asymptotically stable, and if $R_0 > 1$ it is unstable.*

Proof. If Λ is real in (6.5), then it follows by a simple differentiation that $\frac{dR}{d\Lambda} < 0$. Hence, if

$R_0 = R(0) > 1$ it follows that the equation $R(\Lambda) = 1$ has real positive solutions Λ which implies the disease-free equilibrium is unstable. Similarly, if $R_0 < 1$ then the same argument shows that the equation $R(\Lambda) = 1$ has no real positive solutions. Finally, it remains to show that it does not have complex solutions with positive real part either. Let $\Lambda = x + iy$ be complex. Then, if $x \geq 0$ and if one sets $\Lambda_0 = \lambda + \frac{f_S(A_{df})}{A_{df}} S_{df}$, and

$$g(a) = \sigma e_S f_S(A_{df}) W(a)(d + v(a)) e^{-\int_0^a (d+v(\tau)+p_S\theta(\tau)+c(\tau))d\tau} \mu \frac{f_S(A_{df})}{A_{df}} S_{df},$$

it follows that $1 = |R(\Lambda)| = \left| \frac{\int_0^\infty g(a)e^{-xa}e^{-iya}da}{x+\Lambda_0+iy} \right| \leq \frac{\int_0^\infty g(a)e^{-xa}da}{x+\Lambda_0} = R(x) \leq R(0) = R_0$. Hence, if $R_0 < 1$ then the disease-free equilibrium is locally asymptotically stable, and if $R_0 > 1$ it is unstable. □

6.3 Numerical Results

In this section, we analyze how the dependence of R_0 on the disease-induced mortality (v) and extrinsic mortality (θp_S) due to predation is affected by clearance.

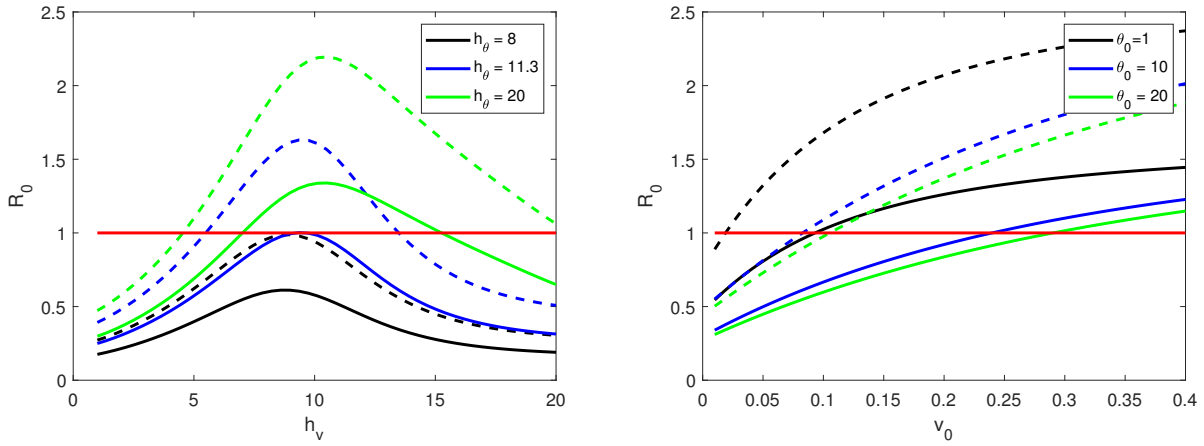

(a) (b)

Figure 6.3: The left panel shows R_0 as a function of h_v for various values of h_θ with $\theta_0 = 3$ when there is no clearance (dashed line) and there is clearance (solid line). The right panel shows R_0 as a function of v_0, for various values of θ_0. The red line is shown as reference to $R_0 = 1$.

Including clearance reduces the value of R_0 for all parameter values as expected. In Figure 6.3a, we compare the effect of the half-saturation constants on R_0 in the cases without clearance

(dashed lines) and with clearance (solid lines). From the panel on the left we see that the maximum value for R_0 happens when virulence kills the host in approximately 8-10 days (i.e. $h_v \approx 8-10$) regardless of their clearance status. When we include clearance we see that the predator is able to control the epidemic when it can detect its prey in less than $h_\theta \approx 11.3$ days, in contrast to $h_\theta \approx 8$ days in the absence of clearance. For the epidemic to ensue, the predator must detect the prey at a slower time scale and the pathogen should kill in approximately $5 \leq h_v \leq 15$ days. We see that the pathogen can reduce its success by killing the host too soon or too late and hence making infected individuals more visible to predators.

This general behavior remains in both cases and suggests that clearance has the same effect as delaying the detection of infected host by the predator for intermediate values of disease induced mortality. We study the effect of the maximum intensity of virulence (v_0) and predation (θ_0) in Figure 6.3b. We see that R_0 is an increasing function of v_0 and a decreasing function of θ_0. With clearance, as θ_0 increases the parasite needs higher values of v_0 in order for the epidemic to persist.

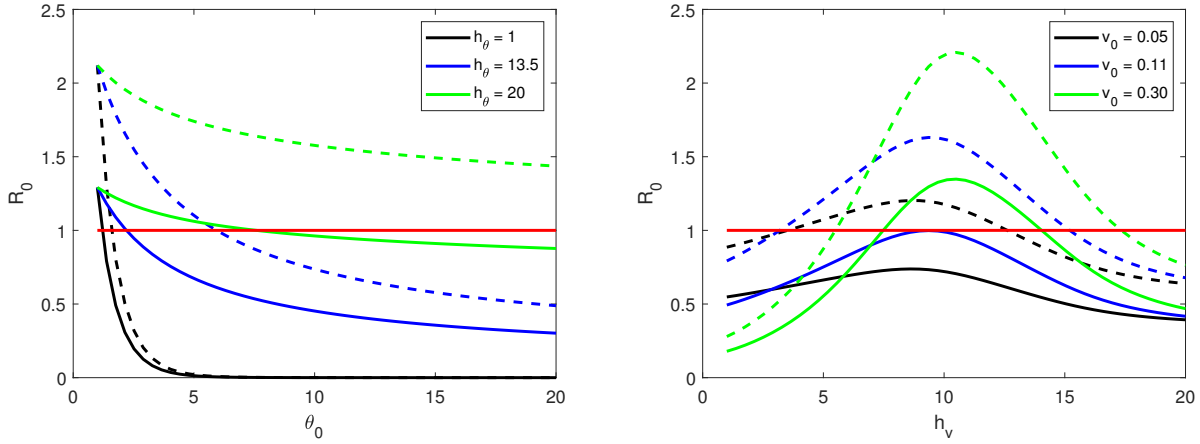

(a) (b)

Figure 6.4: The left panel shows R_0 as a function of v_0 for various values of θ_0 when there is no clearance. The right panel shows the same functional dependence of R_0 on v_0 for various values of θ_0 when we include clearance.

In Figure 6.4a, we compare the effect of the maximum predation intensity (θ_0) and predator detection (h_θ) on R_0. As θ_0 increases, R_0 decreases indicating that as predators eat infected hosts at a higher rate, it becomes more difficult for the pathogen to persist. In the presence to clearance, as h_θ increases the higher R_0 is, however lower values of θ_0 are needed in order to control the

disease. In particular, for late detection by the predator (i.e $h_\theta = 20$) we see that, when clearance is possible, there is a threshold of θ_0 for which the epidemic is controlled, $\theta_0 \leq 8$. We can compare the joint effect of maximum predation and virulence intensity in Figure 6.4b. In the case where there is no recovery, we see that there is a threshold in which if the pathogen kills too soon or too late the disease is contained. This is also the case when clearance is present if virulence is high enough. In contrast, when we include clearance, we notice that the disease is controlled for values of $v_0 \leq 0.11$, for all values of h_v. This indicates that no matter how fast the pathogen kills the host, if virulence is below this threshold, the disease will be contained.

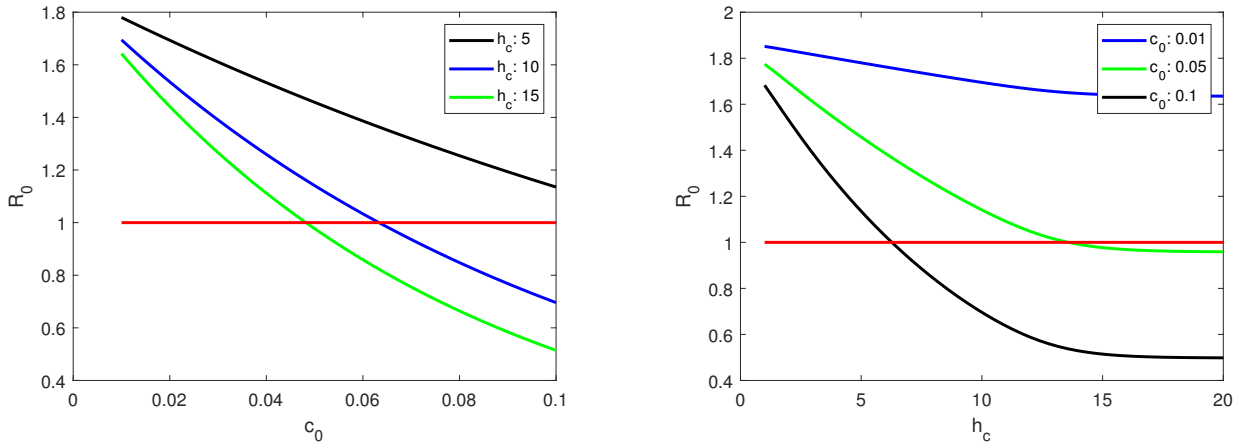

(a) (b)

Figure 6.5: (a) Clearance $c(a) = 0.5c_0(1 - \tanh(a - h_c))$ with a maximum value of $c_0 = 0.05$ and various half-saturation constants $h_c = \{5, 10, 15\}$. (b) R_0 as a function of h_c for various values of c_0 when $\theta_0 = 3$. The default values for the following sections will be $c_0 = 0.05$ and $h_c = 10$.

Prevalence

Prevalence which is estimated as the proportion of infected individuals in the population, $P = \dfrac{Q_e}{S_e + Q_e}$, is an indicator of the burden of a disease in a population. Here, we show how prevalence depends on our model parameters and how it's affected by clearance. In Figures (6.6)–(6.9) by including clearance, prevalence is reduced for all our parameters. Thus we will focus on the the implications of clearance in the viable parameter ranges for which we observe the endemic equilibrium. For example, as shown in Figure 6.6a, higher values of the maximum virulence v_0 (i.e. $v_0 \gtrsim 0.15$) are needed to observe the endemic equilibrium. This is due to the fact that as v_0 increases so does the infected population Q_e while the susceptible population S_e decreases.

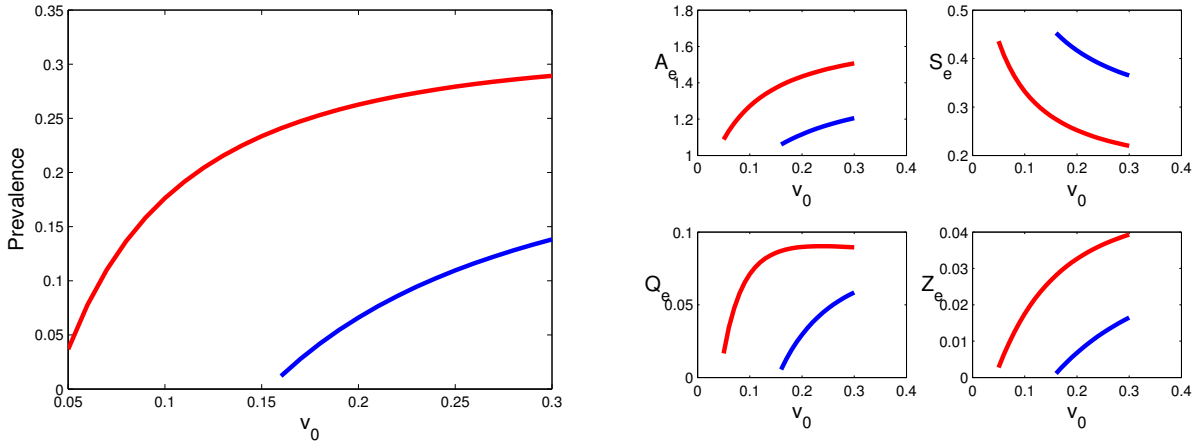

(a) (b)

Figure 6.6: The left panel shows disease prevalence as a function of v_0, and the four panels on the right show the dependence of the endemic equilibrium values on v_0. The red line denotes the instance with no recovery and the blue line with recovery.

In Figure 6.7a, prevalence as a function of h_v displays an increment to a maximum at intermediate values of $h_v \approx 11$ at which point it begins to decrease. At this optimal value, we see that the susceptible population experiences a minimum, while the total infected populations reaches a maximum. In both cases, if the parasite kills the host too soon or too late, (i.e. h_v too low or too high) prevalence is zero. However when clearance is included, we can observe the endemic state for a more narrow range of values of h_v. Thus, when clearance is present, for the pathogen to prevail in the system it needs to kill the host between a period of 8 to 13 days ($h_v \in [8, 13]$) rather than 5 to 17 days ($h_v \in [7, 14]$) in the absence of clearance.

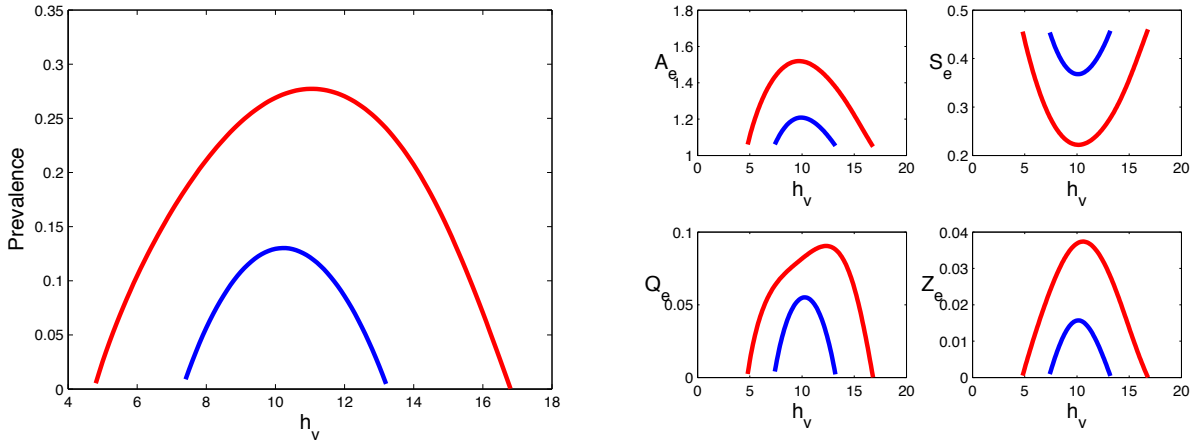

(a) (b)

Figure 6.7: The left panel shows disease prevalence as a function of h_v and the four panels on the right show the dependence of the endemic equilibrium values on h_v. The red line represents when there is no recovery, the blue line when there is recovery.

As seen in Figure 6.8a, predators reduce disease prevalence by reducing the infected population and increasing the susceptible population. Interestingly, the most dramatic effect of clearance can be seen in the maximum predation detection, where only for $\theta_0 \lesssim 8$, the endemic state persists. This indicates that when clearance is possible, lower values of predator intensity are enough to end the epidemic.

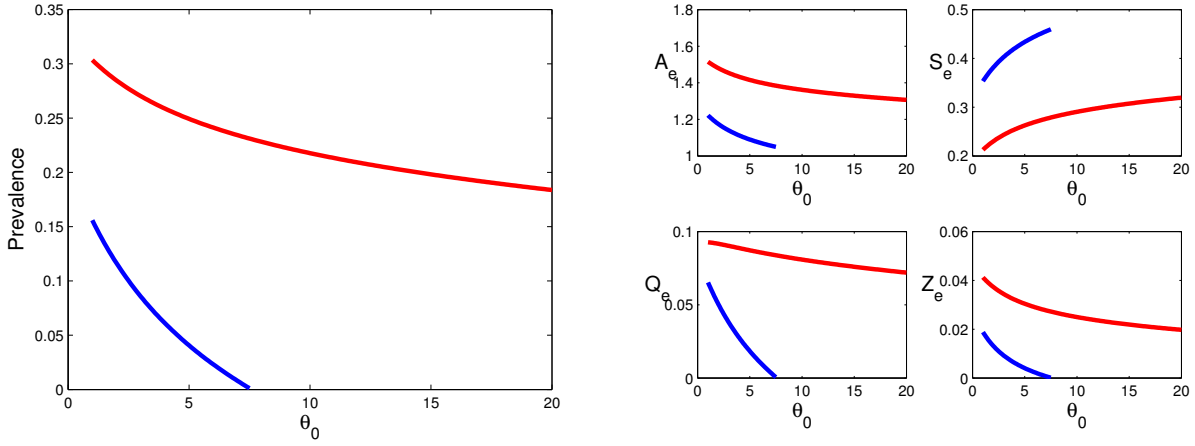

(a) (b)

Figure 6.8: The left panel shows disease prevalence as a function of θ_0 , and the four panels on the right show the dependence of the endemic equilibrium values on θ_0.

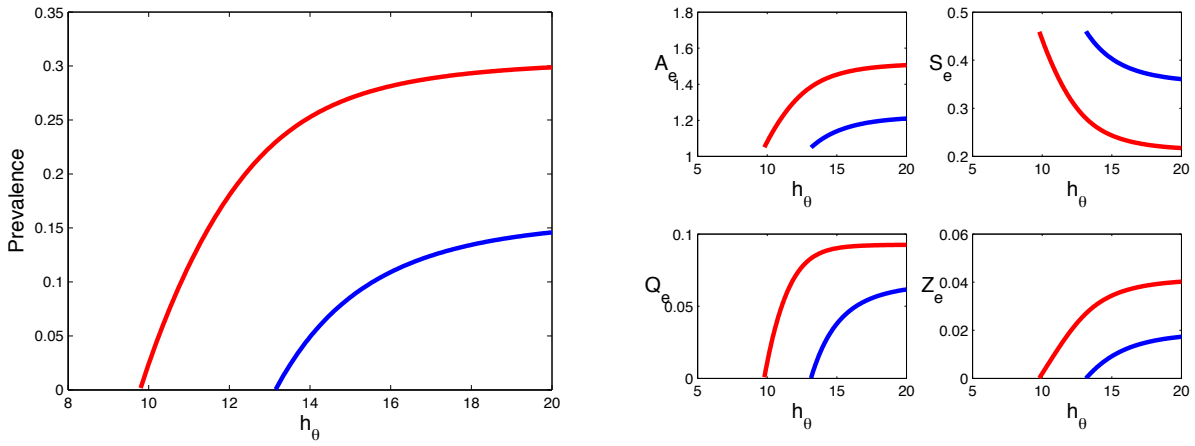

(a) (b)

Figure 6.9: The left panel shows disease prevalence as a function of h_θ when there is recovery, and the four panels on the right show the dependence of the endemic equilibrium values on h_θ.

Finally in Figure 6.9a, we see that prevalence increases with h_θ. Both the total population of infected Q_e and density of spore increase with h_θ, however the susceptible population decreases. Combining Figure 6.8b and 6.9b we see that the predator needs to kills with high intensity and speed to have the maximum effect in reducing disease prevalence. When including clearance, the values for which this maximum reduction occurs are shifted, and the predator must kill the host at a latter time in order for the endemic state to persist, $h_\theta \gtrsim 13$ days.

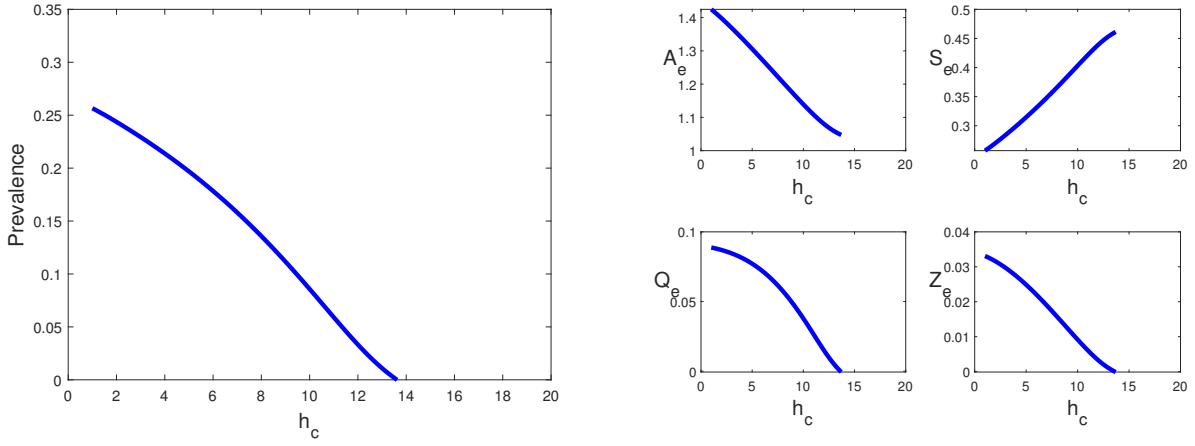

(a) (b)

Figure 6.10: The left panel shows disease prevalence as a function of h_c and the four panels on the right show the dependence of the endemic equilibrium values on h_c.

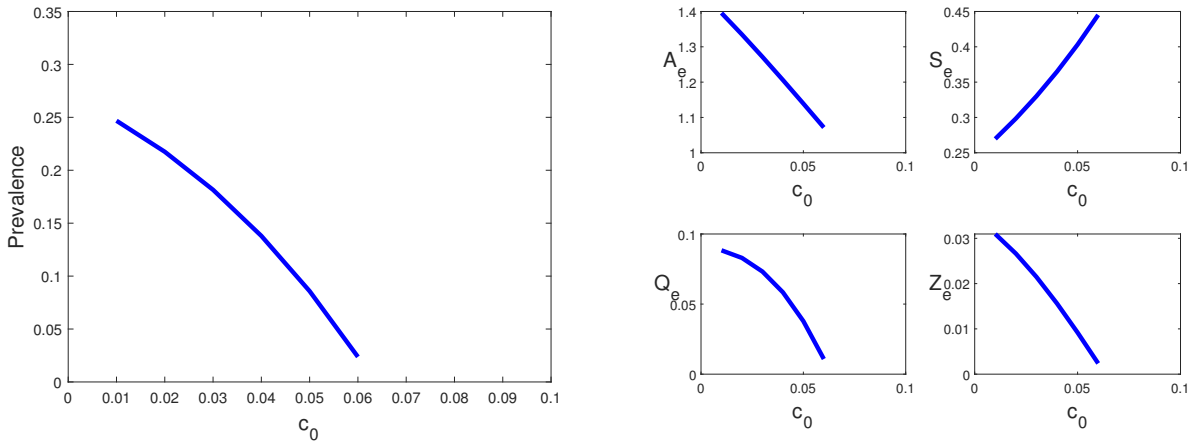

(a) (b)

Figure 6.11: The left panel shows disease prevalence as a function of c_0 and the four panels on the right show the dependence of the endemic equilibrium values on c_0.

In Figure 6.11, we analyze how the speed of clearance and it's intensity impact disease prevalence. Prevalence is a decreasing function of both c_0 and h_c. As the intensity of clearance increases the total population of infected Q_e and spore density Z_e decrease while the susceptible population increases. A similar behavior is observed as h_c increases (i.e. when as infected clear the infection faster). This suggest clearance decrease disease prevalence and might indicate optimal immune responses that would allow the host population to suppress the pathogen in the system.

6.4 Discussion–Future Directions

By using a PDE epidemiological model that incorporates clearance along with mortality as a function of age since infection, we have computed relevant quantities R_0 and infection prevalence. We have shown that clearance suppresses the intensity of an infection and in combination with high intensity of virulence and predation can lead to the termination of an epidemic. In [77], an age since infection model without clearance was analyzed and we used it as a basis of comparison to our model. Qualitatively, these models do not differ much in their behavior.

Modeling clearance as a function of age of infection decreases the basic reproduction number R_0 and reduces disease prevalence which is expected when including a recovery mechanism in a system. However, the parameter regions that lead to the persistence of the pathogen are significantly

reduced. This implies that to persist the pathogen needs to become more virulent and at intermediate rates. On the opposite end, predators, which for our system tend to suppress infection, must detect the infected prey at a lower rate and a higher intensity for the pathogen to persist. In fact, higher predation intensity is shown to terminate an epidemic which was not possible without clearance for the parameter values considered. These findings can be used to further understand the evolution of virulence and possibly other parameters in our system.

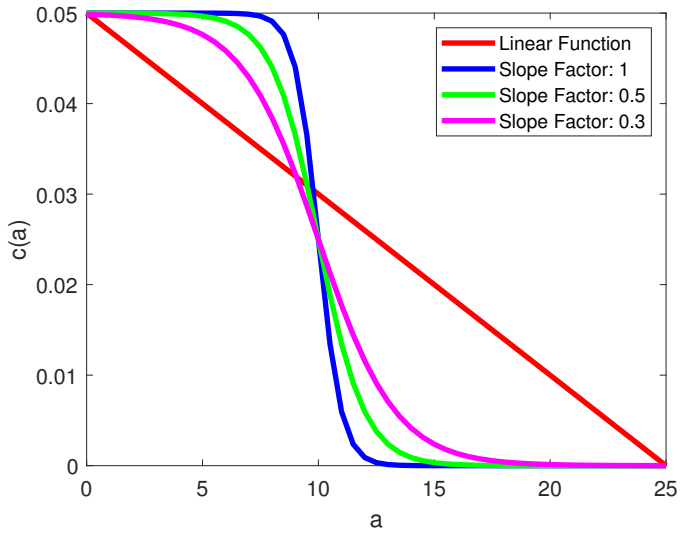

Figure 6.12: Different shapes for clearance as a function of age since infection: Linear (red), $c(a) = 0.5c_0(1 - \tanh(m(a - h_c)))$, where m denotes a factor which alters the slope of the curve.

Future directions for this work could include studying the $SEIZAS$ model introduced in Chapter 4 under this framework. As discussed in Chapter 4, resistance is due to a physical barrier (i.e. the host's gut thickness) and thus would not depend on age since infection. Finally, experimental data could lead to more realistic descriptions of clearance as a function of age since infection for our system. Thus, studying different shapes for clearance and their effect on R_0 and prevalence might be an useful proxy while more data is gathered.

Chapter 7

Conclusions

In Chapter 2, we showed that the short-term evolution of hosts, can lead to the termination of an epidemic and reduced peak disease prevalence. Assuming an explicit trade-off among virulence and two traits: host susceptibility and predator selectivity; we showed virulence evolves to a lower value and increases disease prevalence. In Chapter 3, we analyzed the effect of long-term evolution of host in our system. We determined regions of coexistence between a resident host and a mutant invader by assuming an implicit trade-off among relevant parameters such as virulence, predator selectivity, host susceptibility. While regions of coexistence are possible in our system, the traits considered evolve to an optimal value; thus, evolutionary branching under our assumptions is not possible for our system.

In Chapter 4, we studied how immune responses and physiological barriers impact the disease dynamics of our system. These recovery mechanisms reduce disease prevalence and the number of secondary infections. In the absence of recovery, our system exhibits damped oscillations. Once recovery is introduced, these oscillations begin to dampen at a faster rate. This inspired us to incorporate demographic stochasticity in our model. By using a stochastic differential equation formulation, we capture two behaviors: sustained oscillations and extinction of the disease in Chapter 5. In Chapter 6, we show that clearance as a function of age since infection, leads to a reduction in secondary infections and disease prevalence. However, when compared with a model without clearance, its qualitative behavior does not change significantly.

One of the most exciting aspects of this work is that it opens the door to new biological questions to address. Using new experimental data, we could identify appropriate trade-offs for our system. There is evidence that trade-offs among recovery, virulence, and host-susceptibility are possible ([3], [25], [34]). In addition, we could use these two frameworks to study the evolution of host immunity through our models [40].

Appendix A

In this Appendix, we provide the expression for the equilibrium densities for the two models proposed in Chapter 2 and Chapter 3. The parameters for the SI model are given in Table A.1 while the parameters for the SIZA model are given in Table A.2.

A.1 Equilibrium Points

Using equations (2.1)–(2.2), we obtain that the endemic equilibrium of our SI model is given by,

$$\begin{aligned} S^* &= \frac{(d+v+\theta p_S)}{\beta} \\ I^* &= \frac{b\rho-(\beta+bc+bc\rho)S^*+\sqrt{(b\rho-(\beta+bc+bc\rho)S^*)^2+4bc\rho(b-(d+p_S+bcS^*)S^*)}}{2bc\rho} \end{aligned} \tag{A.1}$$

Using equations (3.17)–(3.19) we obtain that the endemic equilibrium of our SIZA model is given by,

$$S^* = \frac{(d+v+\theta p_S)A^*}{\mu f_S(A^*)}\frac{\lambda+r(1-\frac{A^*}{K})}{\sigma e_S f_S(A^*)(d+v)}, \tag{A.2}$$

$$I^* = \frac{1}{R(A^*)}\frac{r(1-\frac{A^*}{K})A^*(e_S f_S(A^*)-e_S f_S(A_{df}))}{f_S(A^*)(d+v+\theta p_S-\rho e_S f_S(A^*))}, \tag{A.3}$$

$$Z^* = \frac{(d+v+\theta p_S)A^*}{\mu f_S(A^*)}\frac{e_S(f_S(A^*)-f_S(A_{df})}{d+v+\theta p_S-\rho e_S f_S(A^*)}.$$

For the equilibrium points to be biologically feasible, the expressions (A.3)–(A.4) must be greater than or equal to zero. Since $f_S(A)$ is an increasing function of algae, if $A_{df} < A^*$, then $d+v+\theta p_S-\rho e_S f_S(A^*) > 0$.

Finally, we solving equation (3.19) leads to a cubic polynomial expression for A^* given by $p(A) = a_3A^3+a_2A^2+a_1A+a_0 = 0$ the coefficients of the polynomial are given by,

$$
\begin{aligned}
a_3 &= r(d+v+\theta p_S)(v+(\theta-1)p_S+e_S f_{S_0}(1-\rho)) - r\mu\sigma e_S f_{S_0}(d+v)(d+v+\theta p_S-\rho e_S f_{S_0}),\\
a_2 &= r\mu\sigma e_S f_{S_0}(d+v)((d+v+\theta p_S-rhoe_S f_{S_0})K-(d+v+\theta p_S)h_S)\\
&+ r(d+v+\theta p_S)(v+(\theta-1)p_S)h_S\\
&- (v+(\theta-1)p_S+e_S f_{S_0}(1-\rho))(d+v+\theta p_S)((\lambda+r)K-rh_S), \qquad \text{(A.4)}\\
a_1 &= (d+v+\theta p_S)(r\mu\sigma e_S f_{S_0}(d+v)Kh_S-(v+(\theta-1)p_S)((\lambda+r)K-rh_S)h_S\\
&- (\lambda+r)(v+(\theta-1)p_S+e_S f_{S_0}(1-\rho))Kh_S),\\
a_0 &= -(d+v+\theta p_S)(\lambda+r)(v+(\theta-1)p_S)Kh_S^2.
\end{aligned}
$$

A.2 Parameters

Variable	**Unit**
t time	day
$S(t)$ susceptible hosts	nL^{-1}
$I(t)$ infected hosts	nL^{-1}
Parameter	**Value**
b : maximum birthrate	0.4 /day
c : density-dependent reduction in host fecundity	0.05 nL^{-1}
d : background mortality	0.05 /day
f : fecundity reduction due to infection	0.75
p_S: fish predation rate	0.03 /day
θ: selective predation parameter	9
v: virulence	0.05 /day
V_c: clonal variability	0-0.02

Table A.1: Variables and parameters for SI model. The values of the various parameters, unless specified in the text, are the ones given in [45].

SIZA and SIEZA Model

Variable	**Unit**
t time	day
$S(t)$ susceptible hosts	mg C/L
$E(t)$ exposed hosts	mg C/L
$I(t)$ infected hosts	mg C/L
$Z(t)$ fungal spores	mg C/L
$A(t)$ algae	mg C/L
Parameter	**Value**
e_S : conversion efficiency	0.6 mg C / mg C
f_{S_0} : maximal feeding rate	0.32/day mg C/mg C
h_S : half saturation constant	0.50 mg C/L
ρ : fecundity reduction due to infection	0.9
p_S : predation rate	0.1/day
d : background mortality	0.03/day
μ : per spore infectivity	10 mg C/mg C
v : virulence	0.05 /day
θ : selective predation parameter	3
γ : resistance rate	0.1, 0 – 0.6/day (*)
c: clearance	0.12, 0 – 0.6/day (*)
α : infection rate	0.5/day
σ : spore release parameter	31 days × mg C / mg C × mg C/L
λ : spore loss rate	0.2/day
r : algal net maximal growth rate	0.2/day
K : algal carrying capacity	2.0 mg C/L

Table A.2: Variables and parameters for $SEIZA$ model. The values of the various parameters, unless specified in the text, are the ones given in [30]. (*) Denotes parameters considered in this study.

A.3 A Biologically Motivated Approach

To give a more meaningful interpretation of our invasion fitness function we use a method provided in ([25], [69]). We can verify both these derivations, by using linear stability analysis which we explain in detail in Chapter 3. Consider an attempted invasion, characterized by the alone densities, i.e. where the mutant strain is alone in the host population. Assume the invader is initially uninfected and suppose it remains infected for a period of time T_S and that it becomes infected for a period of time T_I. Let R_S and R_I denote the growth rates for S_m and I_m during these time periods. We want to find the average increase in the mutant population per invader. If this expression is positive then the invasion will be successful. Our invasion fitness function will be then given by $s_p(p_m) = R_S T_S + R_I T_I$, where p and p_m denote the parameters corresponding to the

resident and mutant traits respectively. We compute R_S and R_I by considering the growth rate of net change due to births and deaths of susceptible and infected classes.

SI model

At the equilibrium given by $(S^*, I^*, 0, 0)$, we obtain the following expressions for the SI model,

$$\begin{aligned} R_S &= \frac{\partial}{\partial S_m}\left[b_m(S_m+\rho_m I_m)(1-c_m N)-(d+p_S)S_m\right]\Big|_{(S^*,I^*,0,0)} = b_m(1-c_m(S^*+I^*))-(d+p_S) \\ R_I &= \frac{\partial}{\partial I_m}\left[b_m(S_m+\rho_m I_m)(1-c_m N)-(d+v_m+\theta_m p_S)I_m\right]\Big|_{(S^*,I^*,0,0)} \\ &= b_m\rho_m(1-c_m(S^*+I^*))-(d+v_m+\theta_m p_S) \qquad \text{(A.5)} \\ T_S &= \frac{1}{\frac{\partial}{\partial S_m}\left[(d+p_S)S_m+\beta_m S_m(I+I_m)\right]}\Big|_{(S^*,I^*,0,0)} = \frac{1}{d+p_S+\beta_m I^*} \end{aligned}$$

Since the only possibilities for the invader to die is when it remains uninfected or infected, we can use the following relationship to determine T_I,

$$\overbrace{(d+p_S)T_S}^{\substack{\text{Probability of}\\ \text{dying while uninfected}}} + \overbrace{(d+v_m+\theta_m p_S)T_I}^{\substack{\text{Probability of}\\ \text{dying while infected}}} = 1, \text{ we obtain,}$$

$$T_I = \frac{(d+p_S+\beta_m I^*)-(d+p_S)}{(d+p_S+\beta_m I^*)(d+v_m+\theta_m p_S)} = \frac{\beta_m I^*}{(d+p_S+\beta_m I^*)(d+v_m+\theta_m p_S)}$$

Omitting the common positive factor, our invasion fitness function for the mutant is,

$$s_p(p_m) = b_m(1-c_m N^*)-(d+p_S)+\frac{\beta_m I^*}{(d+v_m+\theta_m p_S)}(b_m\rho_m(1-c_m(N^*))-(d+v_m+\theta_m p_S)) \quad \text{(A.6)}$$

SIZA model

Now, consider an attempted invasion, characterized by the alone densities, i.e. where the mutant strain is alone in the host population, S^*, I^*, Z^* and A^*. As in [25], we want to find the average increase in the resident population per invader since if this is positive then the invasion will be successful. Assume the invader is initially uninfected and suppose it remains uninfected for a period of time T_S and that it becomes infected for a period of time T_I. Let R_S and R_I denote the growth

rates for S and I during these time periods. At the equilibrium $(S^*, I^*, Z^*, A^*, 0, 0)$ we obtain,

$$\begin{aligned} R_S &= \frac{d}{dS_m}\left[e_S f_{S_m}(A)(S_m + \rho_m I_m) - (d + p_S)S_m\right] = e_S f_{S_m}(A^*) - (d + p_S) \\ R_I &= e_S f_{S_m}(A^*)\rho_m - (d + v_m + \theta_m p_S) \\ T_S &= \left(\frac{d}{dS_m}\left[(d + p_S)S_m + \mu_1 \frac{f_{S_m}(A)}{A} S_m Z\right]\right)^{-1} = \left((d + p_S) + \mu_m \frac{f_{S_m}(A^*)}{A^*} Z\right)^{-1} \end{aligned}$$

Note, that the probability of the invader dying while uninfected is given by $(d + p_S)T_S$ and the probability of dying while infected is $(d + v_m + \theta_m p_S)T_I$. Since these are the only two possibilities we have, $(d + p_S)T_S + (d + v_m + \theta_m p_S)T_I = 1$, solving for T_I we obtain,

$$T_I = \left(1 - \frac{(d + p_S)}{(d + p_S) + \mu_m \frac{f_{S_m}(A^*)}{A^*} Z^*}\right) \times \frac{1}{(d + v_m + \theta_m p_S)} = \frac{\mu_1 \frac{f_{S_m}(A^*)}{A^*} Z^*}{(d + p_S + \mu_m \frac{f_{S_m}(A^*)}{A^*} Z^*)(d + v_m + \theta_m p_S)}$$

Thus, the number of off-springs per invader is:

$$s_p(p_m) = R_S T_S + R_I T_I = \frac{e_S f_{S_m}(A^*) - (d + p_S)}{\left(d + p_S + \mu_m \frac{f_{S_m}(A^*)}{A^*} Z^*\right)} + \frac{(e_S f_{S_m}(A^*)\rho_m - [d + v_m + \theta_m p_S])\mu_m \frac{f_{S_m}(A^*)}{A^*} Z^*}{(d + p_S + \mu_m \frac{f_{S_m}(A^*)}{A^*} Z^*)(d + v_m + \theta_m p_S)}$$

Neglecting the positive common factor we obtain,

$$s_p(p_m) = e_S f_{S_m}(A^*) - (d + p_S) + (e_S f_{S_m}(A^*)\rho_m - (d + v_m + \theta_m p_S))\frac{\mu_m \frac{f_{S_1}(A^*)}{A^*} Z^*}{(d + v_m + \theta_m p_S)}$$

which shows invasion at equilibrium is successful if and only if $s_p(p_m)$ is positive. Here p, p_m denote the parameter values for the resident and mutant populations respectively. Note, even though this expression explicitly depends on the equilibrium densities of the resources (i.e. algae and spores), S^* and I^* will appear implicitly in Z^* and A^*.

A.4 Trade-off Invasibility Plots

Since the feeding rate $f_S(A)$ is a function of algae, we expect that the carrying capacity K will play a role in our results. In this section, we show how the coexistence regions shown in Figure 3.6 change for different values of carrying capacity for the algae K.

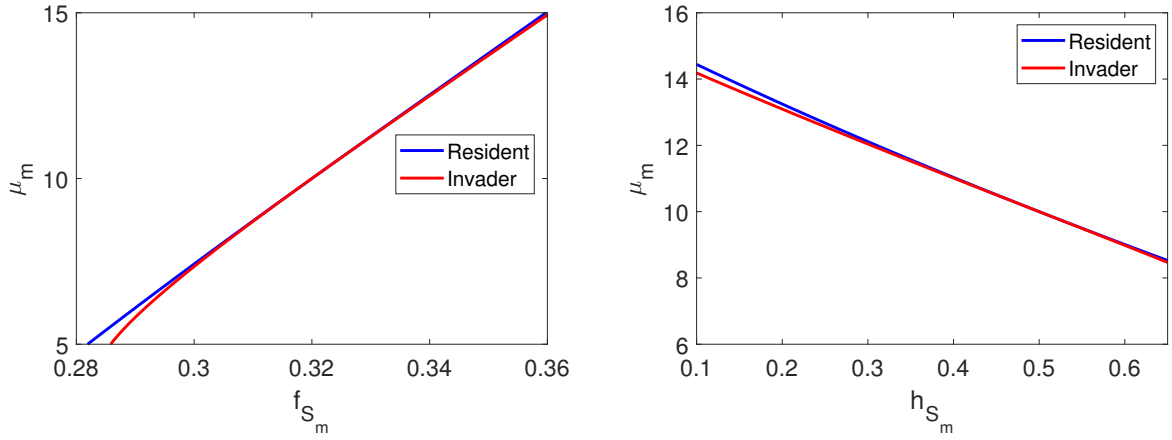

(a) (b)

Figure A.1: Trade-off invasibility plot (TIP) parameters related to per spore infectivity. We compare the outcomes for different levels of infectivity (μ_m) versus (a) the maximal feeding rate (f_{S_m}), and (b) half-saturation constant (h_{S_m}). Default values are $(f_{S_m}, \mu_m) = (0.32, 10)$, $(h_{S_m}, \mu_m) = (0.05, 10)$, and carrying capacity $K = 4$.

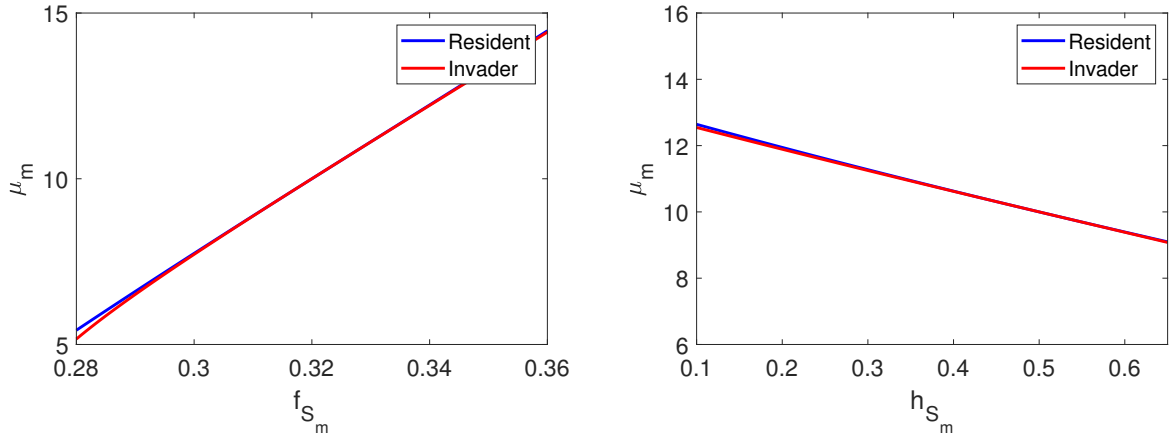

(a) (b)

Figure A.2: Trade-off invasibility plot (TIP) parameters related to per spore infectivity. We compare the outcomes for different levels of infectivity (μ_m) versus (a) the maximal feeding rate (f_{S_m}), and (b) half-saturation constant (h_{S_m}). Default values are $(f_{S_m}, \mu_m) = (0.32, 10)$, $(h_{S_m}, \mu_m) = (0.05, 10)$, and carrying capacity $K = 6$.

This suggests that as the carrying capacity K increases the parameter regions for coexistence become smaller.

Appendix B

B.1 Endemic Equilibria

To find our endemic equilibrium, we solve equation (4.5) for A_e which after calculations will be a root of the following cubic polynomial, $p(A_e) = a_3A_e^3 + a_2A_e^2 + a_1A_e + a_0 = 0$ where,

$$
\begin{aligned}
a_3 &= r\alpha(d+p_S+\gamma+\alpha)(d+v+\theta p_S+c)(v+(\theta-1)p_S) \\
a_2 &= \alpha(2h_Sr-K(\lambda+r))(d+p_S+\gamma+\alpha)(d+v+\theta p_S+c)^2 \\
&+ [(d+p_S+\gamma+\alpha)(K\alpha(c+d+p_S)(\lambda+r) \\
&- 2\alpha rh_S+\alpha\sigma e_S(d+v)f_{S_0}\mu r(e_Sf_{S_0}-(d+p_S+\alpha)](d+v+\theta p_S+c) \\
&+ \sigma e_S(d+v)\mu r\alpha^2f_{S_0}(e_Sf_{S_0}+c) \\
a1 &= \alpha h_S(h_Sr-2K(\lambda+r))(d+p_S+\gamma+\alpha)(d+v+\theta p_S+c)^2 \\
&+ [\alpha(d+p_S+\gamma+\alpha)h_S(d+p_S+c)(-h_Sr+2K(\lambda+r)) \\
&+ \alpha\sigma e_S(d+v)f_{S_0}\mu r(K((d+p_S+\alpha)-e_Sf_{S_0})+\gamma h_S(-(d+p_S+\gamma+\alpha)+1))](d+v+\theta p_S+c) \\
&+ \alpha^2\sigma e_S(d+v)f_{S_0}\mu r(h_Sc-K(c+e_Sf_{S_0})) \\
a_0 &= -Kh_S^2\alpha(\lambda+r)(d+p_S+\gamma+\alpha)(d+v+\theta p_S+v)^2 \\
&+ K\alpha h_S[(h_S(\lambda+r)(c+d+p_S)(d+p_S+\gamma+\alpha)+\sigma e_S(d+v)f_S\mu r(1-\gamma))(d+v+\theta p_S+c) \\
&- \alpha c\sigma e_S(d+v)f_S\mu r]
\end{aligned}
$$

B.2 Stability of Equilibria

In the Chapter 4, we used linear stability analysis to determine the stability our equilibrium points. For the disease-free equilibrium we used the Routh-Hurwitz criterion which we state here for completeness [71].

Definition B.2.1. Given a real polynomial, $P(\lambda) = a_0\lambda^n + a_1\lambda^{n-1} + \cdots + a_{n-1}\lambda + a_5$, the $n \times n$

square matrix,

$$H = \begin{bmatrix} a_1 & a_3 & a_5 & \cdots & 0 \\ a_0 & a_2 & a_4 & \cdots & 0 \\ 0 & a_1 & a_3 & \cdots & 0 \\ \vdots & \vdots & \vdots & \ddots & \vdots \\ 0 & 0 & 0 & \cdots & a_n \end{bmatrix}$$

is called the Hurwitz matrix corresponding to the polynomial $P(\lambda)$.

Definition B.2.2. The leading principal minors are the determinants of the upper left $1 \times 1, 2 \times 2, ..., n \times n$ submatrices of H_n, the upper left $k \times k$ minors are denoted Δ_k for $k = 1, 2, ..., n$. For example, the leading principal minors of the Hurwitz matrices H_1, H_2, and H_3 respectively are:

$$\Delta_1 = |a_1|, \Delta_2 = \begin{vmatrix} a_1 & a_3 \\ a_0 & a_2 \end{vmatrix}, \Delta_3 = \begin{vmatrix} a_1 & a_3 & a_5 \\ a_0 & a_2 & a_4 \\ 0 & a_1 & a_3 \end{vmatrix}.$$

Theorem B.2.1. *(Routh-Hurwitz Criterion) The eigenvalues of a Jacobian matrix J all have negative real part if and only if all of the coefficients of the characteristic polynomial of J are positive and all leading principal minors of the Hurwitz matrix corresponding to the characteristic polynomial are also positive.*

In this section, we give the expression for the full Jacobian matrix for our system. Here we denote N by the total host population, $N = S + E + I$. The stability analysis presented in the main text is performed by evaluating J at each equilibrium point and computing its eigenvalues.

$$J = \begin{bmatrix} e_S f_S(A) - (d+p_S) - \mu\frac{f_S(A)}{A}Z & e_S f_S(A) + \gamma & \rho e_S f_S(A) + c & -\mu\frac{f_S(A)}{A}S & e_S f_S'(A)(S+E+\rho I) - \mu\Big(\frac{f_S(A)}{A}\Big)'SZ \\ \mu\frac{f_S(A)}{A}Z & -(d+p_S+\alpha+\gamma) & 0 & \mu\frac{f_S(A)}{A}S & -\mu\Big(\frac{f_S(A)}{A}\Big)'SZ \\ 0 & \alpha & -(d+v+\theta p_S+c) & 0 & 0 \\ -\frac{f_S(A)}{A}Z & -\frac{f_S(A)}{A}Z & \sigma e_S\frac{f_S(A)}{A}(d+v) - \frac{f_S(A)}{A}Z & -\lambda - \frac{f_S(A)}{A}N & \sigma e_S f_S'(A)(d+v)I - \Big(\frac{f_S(A)}{A}\Big)'NZ \\ -f_S(A) & -f_S(A) & -f_S(A) & 0 & r\Big(1-\frac{2A}{K}\Big) - f_S'(A)N \end{bmatrix}$$

At the disease-free equilibrium, $E_{df} = (S_{df}, 0, 0, 0, A_{df})$ we have,

$$J\Big|_{E_{df}} = \begin{bmatrix} 0 & e_S f_S(A_{df})+\gamma & \rho e_S f_S(A_{df})+c & -\mu\frac{f_S(A_{df})}{A_{df}}S_{df} & e_S f'_S(A_{df})S_{df} \\ 0 & -(d+p_S+\alpha+\gamma) & 0 & \mu\frac{f_S(A_{df})}{A_{df}}S_{df} & 0 \\ 0 & \alpha & -(d+v+\theta p_S+c) & 0 & 0 \\ 0 & 0 & \sigma e_S\frac{f_S(A_{df})}{A_{df}}(d+v) & -\lambda-\frac{f_S(A_{df})}{A_{df}}S_{df} & 0 \\ -f_S(A_{df}) & -f_S(A_{df}) & -f_S(A_{df}) & 0 & r\Big(1-\frac{2A_{df}}{K}\Big)-f'_S(A_{df})S_{df} \end{bmatrix}$$

At the endemic equilibrium $(S^*, E^*, I^*, Z^*, A^*)$,

$$\begin{aligned} e_S f_S(A^*)\left(S^*+E^*+\rho I^*\right) - (d+p_S)S^* - \mu\frac{f_S(A^*)}{A^*}S^*Z^* + cI^* + \gamma E^* &= 0 \\ \mu\frac{f_S(A^*)}{A^*}S^*Z^* - (d+p_S+\gamma+\alpha)E^* &= 0 \\ \alpha E^* - (d+v+\theta p_S+c)I^* &= 0 \\ \sigma e_S\frac{f_S(A^*)}{A^*}(d+v)I^* - \lambda Z^* - f_S(A^*)\left(S^*+E^*+I^*\right)\frac{Z^*}{A^*} &= 0 \\ r\left(1-\frac{A^*}{K}\right)A^* - f_S(A^*)\left(S^*+E^*+I^*\right) &= 0 \end{aligned} \tag{B.1}$$

From which we obtain some useful equalities,

$$\frac{E^*}{S^*} = \frac{e_S(f(A^*)-f(A_{df}))}{d+p_S+\alpha-e_S f_S(A^*)+\frac{\alpha(\rho e_S f_S(A^*)+c)}{d+v+\theta p_S+c}}$$

The jacobian matrix evaluated at the endemic equilibrium can be rewritten as,

$$\begin{bmatrix} e_S f_S(A^*)-(d+p_S)-\mu\frac{f_S(A^*)}{A^*}Z^* & e_S f_S(A^*)+\gamma & \rho e_S f_S(A^*)+c & -\mu\frac{f_S(A^*)}{A^*}S^* & e_S f'_S(A)(S+E+\rho I)-\frac{(d+p_S+\gamma+\alpha)}{h_S+A^*}E^* \\ \mu\frac{f_S(A^*)}{A^*}Z^* & -(d+p_S+\alpha+\gamma) & 0 & \mu\frac{f_S(A^*)}{A^*}S^* & \frac{(d+p_S+\gamma+\alpha)}{h_S+A^*}E^* \\ 0 & \alpha & -(d+v+\theta p_S+c) & 0 & 0 \\ -\frac{f_S(A^*)}{A^*}Z^* & -\frac{f_S(A^*)}{A^*}Z^* & \frac{f_S(A)}{A}(\sigma e_S(d+v)-Z^*) & -(\lambda+r(1-\frac{A^*}{K})) & -\frac{\lambda Z^*}{h_S+A} \\ -f_S(A^*) & -f_S(A^*) & -f_S(A^*) & 0 & \frac{A^*r(K-h_S-2A^*)}{K(h_S+A^*)} \end{bmatrix}$$

Due to the complexity of the expressions found for the endemic equilibrium, we were not able to find explicit expressions for the eigenvalues of the Jacobian matrix evaluated at the endemic equilibrium.

B.3 Elasticity Analysis

The analytic expressions for the elasticity analysis in Chapter 4 are given below.

$$I_{\alpha}^{R_0} = \frac{d+\gamma+p_S}{d+p_S+\gamma+\alpha}$$

$$I_{c}^{R_0} = \frac{-c}{d+v+\theta p_S+c}$$

$$I_{d}^{R_0} = \frac{d}{d-e_S f_S+p_S} - \frac{d}{(\alpha+d+\gamma+p_S)} + \frac{d}{d+v} - \frac{d}{c+d+p_S\theta+v}$$
$$- \frac{d(e_S f_S h_S \lambda K)}{((h_S r(d+p_S)+(\lambda+r)K(d+p_S-e_S f_S)))(h_S(d+p_S)-K(d+p_S-e_S f_S)))}$$

$$I_{e_S}^{R_0} = -\frac{[e_S f_S((K^2(\lambda+r)+(h_S^2 r+2Kh_S r))(d^2+p_S^2)+K^2(e_S^2 f_S^2+2dp_S-2e_S f_S(d+p_S))(\lambda+r)}{((d+p_S-e_S f_S)((K+h_S)(d+p_S)-Ke_S f_S)(K(\lambda+r)(d+p_S Ke_S f_S)+h_S r(d+p_S)))}$$
$$- \frac{2Kh_S r(e_S f_S(d+p_S)-2dp_S)+2dh_S^2 p_S r)]}{((d+p_S-e_S f_S)((K+h_S)(d+p_S)-Ke_S f_S)(K(\lambda+r)(d+p_S Ke_S f_S)+h_S r(d+p_S)))}$$

$$I_{f_{S_0}}^{R_0} = I_{e_S}^{R_0}$$

$$I_{\gamma}^{R_0} = \frac{-\gamma}{\alpha+d+\gamma+p_S}$$

$$I_{h_S}^{R_0} = -\frac{((e_S^2 f_S^2 K^2(\lambda+r)-2e_S f_S K(h_S r+K(\lambda+r))(d+p_S)+(d^2+2dp_S+p_S^2)(h_S^2 r+2h_S Kr+K^2(\lambda+r)))}{((-e_S f_S K+(d+p_S)(h_S+K))(dh_S r+h_S p_S r+dK(\lambda+r)-e_S f_S K(\lambda+r)+Kp_S(\lambda+r))))}$$

$$I_{K}^{R_0} = -\frac{Kh_S\lambda(d+p_S)(d+p_S-e_S f_S)}{((K+h_S)(d+p_S)-Ke_S f_S)(K(\lambda+r)(d+p_S-Ke_S f_S)+h_S r(d+p_S))}$$

$$I_{\lambda}^{R_0} = \frac{-K\lambda(d+p_S-e_S f_{S_0})}{K(\lambda+r)(d+p_S-Ke_S f_{S_0})+h_S r(d+p_S)}$$

$$I_{\mu}^{R_0} = 1$$

$$I_{p_S}^{R_0} = \frac{-p_S}{(\alpha\mu(d-e_S f_S+p_S)^2 r\sigma(d+v)(e_S f_S K-(d+p_S)(h_S+K))^2))}$$
$$\times [(d+p_S+\gamma+\alpha)(d+v+\theta p_S+c)(h_S(d+p_S)+(d+p_S-e_S f_{S_0})]$$

$$I_{r}^{R_0} = \frac{K\lambda(d+p_S-e_S f_{S_0})}{K(\lambda+r)(d+p_S-Ke_S f_{S_0})+h_S r(d+p_S)}$$

$$I_{\sigma}^{R_0} = 1$$

$$I_{\theta}^{R_0} = \frac{-\theta p_S}{d+v+\theta p_S+c}$$

$$I_{v}^{R_0} = \frac{v(c+\theta p_S)}{(d+v)(d+v+\theta p_S+c)}$$

Appendix C

In this Appendix, we provide the parameters used for our age since infection model described by equations (6.2)–(6.4) and the expressions for the endemic equilibrium.

C.1 Parameters

Variable	**Unit**
t time, a age of infection	day
$S(t)$ susceptible hosts	mg C/L
$I(t,a)$ infected hosts	mg C/(L day)
$Z(t)$ fungal spores	mg C/L
$A(t)$ algae	mg C/L
Parameter	**Value**
e_S : conversion efficiency	0.6 mg C/ mg C
f_0 : maximal feeding rate	0.32/day mg C/mg C
h_S : half saturation constant	0.50 mg C/L
$\rho(a)$: fecundity reduction due to infection	0.05–1
p_S : predation rate	0.1/day
d : background mortality	0.03/day
μ : per spore infectivity	10 mg C/mg C
$v(a)$: virulence	0.05-0.4 /day
$\theta(a)$: selective predation parameter	1–20
σ : spore release parameter	31 days $\times$ mg C / mg C
λ : spore loss rate	0.2/day
r : algal net maximal growth rate	0.2/day
K : algal carrying capacity	2.0 mg C/L

Table C.1: Variables and parameters PDE model. The values of the various parameters, unless specified in the text, are the ones given in [30].

C.2 Steady States

From equation (6.2) we obtain that $I(a) = \mu \frac{f_S(A)}{A} SZ \left(e^{-\int_0^a (d+v(\tau)+\theta(\tau)p_S+r(\tau))d\tau} \right)$, thus

$$Q_e = \int_0^{a_0} I_e(a)da = \mu \frac{f_S(A_e)}{A_e} S_e Z_e \int_0^{a_0} e^{-\int_0^a (d+v(\tau)+p_S\theta(\tau)+r(\tau)d\tau} da = \mu \frac{f_S(A_e)}{A_e} S_e Z_e J_0$$

is the total infected host population and J_0 is expected life-span of an infected host. Then, E_e is described by the relationships

$$\begin{aligned} S_e &= \frac{\lambda + r\left(1-\frac{A_e}{K}\right)}{\sigma e_S f_S(A_e)(d\phi+\chi)} \frac{1}{\mu J_0 \frac{f_S(A_e)}{A_e}} \\ Q_e &= \frac{r\left(1-\frac{A_e}{K}\right)A_e}{f_S(A_e)} - S_e = \frac{e_S f_S(A_e) - (d+p_S)}{\frac{1}{J_0} - \psi e_S f_S(A_e) - \eta} S_e, \\ Z_e &= \frac{\sigma e_S f_S(A_e)(d\phi+\chi)}{\lambda + r\left(1-\frac{A_e}{K}\right)} Q_e. \end{aligned} \tag{C.1}$$

Where we denote by,

$$J_1 = \int_0^{a_0} W(a) \exp\left(-\int_0^a (d + v(\tau) + \theta(\tau)p_S + c(\tau))d\tau\right) da \tag{C.2}$$

the expected value of within-host pathogen load in the lifespan of an infected host,

$$J_2 = \int_0^{a_0} v(a)W(a) \exp\left(-\int_0^a (d + v(\tau) + \theta(\tau)p_S + c(\tau))d\tau\right) da \tag{C.3}$$

the expected value of the disease-induced mortality over the lifespan of the infected host, and

$$J_3 = \int_0^{a_0} \rho(a) \exp\left(-\int_0^a (d + v(\tau) + \theta(\tau)p_S + c(\tau))d\tau\right) da \tag{C.4}$$

the expected value of the fecundity reduction parameter over the lifespan of the infected host,

$$J_4 = \int_0^{a_0} c(a) \exp\left(-\int_0^a (d + v(\tau) + \theta(\tau)p_S + c(\tau))d\tau\right) da \tag{C.5}$$

the expected value of the recovery over the lifespan of the infected host,

$$\phi = \frac{J_1}{J_0}, \quad \chi = \frac{J_2}{J_0}, \quad \text{and} \quad \psi = \frac{J_3}{J_0} \quad \eta = \frac{J_4}{J_0}. \tag{C.6}$$

References

[1] P. Abrams. Modelling the adaptive dynamics of traits involved in inter-and intraspecific interactions: an assessment of three methods. *Ecology Letters*, 4(2):166–175, 2001.

[2] P. A. Abrams, Y. Harada, and H. Matsuda. On the relationship between quantitative genetic and ess models. *Evolution*, 47(3):982–985, 1993.

[3] S. Alizon, A. Hurford, N. Mideo, and M. Van Baalen. Virulence evolution and the trade-off hypothesis: history, current state of affairs and the future. *Journal of Evolutionary Biology*, 22(2):245–259, 2009.

[4] S. Alizon and Y. Michalakis. Adaptive virulence evolution: the good old fitness-based approach. *Trends in Ecology & Evolution*, 30(5):248–254, 2015.

[5] L. J. Allen, F. Brauer, P. Van den Driessche, and J. Wu. *Mathematical epidemiology*, volume 1945. Springer, 2008.

[6] R. M. Anderson and R. M. May. The population dynamics of microparasites and their invertebrate hosts. *Philosophical Transactions of the Royal Society of London. B, Biological Sciences*, 291(1054):451–524, 1981.

[7] J. P. Aparicio and H. G. Solari. Sustained oscillations in stochastic systems. *Mathematical Biosciences*, 169(1):15–25, 2001.

[8] L. Arriola and J. M. Hyman. Sensitivity analysis for uncertainty quantification in mathematical models. In *Mathematical and Statistical Estimation Approaches in Epidemiology*, pages 195–247. Springer, 2009.

[9] S. Auld, R. M. Penczykowski, J. Housley Ochs, D. C. Grippi, S. R. Hall, and M. A. Duffy. Variation in costs of parasite resistance among natural host populations. *Journal of Evolutionary Biology*, 26(11):2479–2486, 2013.

[10] S. K. Auld, S. R. Hall, J. Housley Ochs, M. Sebastian, and M. A. Duffy. Predators and patterns of within-host growth can mediate both among-host competition and evolution of transmission potential of parasites. *The American Naturalist*, 184(S1):S77–S90, 2014.

[11] M. S. Bartlett. Measles periodicity and community size. *Journal of the Royal Statistical Society. Series A (General)*, 120(1):48–70, 1957.

[12] C. T. Bauch. The role of mathematical models in explaining recurrent outbreaks of infectious childhood diseases. In *Mathematical Epidemiology*, pages 297–319. Springer, 2008.

[13] L. Becks, S. P. Ellner, L. E. Jones, and N. G. Hairston Jr. Reduction of adaptive genetic diversity radically alters eco-evolutionary community dynamics. *Ecology Letters*, 13(8):989–997, 2010.

[14] P. M. Beldomenico and M. Begon. Disease spread, susceptibility and infection intensity: vicious circles? *Trends in Ecology & Evolution*, 25(1):21–27, 2010.

[15] A. Best, A. White, and M. Boots. Maintenance of host variation in tolerance to pathogens and parasites. *Proceedings of the National Academy of Sciences*, 105(52):20786–20791, 2008.

[16] M. Betti, L. Wahl, and M. Zamir. Reproduction number and asymptotic stability for the dynamics of a honey bee colony with continuous age structure. *Bulletin of Mathematical Biology*, 79(7):1586–1611, 2017.

[17] M. I. Betti, L. M. Wahl, and M. Zamir. Effects of infection on honey bee population dynamics: a model. *PloS one*, 9(10):e110237, 2014.

[18] A. J. Black and A. J. McKane. Stochasticity in staged models of epidemics: quantifying the dynamics of whooping cough. *Journal of The Royal Society Interface*, 7(49):1219–1227, 2010.

[19] A. J. Black and A. J. McKane. Stochastic formulation of ecological models and their applications. *Trends in Ecology & Evolution*, 27(6):337–345, 2012.

[20] C. Boettiger. Adaptive dynamics: Branching phenomena and the canonical equation. 2006.

[21] B. Boldin and É. Kisdi. On the evolutionary dynamics of pathogens with direct and environmental transmission. *Evolution: International Journal of Organic Evolution*, 66(8):2514–2527, 2012.

[22] B. M. Bolker, A. Nanda, and D. Shah. Transient virulence of emerging pathogens. *Journal of the Royal Society Interface*, 7(46):811–822, 2009.

[23] L. Bolzoni and G. A. De Leo. Unexpected consequences of culling on the eradication of wildlife diseases: the role of virulence evolution. *The American Naturalist*, 181(3):301–313, 2013.

[24] M. Boots, A. Best, M. R. Miller, and A. White. The role of ecological feedbacks in the evolution of host defence: what does theory tell us? *Philosophical Transactions of the Royal Society B: Biological Sciences*, 364(1513):27, 2009.

[25] M. Boots and R. G. Bowers. Three mechanisms of host resistance to microparasitesavoidance, recovery and toleranceshow different evolutionary dynamics. *Journal of Theoretical Biology*, 201(1):13–23, 1999.

[26] R. Bowers. A baseline model for the apparent competition between many host strains: the evolution of host resistance to microparasites. *Journal of Theoretical Biology*, 200(1):65–75, 1999.

[27] R. G. Bowers, A. Hoyle, A. White, and M. Boots. The geometric theory of adaptive evolution: trade-off and invasion plots. *Journal of Theoretical Biology*, 233(3):363–377, 2005.

[28] Å. Brännström, J. Johansson, and N. von Festenberg. The hitchhikers guide to adaptive dynamics. *Games*, 4(3):304–328, 2013.

[29] J. Bryden, R. J. Gill, R. A. Mitton, N. E. Raine, and V. A. Jansen. Chronic sublethal stress causes bee colony failure. *Ecology Letters*, 16(12):1463–1469, 2013.

[30] C. E. Cáceres, G. Davis, S. Duple, S. Hall, A. Koss, P. Lee, and Z. Rapti. Complex *Daphnia* interactions with parasites and competitors. *Mathematical Biosciences*, 258:148–161, 2014.

[31] C. E. Cáceres, A. J. Tessier, M. A. Duffy, and S. R. Hall. Disease in freshwater zooplankton: what have we learned and where are we going? *Journal of Plankton Research*, 36(2):326–333, 2014.

[32] N. Chitnis, J. M. Hyman, and J. M. Cushing. Determining important parameters in the spread of malaria through the sensitivity analysis of a mathematical model. *Bulletin of Mathematical Biology*, 70(5):1272, 2008.

[33] K. Choo, P. D. Williams, and T. Day. Host mortality, predation and the evolution of parasite virulence. *Ecology Letters*, 6(4):310–315, 2003.

[34] C. E. Cressler, D. V. McLeod, C. Rozins, J. Van Den Hoogen, and T. Day. The adaptive evolution of virulence: a review of theoretical predictions and empirical tests. *Parasitology*, 143(7):915–930, 2016.

[35] C. Darwin. *On the origin of species, 1859*. Routledge, 2004.

[36] T. Day. Virulence evolution via host exploitation and toxin production in spore-producing pathogens. *Ecology Letters*, 5(4):471–476, 2002.

[37] T. Day and S. R. Proulx. A general theory for the evolutionary dynamics of virulence. *The American Naturalist*, 163(4):E40–E63, 2004.

[38] O. Diekmann, J. A. P. Heesterbeek, and J. A. Metz. On the definition and the computation of the basic reproduction ratio r_0 in models for infectious diseases in heterogeneous populations. *Journal of Mathematical Biology*, 28(4):365–382, 1990.

[39] M. Doebeli. *Adaptive Diversification (MPB-48)*. Princeton University Press, 2011.

[40] R. Donnelly, A. White, and M. Boots. The epidemiological feedbacks critical to the evolution of host immunity. *Journal of Evolutionary Biology*, 28(11):2042–2053, 2015.

[41] M. A. Duffy and S. R. Hall. Selective predation and rapid evolution can jointly dampen effects of virulent parasites on daphnia populations. *The American Naturalist*, 171(4):499–510, 2008.

[42] M. A. Duffy, S. R. Hall, C. E. Cáceres, and A. R. Ives. Rapid evolution, seasonality, and the termination of parasite epidemics. *Ecology*, 90(6):1441–1448, 2009.

[43] M. A. Duffy, S. R. Hall, A. J. Tessier, and M. Huebner. Selective predators and their parasitized prey: are epidemics in zooplankton under top-down control? *Limnology and Oceanography*, 50(2):412–420, 2005.

[44] M. A. Duffy, J. H. Ochs, R. M. Penczykowski, D. J. Civitello, C. A. Klausmeier, and S. R. Hall. Ecological context influences epidemic size and parasite-driven evolution. *Science*, 335(6076):1636–1638, 2012.

[45] M. A. Duffy and L. Sivars-Becker. Rapid evolution and ecological host–parasite dynamics. *Ecology Letters*, 10(1):44–53, 2007.

[46] D. Ebert and W. W. Weisser. Optimal killing for obligate killers: the evolution of life histories and virulence of semelparous parasites. *Proceedings of the Royal Society of London. Series B: Biological Sciences*, 264(1384):985–991, 1997.

[47] R. Erban, J. Chapman, and P. Maini. A practical guide to stochastic simulations of reaction-diffusion processes. *arXiv preprint arXiv:0704.1908*, 2007.

[48] S. Genieys, N. Bessonov, and V. Volpert. Mathematical model of evolutionary branching. *Mathematical and Computer Modelling*, 49(11-12):2109–2115, 2009.

[49] S. Génieys, V. Volpert, and P. Auger. Adaptive dynamics: modelling darwin's divergence principle. *Comptes rendus biologies*, 329(11):876–879, 2006.

[50] S. A. Geritz, J. A. Metz, É. Kisdi, and G. Meszéna. Dynamics of adaptation and evolutionary branching. *Physical Review Letters*, 78(10):2024, 1997.

[51] D. T. Gillespie. A general method for numerically simulating the stochastic time evolution of coupled chemical reactions. *Journal of Computational Physics*, 22(4):403–434, 1976.

[52] P. E. Greenwood and L. F. Gordillo. Stochastic epidemic modeling. In *Mathematical and statistical estimation approaches in epidemiology*, pages 31–52. Springer, 2009.

[53] S. R. Hall, C. R. Becker, J. L. Simonis, M. A. Duffy, A. J. Tessier, and C. E. Cáceres. Friendly competition: evidence for a dilution effect among competitors in a planktonic host–parasite system. *Ecology*, 90(3):791–801, 2009.

[54] S. R. Hall, M. A. Duffy, and C. E. Cáceres. Selective predation and productivity jointly drive complex behavior in host-parasite systems. *The American Naturalist*, 165(1):70–81, 2004.

[55] S. R. Hall, R. Smyth, C. R. Becker, M. A. Duffy, C. J. Knight, S. MacIntyre, A. J. Tessier, and C. E. Cáceres. Why are *Daphnia* in some lakes sicker? Disease ecology, habitat structure, and the plankton. *Bioscience*, 60(5):363–375, 2010.

[56] S. Halsey. Defuse the dilution effect debate. *Nature Ecology & Evolution*, 3:145–146, 2019.

[57] H. W. Hethcote. The mathematics of infectious diseases. *SIAM Review*, 42(4):599–653, 2000.

[58] A. Hurford, D. Cownden, and T. Day. Next-generation tools for evolutionary invasion analyses. *Journal of the Royal Society Interface*, 7(45):561–571, 2009.

[59] W. O. Kermack and A. G. McKendrick. A contribution to the mathematical theory of epidemics. *Proceedings of the Royal Society of London. Series A, Containing papers of a mathematical and physical character*, 115(772):700–721, 1927.

[60] É. Kisdi and S. A. Geritz. Adaptive dynamics in allele space: evolution of genetic polymorphism by small mutations in a heterogeneous environment. *Evolution*, 53(4):993–1008, 1999.

[61] E. Kisdi, S. A. Geritz, and B. Boldin. Evolution of pathogen virulence under selective predation: a construction method to find eco-evolutionary cycles. *Journal of Theoretical Biology*, 339:140–150, 2013.

[62] S. Lion. Theoretical approaches in evolutionary ecology: environmental feedback as a unifying perspective. *The American Naturalist*, 191(1):21–44, 2018.

[63] A. Lloyd. Sensitivity of model-based epidemiological parameter estimation to model assumptions. In *Mathematical and Statistical Estimation Approaches in Epidemiology*, pages 123–141. Springer, 2009.

[64] A. L. Lloyd. Destabilization of epidemic models with the inclusion of realistic distributions of infectious periods. *Proceedings of the Royal Society of London. Series B: Biological Sciences*, 268(1470):985–993, 2001.

[65] A. L. Lloyd. Realistic distributions of infectious periods in epidemic models: changing patterns of persistence and dynamics. *Theoretical Population Biology*, 60(1):59–71, 2001.

[66] S. Luo and K. Koelle. Navigating the devious course of evolution: the importance of mechanistic models for identifying eco-evolutionary dynamics in nature. *The American Naturalist*, 181(S1):S58–S75, 2013.

[67] S. Mandal, R. R. Sarkar, and S. Sinha. Mathematical models of malaria-a review. *Malaria Journal*, 10(1):202, 2011.

[68] J. A. Metz, S. A. Geritz, G. Meszéna, F. J. Jacobs, and J. S. Van Heerwaarden. Adaptive dynamics: a geometrical study of the consequences of nearly faithful reproduction. *IIASA Working Paper*, 1995.

[69] M. R. Miller. *Theoretical models for the evolution and ecological dynamics of host-parasite systems.* PhD thesis, University of Sheffield, 2006.

[70] B. E. Miner, L. De Meester, M. E. Pfrender, W. Lampert, and N. G. Hairston Jr. Linking genes to communities and ecosystems: Daphnia as an ecogenomic model. *Proceedings of the Royal Society B: Biological Sciences*, 279(1735):1873–1882, 2012.

[71] A. Morales and M. Eithun. Stability of control system of intracellular iron homeostasis: A mathematical proof. Texas A&M University, 2016.

[72] A. Morozov and A. Best. Predation on infected host promotes evolutionary branching of virulence and pathogens' biodiversity. *Journal of Theoretical Biology*, 307:29–36, 2012.

[73] A. Y. Morozov and M. Adamson. Evolution of virulence driven by predator–prey interaction: possible consequences for population dynamics. *Journal of Theoretical Biology*, 276(1):181–191, 2011.

[74] R. M. Penczykowski, A.-L. Laine, and B. Koskella. Understanding the ecology and evolution of host–parasite interactions across scales. *Evolutionary Applications*, 9(1):37–52, 2016.

[75] O. Prosper, N. Ruktanonchai, and M. Martcheva. Assessing the role of spatial heterogeneity and human movement in malaria dynamics and control. *Journal of Theoretical Biology*, 303:1–14, 2012.

[76] A. Pugliese. On the evolutionary coexistence of parasite strains. *Mathematical Biosciences*, 177:355–375, 2002.

[77] Z. Rapti and C. Cáceres. Effects of intrinsic and extrinsic host mortality on disease spread. *Bulletin of Mathematical Biology*, 78(2):235–253, 2016.

[78] P. Rohani, M. J. Keeling, and B. T. Grenfell. The interplay between determinism and stochasticity in childhood diseases. *The American Naturalist*, 159(5):469–481, 2002.

[79] T. E. Stewart Merrill and C. E. Cáceres. Within-host complexity of a plankton-parasite interaction. *Ecology*, 99(12):2864–2867, 2018.

[80] A. T. Strauss, M. S. Shocket, D. J. Civitello, J. L. Hite, R. M. Penczykowski, M. A. Duffy, C. E. Cáceres, and S. R. Hall. Habitat, predators, and hosts regulate disease in daphnia through direct and indirect pathways. *Ecological Monographs*, 86(4):393–411, 2016.

[81] T. O. Svennungsen and É. Kisdi. Evolutionary branching of virulence in a single-infection model. *Journal of Theoretical Biology*, 257(3):408–418, 2009.

[82] P. van den Driessche. Reproduction numbers of infectious disease models. *Infectious Disease Modelling*, 2(3):288–303, 2017.

[83] D. Waxman and S. Gavrilets. 20 questions on adaptive dynamics. *Journal of Evolutionary Biology*, 18(5):1139–1154, 2005.

[84] M. J. Wonham, M. A. Lewis, J. Rencławowicz, and P. Van den Driessche. Transmission assumptions generate conflicting predictions in host–vector disease models: a case study in west nile virus. *Ecology Letters*, 9(6):706–725, 2006.